

UNIVERSITÀ DEGLI STUDI DI PADOVA



Facoltà di Ingegneria

Corso di Laurea in Ingegneria Dell'Automazione

Tesi di Laurea Specialistica

**ANALYSIS AND MODELING OF A
THERMOSOLAR PLANT**

RELATORE: Prof.ssa Maria Elena Valcher

CO-RELATORE: Prof. Eduardo Fernandez Camacho

LAUREANDO: Marco Spoladore

Padova, 12/07/2010

*...La forza non deriva dalle capacità fisiche,
ma da una volontà indomita...
(Gandhi)*

Contents

Introduction	7
1 Current Status of Solar Techniques	11
1.1 Concentrating Solar Power	12
1.1.1 Linear Concentrator Systems	13
1.1.2 Dish/Engine System	16
1.1.3 Power Tower System	17
1.1.4 Thermal Storage	19
1.2 Photovoltaic Systems	21
1.3 Solar Heating	22
1.4 Solar Lighting	23
2 Earth-Sun Geometry	25
2.1 Sun Basics	25
2.2 Solar Radiation	29
2.2.1 Earth's Energy Balance	30
2.2.2 Solar Exposure	31
2.2.3 Global, Direct and Diffuse Irradiance	34
2.3 Earth-Sun's Geometry Relation	35
3 Solar Plant of Seville's University	43
3.1 Linear Fresnel Collector Field	44
3.2 Plant's Technical Data	45
3.3 Absorption Machine	52
4 Optical Model of The Solar Plant	57
4.1 Solar Quantities Definition	58
4.2 2D-Model	66
4.2.1 Mirror Rows Inclination	66
4.2.2 Mirrors Shadows	72
4.2.3 Optical Losses	84
4.3 3D-Model	85
4.3.1 Real Radiation Computation	87
5 Thermal Model of The Solar Plant	89
5.1 Implementation of the Model	94
5.2 Solving of the Model	97

6	Practical and Experimental Results	101
6.1	Optical Model	101
6.2	Thermal Model	113
7	Conclusions and Future Developments	119
A	Energy Production of a Solar Plant	123
B	Sun Statistics	125
C	Magnitude of a star	127
D	Wavelength Radiation Relations	129
E	Atmospheric Effects on Incoming Solar Radiation	131
F	Double Effect Absorption Machine Way of Working Scheme	133
G	Mirrors Row Inclination	135
H	Values of Density and Specific Heat Capacity for Waters	137
I	Least Squares Method	139

Introduction

In today's climate of growing energy needs and increasing environmental concerns, alternatives to the use of non-renewable and polluting fossil fuels need to be searched for. One such alternative is Solar Energy.

Solar Energy is simply the energy produced directly by the sun and collected elsewhere, including the Earth. The sun creates its energy through a thermonuclear process that converts about 650,000,000 tons of hydrogen to helium every second. The process creates heat and electromagnetic radiation. The heat remains in the sun and is instrumental in maintaining the thermonuclear reaction. The electromagnetic radiation (including visible light, infra-red light, and ultra-violet radiation) streams out into space in all directions.

Only a very small fraction of the total radiation produced reaches the Earth. The radiation that reaches the Earth is the indirect source of many types of energy used today. Some exceptions are geothermal energy, nuclear fission and fusion. Even fossil fuels owe their origins to the sun; they were once living plants and animals whose life was for most dependent upon the sun.

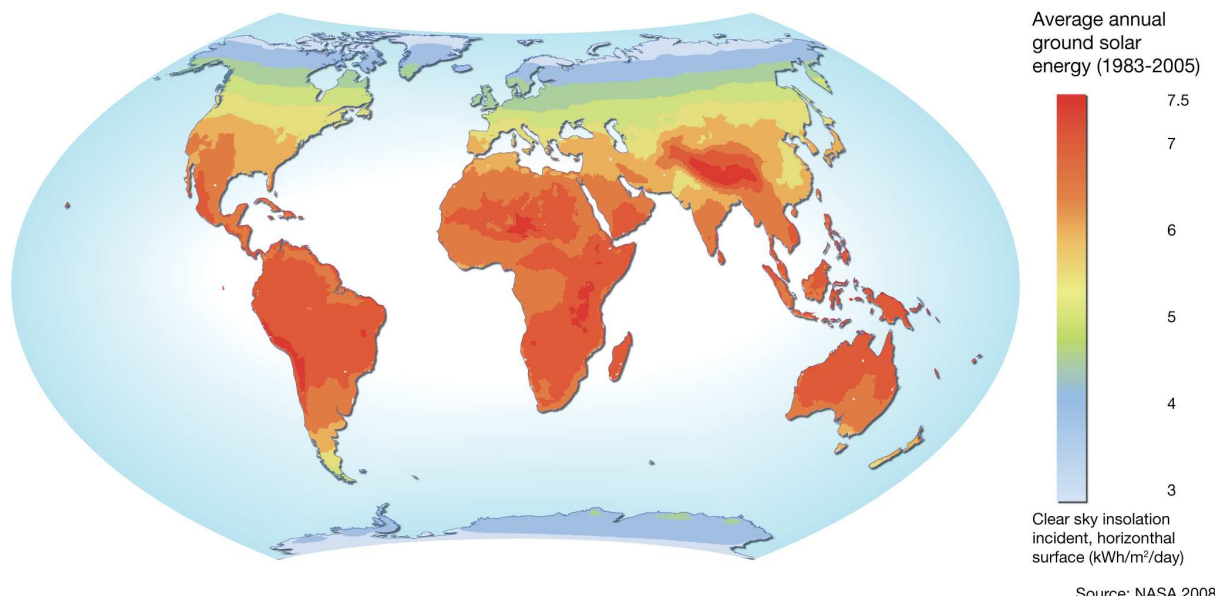


Figure 1: Map of Solar Energy Hitting Earth's Surface: Red is highest level.

Solar energy is radiated from the sun through forms of heat and light, and this determines the Earth's climate and sustains its life. All Solar Technology Systems capture the energy of the sun by absorbing light as heat. There are two main types of solar technologies:

★ ThermoSolar technology**★ Photovoltaic technology**

ThermoSolar Power Systems concentrate sunlight, usually with mirrors, to heat to high temperatures a fluid that drives an engine. This approach differs from the one used by Photovoltaic Solar Power Systems, where light interacts directly with special materials to separate charges and generate electricity. Photovoltaic power exhibits many advantages, such as untended operation and small-scale feasibility, but it remains significantly more expensive, as a source of large-scale power, than solar thermal technologies.

Generally speaking, solar electricity may be seen as the result of a process through which directly collected solar energy is converted into electricity through the use of some sort of heat/light to electricity conversion device. In most of the cases, this is a heat engine, but there are other options such as a thermoelectric pile converter or a fan converter, as in solar chimneys.

Solar thermal electricity on grid¹ was not achieved until the 1980s, although the basic technology for the production of mechanical energy (which could be converted to electricity using a conventional generator) had been under development for about 140 years, beginning with Mouchot and Pifre (1882) in France, and continuing with extraordinary pioneers such as Ericsson (1888), Eneas (1901), Shuman (1913), and Francia (1961, 1968).

The modern era of large scale solar power generation was born in California's Mojave Desert in the 1980s, when Luz Industries² built a total of 354 MegaWatts of Solar Electric Generating System, or SEGS, power plants. The SEGS plants use long parabolic mirrors with pipes located at the focus point, where circulating oil is heated to 700° F (350° C). The oil is pumped through heat exchangers which boil water to make high-pressure steam, which in turn drives turbine generators to make electric power. For many years the SEGS plants produced the majority of the world's solar electric power, and they are still operating.

Solar thermal power has probably the greatest potential within the renewable energies area, but its development has been delayed since the 1980s because of market resistance to large plant sizes and poor political and financial support from incentive programmes.

However, nowadays a rapid development is occurring, both in the basic technology and the market strategy, and prospects for a rapid growth appear to be very bright for newer approaches.

Of all the energy sources available, solar one is undoubtedly the most promising. Numerically, it is capable of potentially producing the power required to satisfy the entire planet's energy needs. Environmentally, it is one of the least destructive among all the sources of energy. Practically, it can be set up to power, with very little adjustment, nearly everything except for transportation systems, and even in that case it could be handled with some reasonable modifications of the current general system of travel. So, clearly, solar energy is the resource of the future.

¹The term "on grid" is used in the field of solar electricity to indicate the area in which are collocated photovoltaic cells or solar mirrors, because of the aspect that assumes when seen overhead from above.

²Luz International Limited ('Luz'). The Luz team revolutionized the power world by proving that solar energy could reliably produce commercially competitive electricity during the heavy use, peak load, day time hours. Between 1984 and 1991, Luz designed, developed, built, financed, and operated nine Solar Electricity Generating Stations (SEGS) in California's Mojave Desert, generating a total of 354 MegaWatts.



Figure 2: The Revolutionary Mojave's Desert Power Plant built by Luz International.

In this thesis, an overview of the current technologies which are available, or are being developed, is given, together with an assessment of their market prospects.

Then a particular technology, employed in the Linear Fresnel Reflector System of Seville Engineer University's thermosolar plant, will be analyzed and discussed in detail.

Chapter 1

Current Status of Solar Techniques

The world of Solar Technology consists of four major areas: Concentrating Solar, also known as ThermoSolar Power; Solar Electricity, also known as Photovoltaics (PV) Power; Solar Heating and Solar Lighting.

- **Concentrating Solar Power**

These systems - such as dish/engine systems, linear concentrator systems and central power tower - are made of reflective materials that focus or concentrate the sun's considerable heat energy. This concentrated solar energy then drives a generator to produce electricity.

- **Photovoltaic System**

This solar electric technology makes use of semiconductors to convert sunlight directly to electricity. Photovoltaic systems can be used to provide both a very small amount of electric power to solar watches or calculators, and a very large amount of power to local electric utilities.

- **Solar Heating**

Solar heating technologies make use of low-temperature solar collectors that absorb the sun's heat energy, to be used directly for water or space heating in residential, commercial, and industrial buildings.

- **Solar Lighting**

Solar lighting technologies rely on solar concentrators to collect sunlight; then, they distribute that light through optical fibers to hybrid lighting fixtures in the building's interior/exterior or in the street. These fixtures are called hybrid because they combine natural light with artificial light to illuminate spaces.

All these solar energy technologies use the sun's energy to serve the man in industry, home, public buildings and everyday's life. They are being developed because they are feasible and reliable, they have very little environmental impact, and they make use of an abundant energy resource: sunlight.

In this section, a basics description of today's solar energy technologies is introduced, explaining the reasons why they are important, how can be used to produce heat, light, and power. Also, research and development on the latest materials, methods, and manufacturing processes that will lead to the solar technologies of the future will be described.

1.1 Concentrating Solar Power

Concentrating solar power (CSP) technologies use mirrors to reflect and concentrate sunlight onto receivers that collect the solar energy and convert it to heat. This thermal energy can then be used to produce electricity via a steam turbine or a heat engine driving a generator.

Due to the nature of solar energy, two components are required to have a functional solar energy generator. These two components are a **Solar Collector** and a **Thermal Storage Unit**. The Solar Collector simply collects the radiation that falls over it and converts a fraction of it into other forms of energy (either electricity and heat, or heat alone). The Thermal Storage Unit is required because of the non-constant nature of solar energy; indeed, sometimes, due to the time of the day, the season or the weather conditions, only a very small amount of radiation will be received. When so, the amount of energy produced by the collector is quite small. So, the storage unit can hold the excess energy produced during the periods of maximum productivity, and release it when the productivity drops. In practice, a backup power supply is usually added, too, for the situations when the amount of energy required is greater than both what is being produced and what is stored in the container.

Methods of classifying Collecting Solar Energy depend on the main aspect that is considered.

There are many different typologies of solar technologies classification, for example based on the way the various systems collect solar energy or the method of energy transformation. The most diffused and functional is the one based on the way the various systems collect solar energy. According to this classification, there are three principal types of solar systems:

- **Linear Concentrator Systems**
- **Dish/Engine Systems**
- **Power Tower Systems**

Presently, smaller CSP systems can be located directly where the power is needed. Single dish/engine systems can produce 3 to 25 kilowatts¹ of power and are well suited for such distributed applications. Larger, utility-scale CSP applications provide hundreds of megawatts of electricity for the power grid. Both linear concentrator and power tower systems can be easily integrated with thermal storage, helping to generate electricity during cloudy periods or at night. Alternatively, these systems can be combined with natural gas, and the resulting hybrid power plants can provide high-value, dispatchable power throughout the day.

¹This data refers to rated power (or maximum power or peak power) that is the electrical power of the plant measured in accordance with International Standard Conditions (ISC) specified at a temperature of 25 °C, an irradiance of 1000 W/m² and relates to sunlight that has passed through the atmosphere (that has an air mass of 1.5 (air mass is a unit used in astronomy in measuring the absorption of light from the stars by the atmosphere. One air mass is the amount of absorption of light from a star directly overhead)). These conditions correspond to the irradiance and spectrum of sunlight incident on a clear day upon a sun-facing 37°-tilted surface with the sun at an angle of 41.81° above the horizon. This condition approximately represents solar noon near the spring and autumn equinoxes in the United States. For more details see Appendix A.

These attributes - along with growing solar-to-electric conversion efficiencies - make CSP an attractive renewable energy option in the southwestern of Spain and in other sunbelts worldwide.

1.1.1 Linear Concentrator Systems

Linear concentrating solar power (CSP) collectors are one of the three types of CSP systems in use today. They include the two major types of linear concentrator systems: *Parabolic Trough Systems* and *Linear Fresnel Reflector Systems*.

Linear CSP collectors capture the sun's energy with large mirrors that reflect and focus the sunlight onto a linear receiver tube. The receiver contains a fluid that is heated by the sunlight, and then used to create superheated steam that spins a turbine that drives a generator to produce electricity. Alternatively, steam can be generated directly in the solar field, eliminating the need for costly heat exchangers.

Linear concentrating collector fields consist of a large number of collectors in parallel rows that are typically aligned in a north-to-south orientation to maximize both annual and summertime energy collection. With a single-axis sun-tracking system, this configuration enables the mirrors to track the sun from east to west during the day, ensuring that the sun reflects continuously onto the receiver tubes.

Parabolic Trough Systems

This is the predominant kind of CSP systems currently in operation in the United States. In these systems, the receiver tube is positioned along the focal line of each parabola-shaped reflector. The tube is fixed to the mirror structure and the heated fluid - either a heat-transfer fluid or water/steam - flows through and out of the field of solar mirrors to the tank, where it is used to create steam (or, for the case of a water/steam receiver, it is sent directly to the turbine).

Currently, the largest individual trough systems generate 80 Megawatts² of electricity. However, individual systems presently under development will generate 250 megawatts. In addition, individual systems can be collocated in power parks. This capacity would be constrained only by the transmission capacity and the availability of contiguous land area.

Trough design can incorporate thermal storage. In such systems, the collector field is oversized to heat during the day a storage system that can be used in the evening or during cloudy weather to generate additional steam to produce electricity. Parabolic trough plants can also be designed as hybrids, meaning that they can use fossil fuel to supplement the solar output during periods of low solar radiation. In such a design, a natural-gas-fired heater or a gas-steam boiler/reheater is used. In the future, troughs may be integrated with existing or new combined-cycle natural-gas- and coal-fired plants.

Linear Fresnel Reflector Systems

A second linear concentrator technology is exploited in linear Fresnel reflector systems. Flat or slightly curved mirrors mounted on trackers on the ground are configured to reflect

²This data refers to rated power (or maximum power or peak power). For more details see Appendix A.



Figure 1.1: A parabolic trough collector system

sunlight onto a receiver tube located above these mirrors. A small parabolic mirror is sometimes added atop the receiver, to further focus the sunlight.



Figure 1.2: A Linear Fresnel collector system

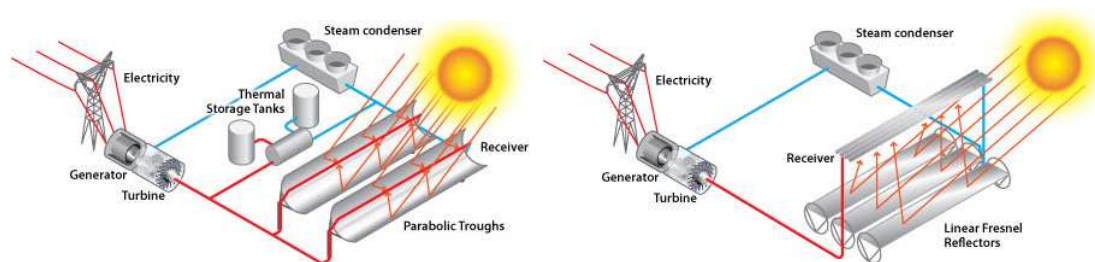


Figure 1.3: A linear concentrator power plant using parabolic trough collectors (on the left) and linear Fresnel reflector (on the right).

The classical linear Fresnel system uses an array of mirror strips close to the ground, to direct solar radiation to a single linear elevated fixed receiver. The first to apply this principle in a real system for solar collection was Francia (1968) who developed both linear and two axis tracking Fresnel reflector systems. One substantial difficulty with the Linear Fresnel Reflector (LFR) technology is that avoidance of shading and blocking leads to increased spacing between reflectors, which in turn leads to larger ground collector area.

Compact linear Fresnel reflector (CLFR) technology has proposed a new configuration of the Fresnel Reflector field to overcome the problem of reflector spacing. Traditional LFR technology design is based on one absorber receiver. The classical linear Fresnel system has only one linear receiver, and therefore there is no choice about the direction of orientation of a given reflector. However, if one assumes that the size of the field will be large, as it must be to supply electricity in the multi-Megawatt class, it is reasonable to assume that there will be many linear receivers in the system. If they are close enough, then individual reflectors have the option of directing reflected solar radiation to at least two receivers. This additional degree of freedom in reflector orientation allows for much more densely packed arrays and lower absorber receiver heights, because patterns of alternating reflector orientation can be set up so that closely packed reflectors can be positioned without shading and blocking. The interleaving of mirrors between two linear receiving towers is shown in the figure below.

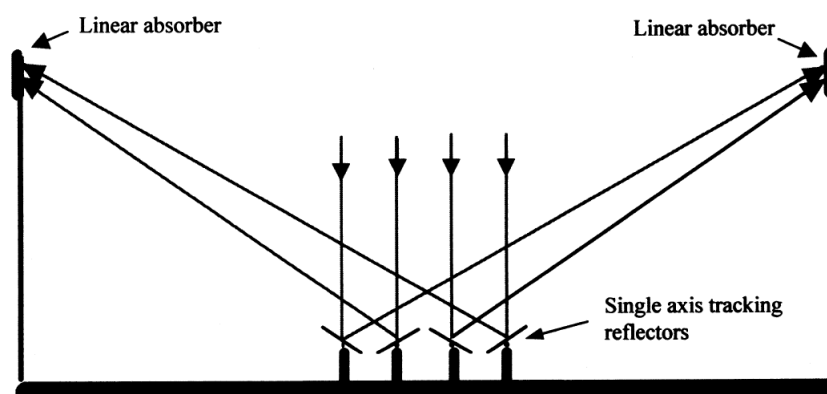


Figure 1.4: Compact Linear Fresnel Scheme with two linear receivers. In this way, individual reflectors have the option of directing reflected solar radiation to at least two receivers.

The avoidance of large reflector spacings and absorber receivers heights is an important issue in determining the cost of ground preparation, array substructure and absorber receiver structure costs, steam line thermal losses and steam line cost.

The more flexible CLFR still delivers the traditional benefits of a Fresnel reflector system, namely small reflector size, low structural cost, fixed receiver position without moving joints, and the ability to use non-cylindrical receiver geometry. The CLFR power plant concept is a new optical layout that includes the following additional features which enhance the system cost/performance ratio :

1. The array uses flat or elastically curved reflectors, instead of costly sagged glass reflectors. The reflectors are mounted close to the ground, minimizing structural requirements.
2. The heat transfer loop is separated from the reflector field and is fixed in space, thus avoiding the high cost of flexible high pressure lines or high pressure rotating joints as required in the trough and dish concepts.
3. The heat transfer fluid is water, and passive direct boiling heat transfer could be used to avoid parasitic pumping losses and the use of expensive flow controllers. Steam supply may either go directly to the power plant steam drum, or via a heat exchanger.
4. Maintenance will be lower than in other types of solar concentrators because of nearly flat reflectors and ease of access for cleaning, and because the single ended evacuated tubes can be removed without breaking the heat transfer fluid circuit.

1.1.2 Dish/Engine System

The dish/engine system is a concentrating solar power (CSP) technology that produces relatively small amounts of electricity compared to other CSP technologies, typically in the range of 3 to 25 kilowatts.

A parabolic dish of mirrors directs and concentrates sunlight onto a central engine that produces electricity. The two major parts of the system are the Solar Concentrator and the Power Conversion Unit.

- **Solar Concentrator**

The solar concentrator, or dish, gathers the solar energy coming directly from the sun. The resulting beam of concentrated sunlight is reflected onto a thermal receiver that collects the solar heat. The dish is mounted on a structure that tracks the sun continuously throughout the day to reflect the highest percentage of sunlight possible onto the thermal receiver.

- **Power Conversion Unit**

The power conversion unit includes the thermal receiver and the engine/generator.

The thermal receiver is the interface between the dish and the engine/generator. It absorbs the concentrated beams of solar energy, converts them to heat, and transfers the heat to the engine/generator. A thermal receiver can be a bank of tubes with a cooling fluid (usually hydrogen or helium) that typically is the heat-transfer medium

and also the working fluid for an engine. Alternate thermal receivers are heat pipes, where the boiling and condensing of an intermediate fluid transfers the heat to the engine.

The engine/generator system is the subsystem that takes the heat from the thermal receiver and uses it to produce electricity. Currently, the most common type of heat engine used in dish/engine systems is the Stirling engine. A Stirling engine uses the heated fluid to move pistons and create mechanical power. The mechanical work, in the form of the rotation of the engine's crankshaft, drives a generator and produces electrical power.



Figure 1.5: Two types of Dish/Engine Systems: Compact Mirror Dishes (on the left) and Multiple Mirror Dishes (on the right). Each of this solar concentrators has a fixed-focus faceted dish with a concentration of up to 250 suns.

1.1.3 Power Tower System

In this CSP technology, numerous large, flat, sun-tracking mirrors, known as heliostats, focus sunlight onto a receiver at the top of a tower. A heat-transfer fluid heated in the receiver is used to generate steam, which, in turn, is used in a conventional turbine generator to produce electricity. Some power towers use water/steam as the heat-transfer fluid.

Other advanced designs are experimenting with molten nitrate salt, because of its superior heat-transfer and energy-storage capabilities. Individual commercial plants can be sized to produce up to 200 megawatts of electricity.

Two large-scale power tower demonstration projects have been deployed in the United States. During its operation from 1982 to 1988, the 10-megawatt Solar One plant near Barstow, California, demonstrated the viability of power towers, producing more than 38 million kilowatt-hours of electricity.

The Solar Two plant was a retrofit of Solar One to demonstrate the advantages of molten salt for heat transfer and thermal storage. Using its highly efficient molten-salt energy storage system, Solar Two successfully demonstrated efficient collection of solar energy and dispatch of electricity. It also demonstrated the ability to routinely produce electricity during cloudy weather and at night. In one demonstration, Solar Two delivered



Figure 1.6: A Power Tower Plant: Stretched-membrane heliostats with silvered polymer reflectors surround the Solar Two Power Tower in Sanlúcar La Mayor, Andalusia (20km from Seville). This Plant can produce up to 23 GW per hour during all year.

power to the grid for 24 hours a day for almost seven consecutive days before cloudy weather interrupted operation.

Currently, Spain has several power tower systems, either operating or under construction, including the Europe biggest Thermo Solar Plant of Sanlúcar La Major, at 20 km from Seville (Figure 1.6). Furthermore, Planta Solar 10 and Planta Solar 20, water/steam systems with capacities of 11 and 20 megawatts, respectively, are presently under construction. Solar Tres will produce some 15 megawatts of electricity and has the capacity for molten-salt thermal storage.

Power towers also offer good longer-term prospects because of the high solar-to-electrical conversion efficiency. Additionally, costs will likely drop as the technology matures.

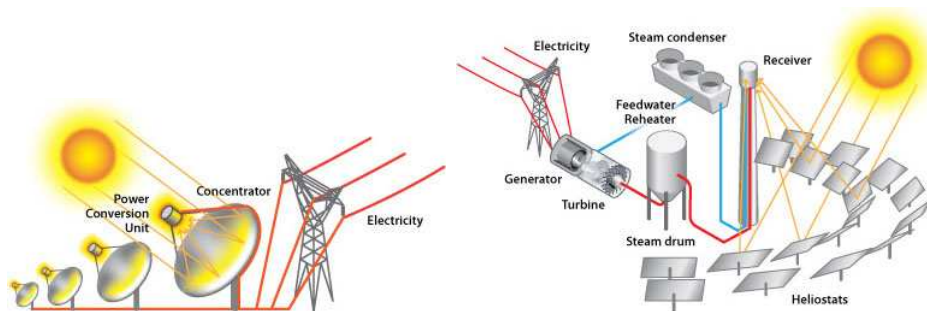


Figure 1.7: Dish/Engine Plant Scheme (on the left); Power Tower Plant Scheme (on the right).

1.1.4 Thermal Storage

Thermal Energy Storage (TES) has become a critical aspect of any concentrating solar power (CSP) system deployed today.

One challenge to face in order to achieve a widespread use of solar energy, as described above, is the reduced or curtailed energy production: thermal energy storage provides a workable solution to this challenge.

In a CSP system, the sun's rays are reflected onto a receiver, creating heat that is then used to generate electricity. If the receiver contains oil or molten salt as the heat-transfer medium, then the thermal energy can be stored for later use. This allows CSP systems to be a cost-competitive option for providing clean, renewable energy. Presently, steam-based receivers cannot store thermal energy for later use. Thermal storage research in the United States and Europe seeks to develop such capabilities.

Several TES technologies have been tested and implemented since 1985. These include:

- Two-Tank Direct Systems;
- Two-tank Indirect Systems;
- Single-Tank Thermocline Systems.

Two-Tank Direct Systems

Solar thermal energy in these systems is stored in the same fluid used to collect it. The fluid is stored in two tanks, one at high temperature and the other at low temperature. Fluid from the low-temperature tank flows through the solar collector or receiver, where solar energy heats it to the high temperature and it then flows to the high-temperature tank for storage. Fluid from the high-temperature tank flows through a heat exchanger, where it generates steam for electricity production. The fluid exits the heat exchanger at the low temperature and returns to the low-temperature tank. Two-tank direct storage was used in early parabolic trough power plants and at the Solar Two Power Tower in California. The trough plants used mineral oil as heat-transfer and storage fluid; Solar Two used molten salt.

Two-Tank Indirect Systems

These systems function in the same way as the two-tank direct system, except that different fluids are used as heat-transfer and storage fluids. These systems are used in plants where the heat-transfer fluid is too expensive or not suited for use as the storage fluid. The storage fluid from the low-temperature tank flows through an extra heat exchanger, where it is heated by the high-temperature heat-transfer fluid. The high-temperature storage fluid then flows back to the high-temperature storage tank. The fluid exits this heat exchanger at a low temperature and returns to the solar collector or receiver, where it is heated back to the high temperature. Storage fluid from the high-temperature tank is used to generate steam in the same manner as the two-tank direct system. The indirect system requires an extra heat exchanger, which adds cost to the system. This system will be used in many of the parabolic power plants in Spain and has also been proposed for several U.S. parabolic plants. The plants will use organic oil as heat-transfer fluid and molten salt as storage fluid.

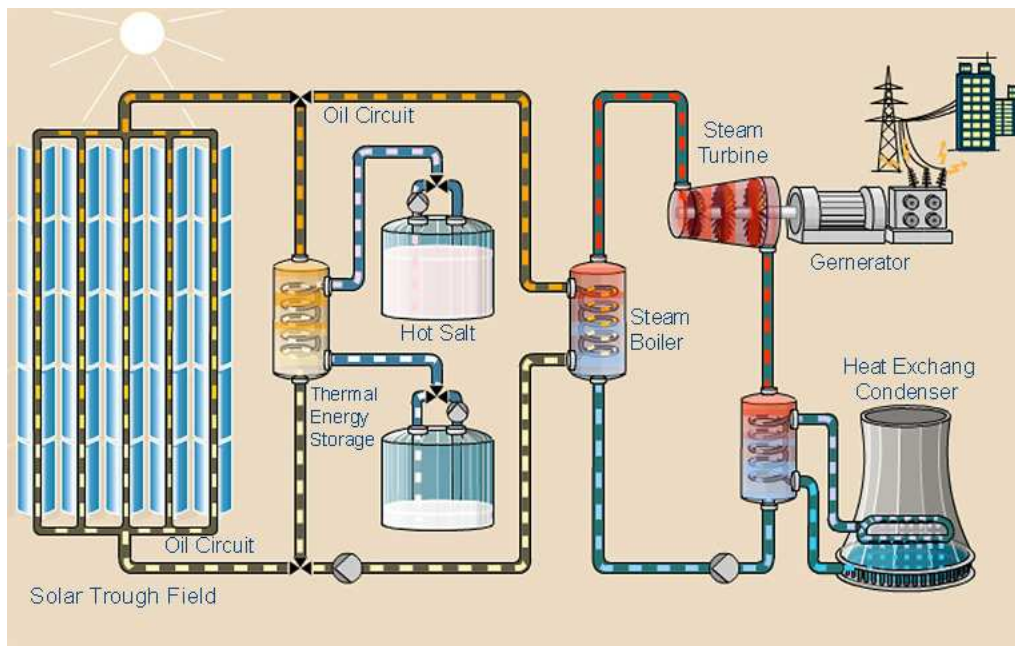


Figure 1.8: Two-Tank Indirect System Storage: part of solar ray energy heats salt fluid to high temperature and hot salt is stored at the thermal energy storage system. When it is dark, the solar trough field oil circuit is shut off. Hot fluid salt releases heat energy back to oil. The oil transforms heat to steam boiler. Thus steam turbine keeps working at night.

Single-Tank Thermocline Systems

These systems store thermal energy in a solid medium, most commonly silica sand, located in a single tank. At any time during operation, a portion of the medium is at high temperature and a portion is at low temperature. The hot and cold temperature regions are separated by a temperature gradient or thermocline. High-temperature heat-transfer fluid flows into the top of the thermocline and exits from the bottom at low temperature. This process moves the thermocline downward and adds thermal energy to the system for storage. Reversing the flow moves the thermocline upward and removes thermal energy from the system to generate steam and electricity. Buoyancy effects create thermal stratification of the fluid within the tank, which helps stabilizing and maintaining the thermocline.

Using a solid storage medium and only needing one tank reduce the cost of this system among the two-tank systems. This system was implemented at the Solar One power tower, where steam was used as heat-transfer fluid and mineral oil was used as storage fluid.

Nowadays advanced heat-transfer fluids are being tried and novel thermal-storage concepts are being developed. The goal is to increase efficiency and reduce costs for thermal energy storage, to identify and characterize novel fluids that possess physical and chemical properties needed to improve thermal storage. This research also identifies novel thermal storage concepts that may offer improved performance and lower costs with respect to the current thermal storage systems. This research is applied to all CSP technologies.

Incorporating TES into CSP power plants allows utilities to enhance dispatchability. As research in TES technologies allows for longer storage periods and lower costs, more utilities may consider CSP as a viable addition to power plants that depend solely on fossil fuels.

1.2 Photovoltaic Systems

The term photovoltaic is composed of “photo”, the Greek root for “light”, and “volt”, a common measurement of electricity. Together, these terms literally mean “light electricity”. Photovoltaic technology is referred to, for short, as Photovoltaics or PV. Photovoltaic technology relies on the electrical properties of certain materials known as semiconductors. When hit by sunlight, a semiconductor material responds by creating an electrical charge which can then be transferred to anything that uses electricity.

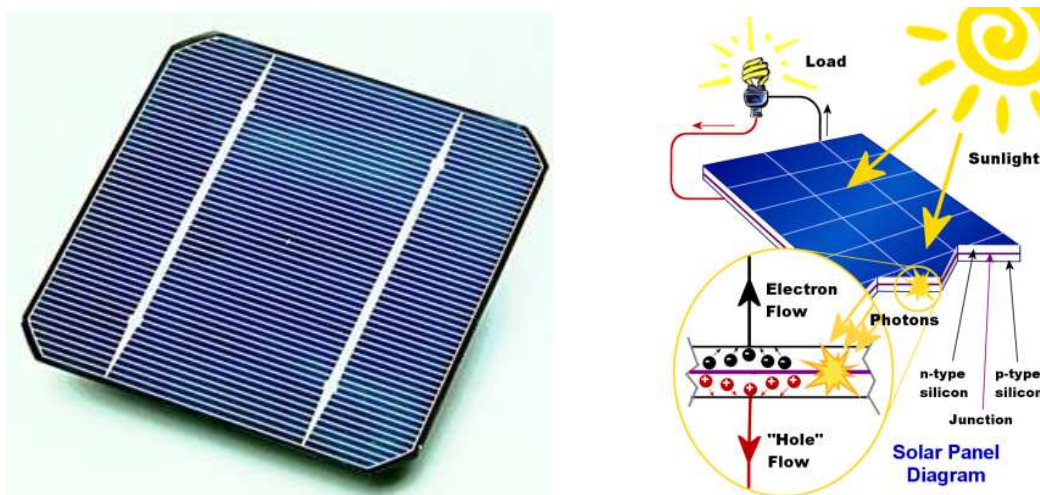


Figure 1.9: A photovoltaic cell(on the left), and a scheme of its way of working(on the right).

These semiconductors are produced in the form of cells, which can then be assembled in groups in a panel. There are many different types of panels available, and each has its particular advantages. Individual panels are often used to charge batteries that power small or remote electric equipments. Depending on the amount of electricity needed, these panels can then be connected in an array, to provide larger amounts of electricity to a building or other large user of electricity.

Photovoltaic cells and panels can be manufactured and installed at almost any scale, and as a result they are used to power a broad variety of applications. At its smallest, photovoltaic technology powers calculators, laptop computers and other applications that run on batteries. At its largest, it powers homes, offices and other buildings that use large amounts of electricity, and can be connected to utilities to increase the diversity of our collective electricity supply.

In connecting a photovoltaic system to an end use, several additional structures and technologies are needed. While photovoltaics can be mounted on roofs, it is important to consider the angle at which they face the sun. To transfer electricity to its end use,

photovoltaics are connected through solar technical devices that condition and modify the electricity they produce. These considerations are known as *Balance of System Components*, as they maximize the system's efficiency and allow higher amounts of electricity to reach its end use.

There are many benefits in using photovoltaics as an electricity source, most notably their environmental benefits.

As one of the cleanest electricity-generating technologies available, photovoltaics hold much promise for reducing environmental impacts from energy production. At the same time, several barriers exist for widespread use of this technology, the largest of which is its current cost.

In spite of its barriers, photovoltaics are becoming more widely used each year, and many examples exist throughout the world.



Figure 1.10: An example of Photovoltaic Arrays for energy production. The Europe biggest Photovoltaic Park is under construction in Italy, in the district of Rovigo, by the American SunEdison. The Park will have a surface of 850.000 m^2 (equal to 120 Football Fields) and a Power of 72 Megawatts.

1.3 Solar Heating

Solar heating utilizes the power of the sun to provide solar thermal energy for solar hot water, solar space heating, and solar pool heaters. A solar heating system saves energy, reduces utility costs, and produces clean energy.

The efficiency and reliability of solar heating systems have increased dramatically, making them attractive options in the home or business environment. But there is still room for improvement. The world research is working to design even more cost-effective

solar heating systems and to improve the durability of materials used in those systems. This research is helping make these systems more accessible to the average consumer and helping individuals reduce their utility bills and the nation reduce its consumption of fossil fuels.

To help more citizens benefit from these systems, there are facilities for consumers who install solar water heating systems in their home in all European Union Countries.

Since the early 1970s, the efficiency and reliability of solar heating systems and collectors have increased greatly, and costs have dropped. Current research and development is focused on improving solar-heating technologies to make them even more efficient and affordable, with special emphasis on the following:

- ◆ Testing materials for durability;
- ◆ Conducting thermal analysis of solar water-heating systems that work in different climates;
- ◆ Developing advanced applications, such as low-cost solar water heating and collectors for crop drying.



Figure 1.11: Examples of Solar Heating

1.4 Solar Lighting

Solar lighting can be used to illuminate most of the outdoor landscape elements, with significant advantages: they are a truly environmentally-friendly option with no running costs, low initial investment and an easy installation.

Solar lights absorb energy from sunlight and convert it into electricity that is stored in batteries; at dusk the solar lights turn on automatically, due to a small photocell device.

Solar outdoor lighting is excellent to mark and outline locations in dark areas, namely whenever the access to power source is difficult (no wiring is required in solar outdoor lighting).

There are many types of solar light fixtures, with different roles: general solar garden lights, solar spot lights, solar wall lights, floodlights, pathway lights, deck and patio lights, underwater lights and many others.

Some of them are very cheap but also of poor quality. This aspect must also be taken into account.

Solar lighting does not require any cables or external power sources. The fixture should simply be positioned in order to get as much sunlight as possible (every minute of sunlight is important in cold and cloudy climates).

Outdoor solar lighting systems work satisfactorily in most climates. In some cases fully charged solar lights can remain on for up to 12-15 hours.

However, solar outdoor lighting may not work well-enough on persistent cloudy days and climates, namely if you want more than just safe night-time navigation or spot lighting. The final performance of the system is always dependent on the amount of sunlight received during the day.

Due to these reasons, for non-sunny climates, there are also low-voltage outdoor lighting solutions. Some good solar lights can operate perfectly all night, even after several days of bad weather with little sunshine. As a rule, solar lights turn on and off automatically. Fixtures have a built-in photocell device, that switches on and off the light at dusk and early morning.

Hence the climate, the season and the weather conditions have a considerable importance. Persistently non-sunny weather will mean less charged batteries, which can reduce the lighting power of the system.

Most outdoor solar light batteries are AA type inexpensive batteries, that can be bought from many retailers. These batteries may last 1-3 years, but there are high quality batteries (much more expensive) with a lifespan of up to 10 years or more.

Moreover, most solar lights use LEDs (not bulbs) as light's source, and LEDs have a life expectancy of up to 20 years. Obviously, if the solar lights use bulbs, these can be replaced as any other bulb.



Figure 1.12: Examples of Solar Lighting: optical fibers street lights (also called "Light-Up Path" or "Spot-light") and street lamp heat lighting.

Chapter 2

Earth-Sun Geometry

In this section a description of basics concept and notions about Solar Geometry are given, that are fundamental to understand the interaction between the Earth and the Sun, and consequently the way of working of each Solar plant.

2.1 Sun Basics

The sun is the most prominent feature in our solar system. It is the largest star and contains approximately 98% of the total solar system mass¹.

It has a power output of about 10^{26} watts and is expected to continue producing energy at that rate for other 5 billion years². The sun is said to have a diameter of 1.4 million kilometers, about 109 times the diameter of earth, but this is not a properly correct statement because the sun has no true 'surface'. There is nothing definite, or hard, about the sun; in fact, the matter that makes up the apparent surface is so rarified that it would be consider as a vacuum here on earth. It is more accurate to think of the sun's boundary as extending far out into the solar system, well beyond earth.

Usually in studying the structure of the sun, solar physicists divide it into three domains:

1. The Interior;
2. The Surface Atmospheres;
3. The Corona.

The Interior

The sun's interior domain includes the *core*, *the radiative layer*, and *the convective layer*.

¹A more detailed description of basic structural and chemical properties of the sun can be found in Appendix B.

²At the end of its life, the sun will start to fuse helium into heavier elements and begin to swell up, ultimately growing so large that it will swallow the earth. After a billion years as a red giant, it will suddenly collapse into a white dwarf, the final end product of a star like this. It may take a trillion years to cool off completely.

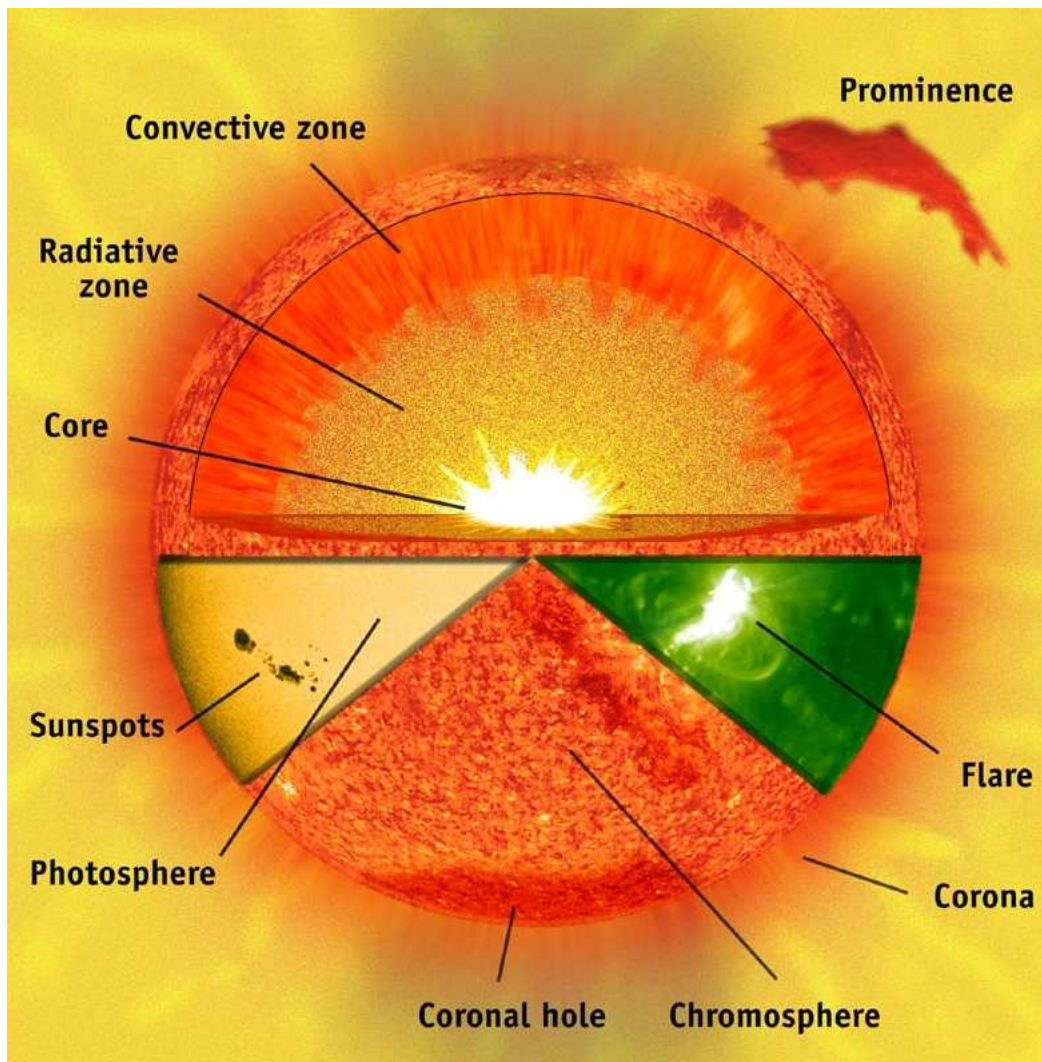


Figure 2.1: Solar Structure.

The core is the source of the sun's energy, the site of thermonuclear fusion. At a temperature of about $15 \cdot 10^6$ Kelvin, matter is in the state of 'plasma': atomic nuclei (principally protons) and electrons moving at very high speeds. Under these conditions, two protons can collide, overcome their electrical repulsion, and become cemented together by the strong nuclear force. This process is known as *nuclear fusion*, and it results in the formation of heavier elements as well as in the release of energy in the form of gamma ray photons³.

The immense energy produced in the core is bound by the surrounding radiative layer. This layer has an insulating effect that helps maintaining the high temperature of the core. The gamma photons produced by fusion in the core are absorbed and re-emitted repeatedly by nuclei in the radiative layer, with the re-emitted photons having successively lower energies and longer wavelengths.

By the time the photons leave the sun, their wavelengths are mostly in the visible

³The energy output of the sun's core is so large that it would shine about 10^{13} times brighter than the solar surface if it could be seen.

range⁴.

Above the radiative layer is the convective layer where the temperature is lower, and radiation is less significant. Energy is transported outward mostly by convection. Hot regions at the bottom of this layer become buoyant and rise. At the same time, cooler material from above descends, and giant convective cells are formed.

This convection is widespread throughout the sun, except in the core and radiative layer where the temperature is too high. The tops of convective cells can be seen on the photosphere as *granules*. Convective circulation of plasma (charged particles) generates large magnetic fields that play an important role in producing sunspots and flares.

The surface atmospheres

The solar surface atmospheres are composed of the *photosphere* and the *chromosphere*. The photosphere is the part of the sun that could be seen and it produces most of the visible (white) light. Bubbles of hotter material well up from within the sun, dividing the surface of the photosphere into bright granules that expand and fade in several minutes, only to be replaced by the next upwelling. The photosphere is one of the coolest layers of the sun; its temperature is about 6000 K.

Sometimes huge magnetic-field bundles break through the photosphere, disturbing this boiling layer with a set of conditions known collectively as solar activity. These magnetic fields create cooler, darker regions, which are seen as sunspots⁵.

The chromosphere lies just above the photosphere, and is slightly cooler at its base. It is called chromo because of its color, which can only be seen when the brighter photosphere's light is eliminated⁶. The chromosphere's distinctive features are long dark filaments and bright areas known as plage that surround sunspot regions.

The chromosphere is also characterized by cellular convection patterns, but these cells are much larger than the granules of the photosphere. Near the boundaries of these cells are concentrated magnetic fields that produce vertical jets of material called *spicules*⁷.

The active regions associated with sunspots produce strong magnetic fields, which arch up through the chromosphere and become conduits for material when explosive flares erupt.

The cause and timing of these eruptions are of great interest to scientists but are not well understood. Solar activity is very apparent in the chromosphere, and has a wide range of time scales. Flares begin in seconds and end after minutes or hours. Active regions last many weeks, and may flare many times before fading away.

⁴The energy produced in the core can take as long as 50 million years to pass through the radiative layer of the sun. If the processes in the core of the sun suddenly stopped, the surface would continue to shine for millions of years.

⁵Early observations of sunspots have shown that they appear to migrate across the disk of the sun as it rotates. The sun's rotational period as observed from earth is known as the *synodic period*. Because the earth moves about 1/12 of the way around the sun while the sun makes one rotation, the synodic period is somewhat greater than the period that would be observed from the fixed stars, known as the *sidereal period*. The sun's rotation rate differs according to latitude: as seen from the earth, the equatorial region rotates with a period of about 27 days, while the rotational period closer to the poles is about 32 days.

⁶When a solar eclipse occurs, the red chromosphere is seen briefly just before and after the period of total eclipse.

⁷Although spicules are considered to be small features of the quiet sun, they are actually about the size of earth.

The activity that can be observed on the photosphere and chromosphere is simply a ‘symptom’ of what is happening inside the sun: the detailed physics of stellar interiors is still largely a mystery.

The Corona

The corona is the outer part of the sun’s atmosphere. It is in this region that prominences appears. Prominences are immense clouds of glowing gas that erupt from the upper chromosphere. The Corona can be divided into two different regions: inner and outer corona.

The *inner corona* is the wispy halo, extending more than a million kilometers into space, that can be seen when the sun is blocked by the Moon during a total eclipse.

The cause of the high temperature of the corona, about $2 \cdot 10^6$ K, is not well understood. The corona is a large source of x-rays which do not penetrate earth’s atmosphere.

Magnetic arches dominate the structure of the corona, while open magnetic field⁸ structures appear as gaping coronal holes.

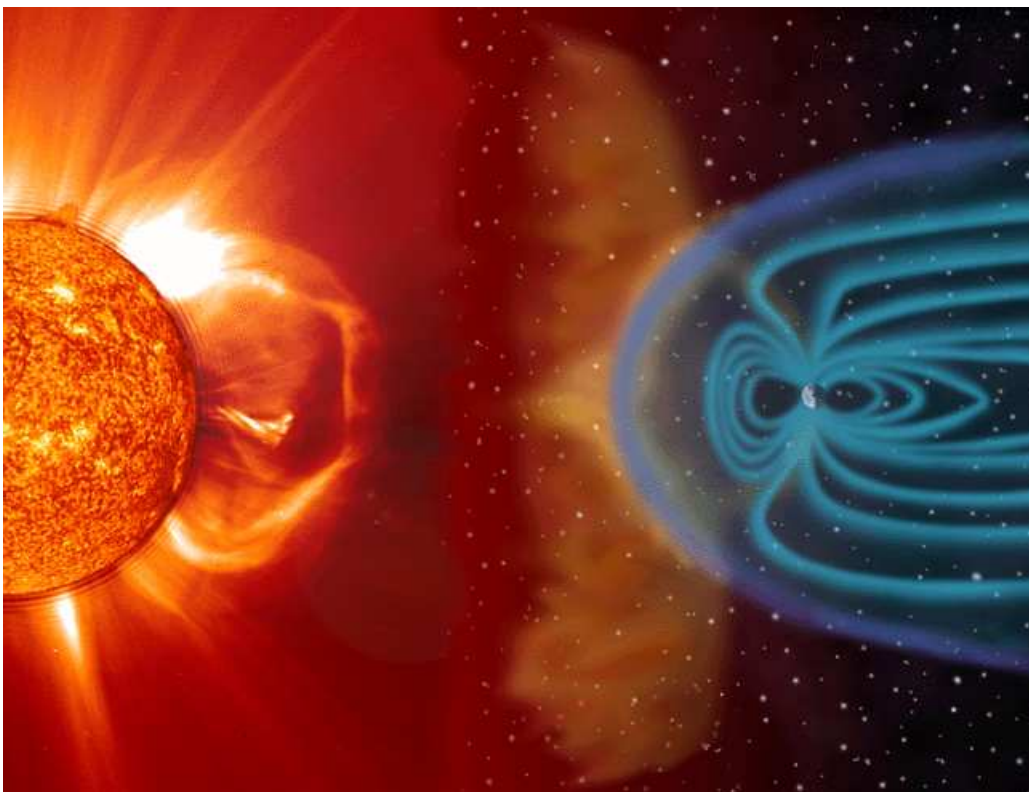


Figure 2.2: Visual Representation of Corona’s Magnetic Field. In this picture can also be noted how the solar wind causes disturbances in the earth’s magnetic field.

The coronal material is generally confined by closed magnetic field structures, anchored at both ends, but the open field structure of coronal holes allows the corona to escape

⁸The reason of the word ‘open’ is because the magnetic field line extends so far out before returning, that in the close proximity of the earth-sun system seems ‘open’.

freely to form fast, low density streams in the *solar wind*. This material travels outward and causes disturbances in earth's magnetic field.

Because of their effect on earth, in the future it will be possible to predict when and where coronal holes will form, but as yet this cannot be done.

The *outer region of the corona* extends to earth and beyond. Its existence is not immediately obvious, since it cannot be seen directly; astrophysicists did not become aware of it until the 1950's.

This region stretches far into space and consists of particles traveling slowly away from the sun. Particles streaming off the sun are necessary to maintain the dynamic equilibrium of the corona.

The solar wind streams radially outward from the sun. Solar rotation swings the source around so that the individual streams describe Archimedian spirals; the solar wind speed⁹ and density vary according to the conditions on the sun. This variation in the solar wind intensity began to make more sense after the discovery of coronal holes during the Skylab missions in the early 1970s.

Coronal holes are large, dark regions with open magnetic field lines where the corona streams outward. These regions grow and shrink, and move around on the sun in ways that are not yet understood. When a coronal hole is facing earth, the solar wind reaching earth is more intense. The nature of the solar wind is also determined by flare and prominence activity on the sun. During times of high activity, plasma is hurled off the sun in vast eruptions that are energized by the turbulent magnetic fields in the inner corona.

2.2 Solar Radiation

Solar radiation is a general term for the visible and near visible (ultraviolet and near-infrared) electromagnetic radiation that is emitted by the sun. It has a spectral, or wavelength, distribution that corresponds to different energy levels; short wavelength radiation has a higher energy than long-wavelength radiation¹⁰.

Every location on earth receives sunlight at least part of the year. The amount of solar radiation that reaches any "spot" on the earth's surface varies according to these factors:

- Geographic location
- Time of day
- Season
- Local landscape
- Local weather.

Because the earth is round, the sun strikes the surface at different angles¹¹ ranging from 0° (just above the horizon) to 90° (directly overhead). When the sun's rays are vertical, the earth's surface gets all the energy possible. The more slanted the sun's rays

⁹Solar wind speed average is about 400 km/s.

¹⁰For more details see Appendix D.

¹¹The effects of different angles' sunlight will be deepened in section 2.3.

are, the longer they travel through the atmosphere, becoming more scattered and diffuse. Because the earth is round, the frigid polar regions never get a high sun, and because of the tilted axis of rotation, these areas receive no sun at all during part of the year.

The earth revolves around the sun in an elliptical orbit and is closer to the sun during part of the year. When the sun is closer to the earth, the earth's surface receives a little more solar energy. The earth is closer to the sun when it is summer in the southern hemisphere and winter in the northern hemisphere. However the presence of vast oceans moderates the hotter summers and colder winters that would be expected to be in the southern hemisphere as a result of this difference.

The 23.5° tilt in the earth's axis of rotation is a more significant factor in determining the amount of sunlight striking the earth at a particular location. Tilting results in longer days in the northern hemisphere from the spring (vernal) equinox to the fall (autumnal) equinox and longer days in the southern hemisphere during the other six months. Days and nights are both exactly 12 hours long on the equinoxes, which occur each year on or around March 23 and September 22.

Countries like the United States and Spain, which lie in the middle latitudes, receive more solar energy in the summer not only because days are longer, but also because the sun is nearly overhead. The sun's rays are far more slanted during the shorter days of the winter months.

The rotation of the earth is responsible for hourly variations in sunlight. In the early morning and late afternoon, the sun is low in the sky. Its rays travel further through the atmosphere than at noon, when the sun is at its highest point. On a clear day, the greatest amount of solar energy reaches a solar collector around solar noon.

2.2.1 Earth's Energy Balance

As sunlight passes through the atmosphere, some of it is absorbed, scattered, and reflected¹² by the following:

- Air molecules
- Water vapor
- Clouds
- Dust
- Pollutants
- Forest fires
- Volcanoes.

¹²The earth's energy balance can be seen in Figure 2.3 and in Appendix E there is a resuming on this argument.

Clouds

The amount of solar radiation reaching the earth's surface varies greatly because of changing atmospheric conditions and the changing position of the sun, both during the day and throughout the year.

Clouds are the predominant atmospheric condition that determines the amount of solar radiation that reaches the earth. Consequently, regions with cloudy climates receive less solar radiation than the cloud-free desert climates.

For any given location, the solar radiation reaching the earth's surface decreases with increasing cloud cover. Local geographical features, such as mountains, oceans, and large lakes, influence the formation of clouds; therefore, the amount of solar radiation received by these areas may be different from that received by adjacent land areas. For example, mountains may receive less solar radiation than adjacent foothills and plains located a short distance away. Winds blowing against mountains force some of the air to rise, and clouds form from the moisture in the air as it cools. Coastlines may also receive a different amount of solar radiation than areas further inland.

The solar energy which is available during the day varies and depends strongly on the local sky conditions. At noon in clear sky conditions, the global solar irradiation can, in Central Europe, reach 1000 W/m^2 on a horizontal surface (under very favourable conditions, even higher levels can occur) while in very cloudy weather, it may fall to less than 100 W/m^2 even at midday.

Pollution, Dust, Forest fires and Volcanoes

Both man-made and naturally occurring events can limit the amount of solar radiation at the earth's surface.

Urban air pollution, smoke from forest fires, and airborne ash resulting from volcanic activity reduce the solar resource by increasing the scattering and absorption of solar radiation.

This has a larger impact on radiation coming in a direct line from the sun (direct radiation) than on the global solar radiation. On a day with severely polluted air (usually called as 'smog alert'), the direct solar radiation can be reduced by 40%, whereas the global solar radiation is reduced by 15% to 25%. A large volcanic eruption¹³ may decrease, over a large portion of the earth, the direct solar radiation by 20% and the global solar radiation by nearly 10% for 6 months up to 2 years. As the volcanic ash falls out of the atmosphere, the effect is diminished, but complete removal of the ash may take several years.

2.2.2 Solar Exposure

Global solar exposure is the total amount of solar energy falling on a horizontal surface. The *daily global solar exposure* is the total solar energy for a day. Typical values for daily global solar exposure range from 1 to 35 MJ/m^2 (megajoules per square metre). The values are usually higher in clear sun conditions during the summer, and lower during winter or very cloudy days.

Diffuse solar exposure is the total amount of solar energy falling on a horizontal surface from all parts of the sky apart from the direct sun. The daily diffuse solar exposure is the

¹³As for example that of Island's volcanoes on the middle of April 2010.

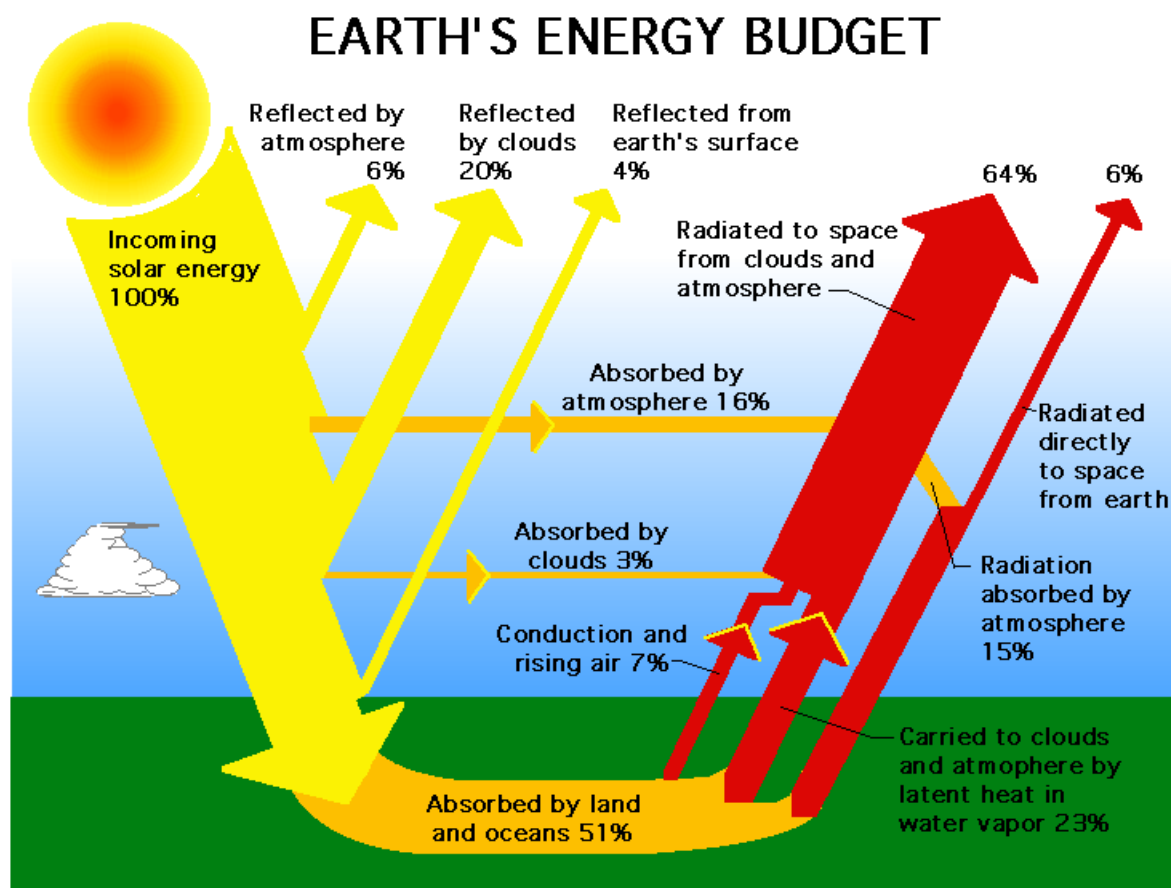


Figure 2.3: Balance of incoming solar radiation.

total diffuse solar energy for a day. Typical values for daily diffuse solar exposure range from 1 to 20 MJ/m² (megajoules per square metre). The values are usually highest during the cloudy conditions, and lowest during clear sky days. Obviously the diffuse exposure is always less than or equal to the global exposures for the same period.

Solar energy received at the earth's surface can be separated into two basic components: *direct solar energy* and *diffuse solar energy*.

Direct solar energy is the energy arriving at the earth's surface with the sun's beam. The sun's beam is quite intense, and hence has also been described a "shadow producing" radiation.

On the contrary, diffuse solar energy is the result of the atmosphere attenuating, or reducing the magnitude of the sun's beam. Some of the energy removed from the beam is redirected or scattered towards the ground; the rate at which this energy falls on a unit horizontal surface per second is called the *diffuse solar irradiance*.

The remaining energy from the beam is either scattered back into space, or absorbed by the atmosphere. Absorption only occurs at specific wavelengths, for example, UVB solar energy is absorbed by ozone in the stratosphere. Scattering occurs at all wavelengths; hence the mechanism by which solar energy is scattered from water droplets and ice particles makes possible the majestic satellite pictures of clouds. The combination of both forms of solar energy incident on a horizontal plane at the earth's surface is referred to as *global solar energy* and all three quantities (specifically their rate or *irradiance*) are

linked mathematically by the following expression:

$$E_g = E_d + E_b \cos z$$

where:

- E_g = global irradiance on a horizontal surface
- E_d = diffuse irradiance
- E_b = direct beam irradiance on a surface perpendicular to the direct beam
- z = sun's zenith¹⁴ angle.

By measuring the three components independently, a useful quality assurance test is immediately obtained by comparing the measured quantity with the one calculated from the other two.

Scientists measure the amount of sunlight falling on specific locations at different times of the year. They then estimate the amount of sunlight falling on regions at the same latitude with similar climates. Measurements of solar energy are typically expressed as total radiation on a horizontal surface, or as total radiation on a surface tracking the sun.

Radiation quantities are generally expressed in terms of either irradiance or radiant exposure. *Irradiance* is a measure of the rate of energy received per unit area, and it is measured in Watts per square metre (W/m^2), where 1 Watt (W) is equal to 1 Joule (J) per second. *Radiant exposure* is the energy that reaches a surface area due to an irradiance maintained for a time duration.

Thus a 1 minute radiant exposure is a measure of the energy received per square metre over a period of 1 minute. Therefore a 1-minute radiant exposure is equal to mean irradiance (W/m^2) per 60 seconds, and has units of joules per square metre (J/m^2). A half-hour radiant exposure would then be the sum of 30 one-minute (or 1800 one-second) radiant exposures¹⁵.

Usually the output of a meteorology's computer model, which estimates the daily global solar exposure from satellite data, provides irradiance integrated over a period of a day, i.e. radiant or global exposure, with units of megajoule per square metre. In terms of remote sensing by satellite, radiance refers to energy received by a satellite sensor and is the rate of energy received per unit area per unit of solid angle (with units of watt per square metre per steradian¹⁶).

Nowadays, radiation data for solar electric (photovoltaic) systems are often represented as kilowatt-hours per square meter (kWh/m^2); direct estimates of solar energy usually are expressed as watts per square meter (W/m^2).

However, the radiation data for solar water heating and space heating systems are usually represented in British thermal units per square foot.

¹⁴The angle between the direction to the zenith and the direction of the sunlight. For more details see Chapter 4.

¹⁵For example: a mean irradiance of $500 \text{ W}/\text{m}^2$ over 1 minute yields a radiant exposure of $30,000 \text{ J}/\text{m}^2$ or $30 \text{ kJ}/\text{m}^2$.

¹⁶The steradian (symbol: sr) is the unit of solid angle in the International System. It is used to describe two-dimensional angular spans in three-dimensional space, analogously to the way in which the radian measures angles in a plane. The steradian, like the radian, is dimensionless because $1 \text{ sr} = \text{m}^2 \cdot \text{m}^{-2} = 1$.

2.2.3 Global, Direct and Diffuse Irradiance

Global solar irradiance is a measure of the rate of total incoming solar energy on a horizontal plane at the earth's surface. It is the sum of two components: *direct solar irradiance* and *diffuse solar irradiance*. A pyranometer¹⁷ sensor can be used to measure this quantity, but with limited accuracy. The most accurate measurements are obtained by summing the diffuse and horizontal component of the direct irradiance.

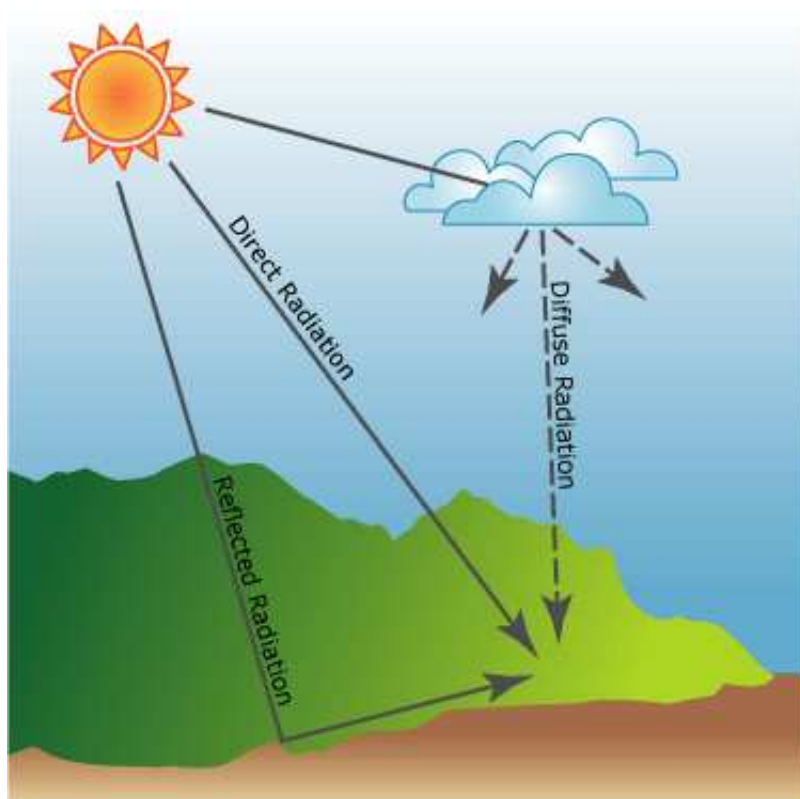


Figure 2.4: Visual representation of the three principal components of solar radiation that can reach a spot of the earth.

The direct solar irradiance is the rate of solar energy arriving at the earth's surface from the sun's direct beam, on a plane perpendicular to the beam, and it is usually measured by a pyrheliometer mounted on a solar tracker. The tracker ensures that the sun's beam is always directed toward the instrument's field of view during the day. In order to use this measurement for comparison with global and diffuse irradiances, it is necessary to obtain the horizontal components of the direct solar irradiance. This is achieved by multiplying the direct solar irradiance by the cosine of the sun's zenith angle.

Using a pyrheliometer it is also possible to obtain a particular and widely used magnitude, the *sunshine duration*, that is defined as the sum of all time periods during the day when the direct solar irradiance equals or exceeds 120 W/m^2 .

The diffuse solar irradiance is a measure of the rate of incoming solar energy on a horizontal plane at the earth's surface resulting from scattering of the sun's beam due to

¹⁷A pyranometer is a device that measure the global radiation that reach a particular place.

atmospheric constituents. This is measured by a pyranometer, with its glass dome shaded from the sun's beam.

As diffuse solar irradiance is a component of global solar irradiance, it should be less than or equal to global irradiance measured at the same time. Global and diffuse irradiances will be equal when the contribution from direct solar irradiance is zero, that is, when the sun is obscured by thick clouds, or the sun is below the horizon. Atmospheric conditions can reduce direct beam radiation by 10% on clear, dry days and by 100% during thick, cloudy days.



Figure 2.5: Solar devices to measure the two principal components of solar irradiance: Pyranometer, used to obtain the value of global irradiance (on the left); Pyrhelioscope, used to obtain the value of direct irradiance (on the right).

2.3 Earth-Sun's Geometry Relation

The term earth rotation refers to the spinning of the planet on its axis. Because of rotation, the earth's surface moves at the equator's level at a speed of about 467 m per second (slightly over 1675 km per hour). Viewed from the north pole, the direction of rotation is counter-clockwise; the opposite is true if the earth is viewed from the south pole.

One rotation takes twenty-four hours and is called a mean solar day. The earth's rotation is responsible for the daily cycles of day and night. At any one moment in time, one half of the earth is in sunlight, while the other half is in darkness. The edge dividing the daylight from night is called the *circle of illumination*.

The earth's rotation also creates the apparent movement of the sun across the horizon.

The orbit of the earth around the sun is called earth revolution. This celestial motion takes 365.25^{18} days to complete one cycle. Further, the earth's orbit around the sun is not circular, but elliptical (see Figure 2.6), with the sun occupying one of the two foci.

The elliptical orbit causes the earth's distance from the sun to vary over a year. This variation in the distance from the sun causes the amount of solar radiation received by the

¹⁸For this reason every 4 years there is a leap year of 366 days.

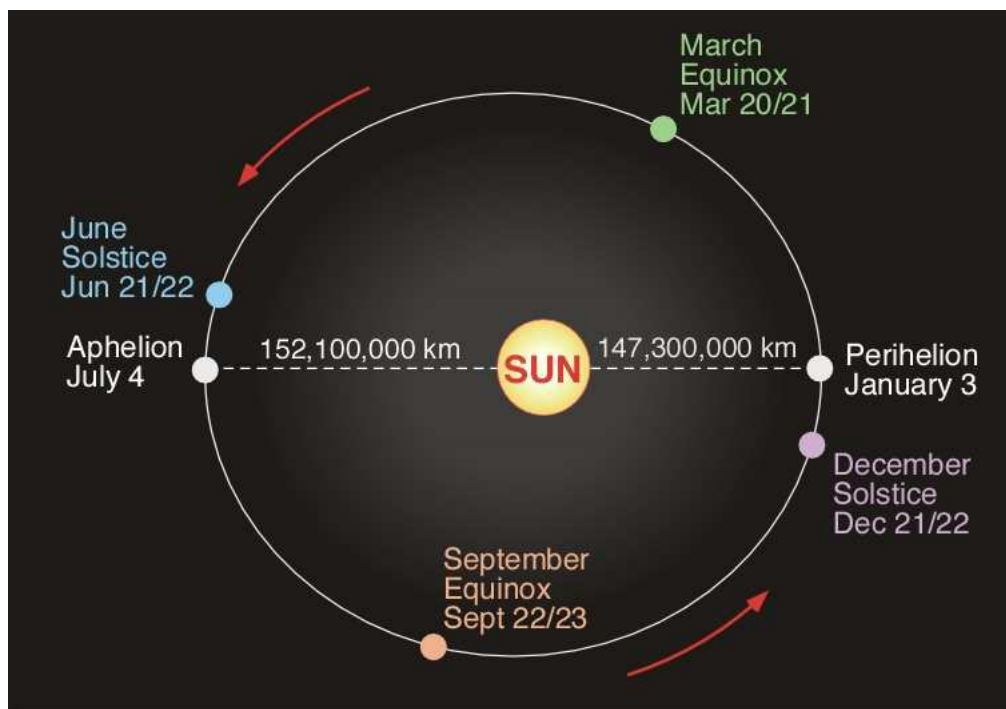


Figure 2.6: Elliptical orbit of the earth. Highlighted focus' distance, position of the equinoxes, solstices, aphelion and perihelion.

earth to annually vary by about 6%. Figure 2.6¹⁹ illustrates the positions, in the earth's revolution, where it is closer and farther from the sun. On early January, *perihelion*, the earth is closest to the sun (147.3 million km). The earth is farthest from the sun on early July, or *aphelion* (152.1 million km). The average distance of the earth from the sun over a one-year period is about 149.6 million km.

Tilt of the axis and Elliptic Plane

The *ecliptic plane* can be defined as a two-dimensional flat surface that geometrically intersects the earth's orbital path around the sun. On this plane, the earth's axis is inclined at an angle of about 23.5° from the perpendicular.

Figure 2.8 shows a side view of the earth in its orbit around the sun on four important dates: June solstice, September equinox, December solstice, and March equinox. Note that the angle of the earth's axis in relation to the ecliptic plane and the North Star on these four dates remains unchanged.

Yet, the relative position of the earth's axis to the sun changes during this cycle. This circumstance is responsible for the annual changes in the height of the sun above the horizon. It also causes the seasons, by controlling the intensity and duration of sunlight received by locations on the earth.

Also the circle of illumination changes its position on the earth's surface. During the two equinoxes, the circle of illumination cuts through the north pole and the south pole. On the June solstice, the circle of illumination is tangent to the arctic circle (66.5° N)

¹⁹The aphelion and perihelion day of the Figure are referred to year 2008.

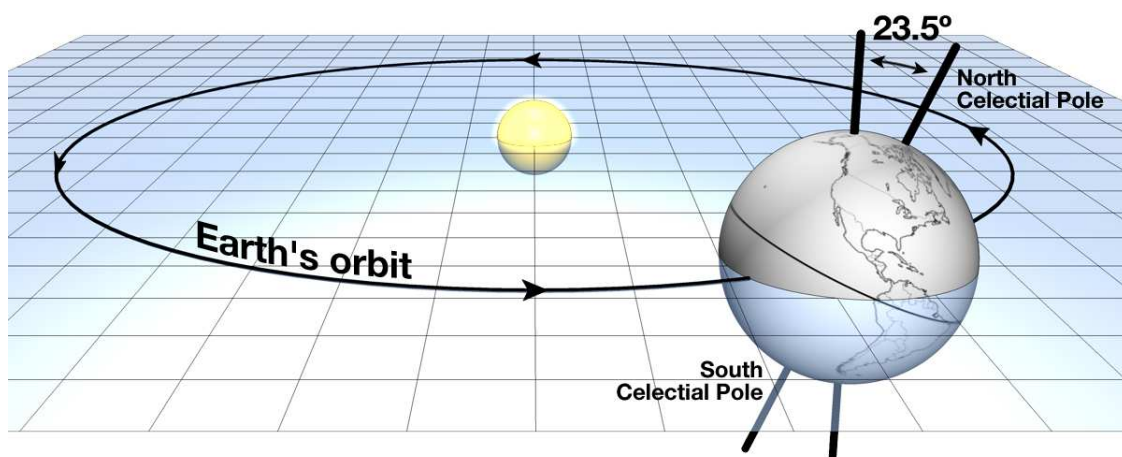


Figure 2.7: Three-dimensional representation of the elliptic plane, with earth axis's tilt in evidence.

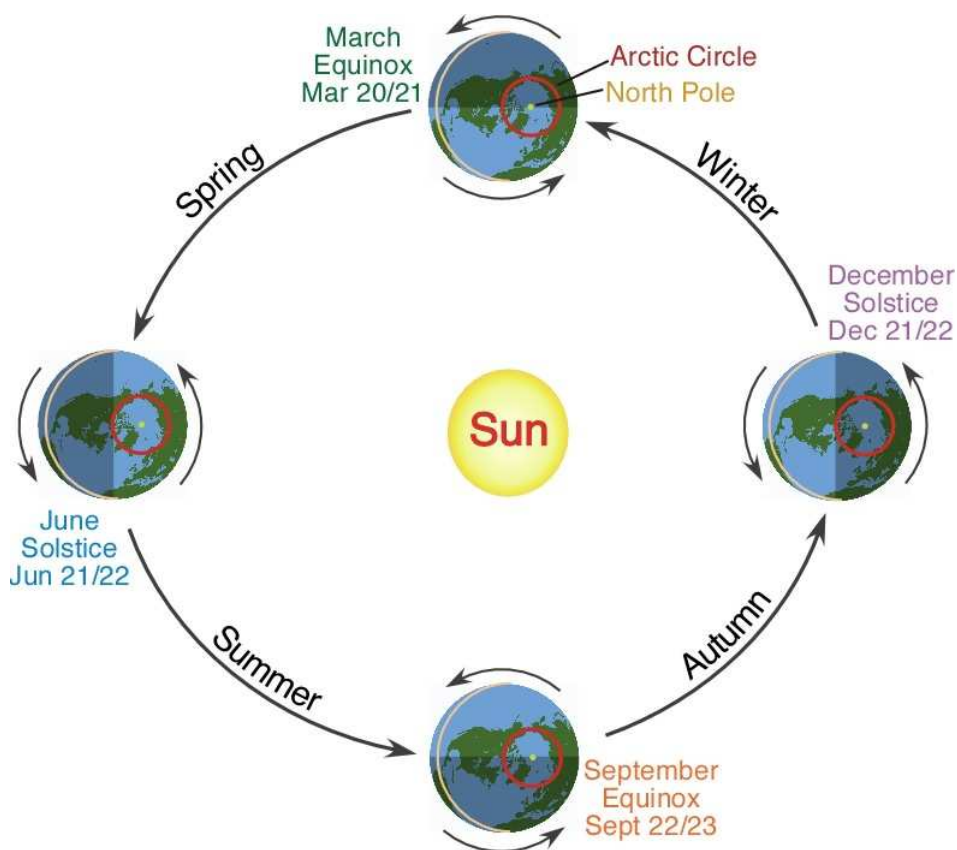


Figure 2.8: Annual change in the position of the earth in its revolution around the sun. In this graphic, the earth is viewed from a position in space that is above the north pole at the summer solstice, the winter solstice, and the two equinoxes. Note how the position of the north pole on the earth's surface does not change, while its position relative to the sun does change and this shift is responsible for the seasons.

and the region above this latitude receives 24 hours of daylight. The arctic circle is in 24 hours of darkness during the December solstice.

On June 21 or 22 the earth is positioned in its orbit so that the north pole is leaning 23.5° toward the sun. During the June solstice (also called the summer solstice in the northern hemisphere), all locations north of the equator have day lengths greater than twelve hours, while all locations south of the equator have day lengths less than twelve hours. On December 21 or 22 the earth is positioned so that the south pole is leaning 23.5 degrees toward the sun. During the December solstice (also called the winter solstice in the northern hemisphere), all locations north of the equator have day lengths less than twelve hours, while all locations south of the equator have day lengths exceeding twelve hours.

On September 22 or 23, also called the autumnal equinox in the northern hemisphere, neither pole is tilted toward or away from the sun. In the northern hemisphere, March 20 or 21 marks the arrival of the vernal equinox or spring when once again the poles are not tilted toward or away from the sun. Day lengths on both of these days, regardless of latitude, are exactly 12 hours.

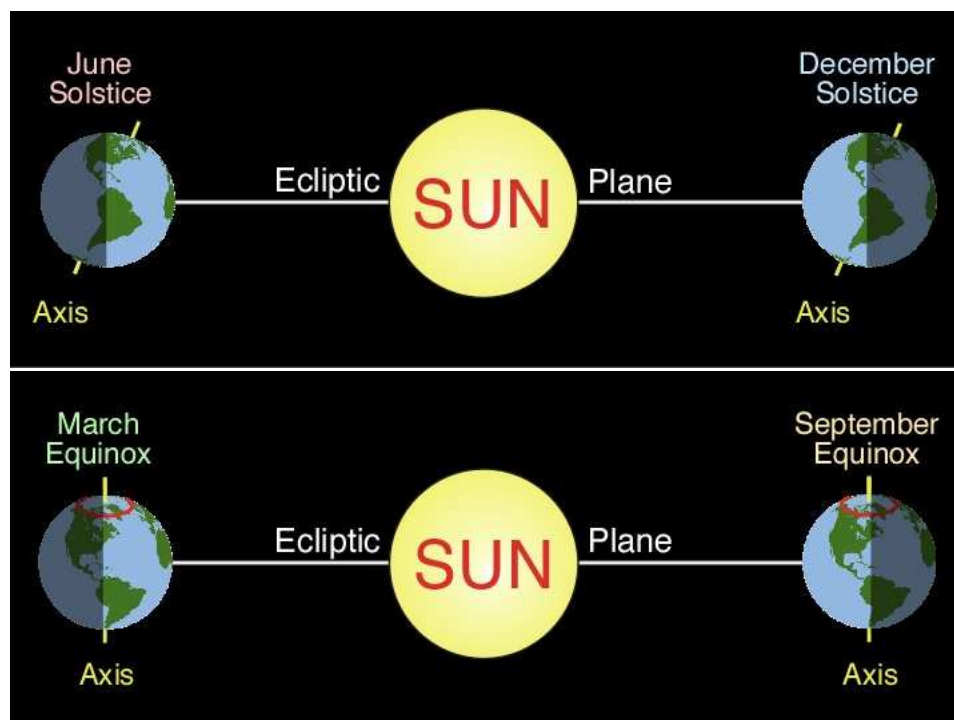


Figure 2.9: During the June solstice the earth's north pole is tilted 23.5 degrees towards the sun relative to the circle of illumination. This phenomenon keeps all places above a latitude of 66.5 degrees N in 24 hours of sunlight, while locations below a latitude of 66.5 degrees S are in darkness (Figure above). During the equinoxes, the axis of the earth is not tilted toward or away from the sun and the circle of illumination cuts through the poles (Figure below).

Axis Tilt and Solar Altitude

The annual change in the relative position of the earth's axis in relationship to the sun causes the height of the sun or solar altitude to vary in the sky.

Solar altitude is normally measured from either the southern or northern point along the horizon and begins at zero degrees. Maximum solar altitude occurs when the sun is directly overhead and has a value of 90° . The total variation in maximum solar altitude for any location on the earth over a one-year period is 47° ²⁰.

This variation is due to the annual changes in the relative position of the earth to the sun. At 50 degrees north, for example, the maximum solar altitude varies from 63.5 degrees on the June solstice to 16.5 degrees on the December solstice (Figure 2.10). Maximum solar height at the equator goes from 66.5 degrees above the northern end of the horizon during the June solstice, to directly overhead on the September equinox, and then down to 66.5 degrees above the southern end of the horizon during the December solstice (Figure 2.10).

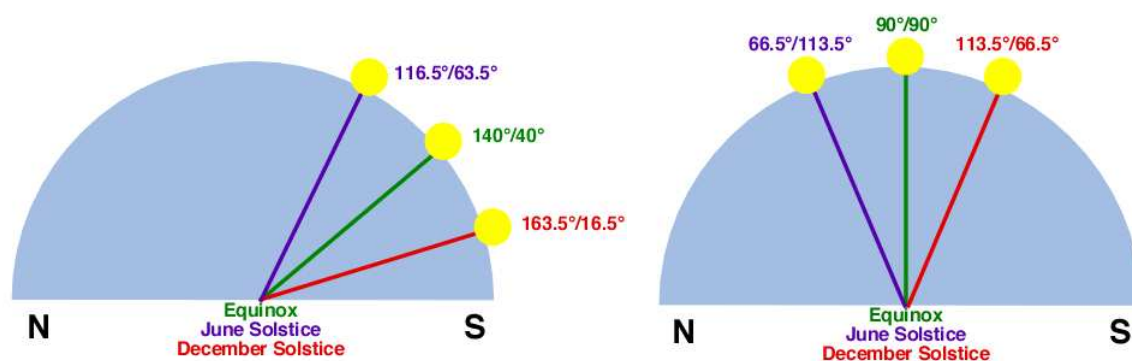


Figure 2.10: Variations in solar altitude at solar noon for 50 degrees north (on the left) and for the equator (on the right) during the June solstice, equinox, and December solstice. First measure represent the angle from the northern side of the horizon, the second the angle from the southern.

The location on the earth where the sun is directly overhead at solar noon is known as the *subsolar point*. The subsolar point occurs on the equator during the two equinoxes. On these dates, the equator is lined up with the ecliptic plane and the poles are in line with the circle of illumination (Figure 2.9).

During the summer solstice, the subsolar point moves to the Tropic of Cancer (23.5° N) because at this time the north pole is inclined 23.5° toward the sun (Figure 2.9).

Angle of Incidence and Insolation

The earth's seasons are controlled by changes in the duration and intensity of solar radiation or *insolation*. Both these factors are in turn governed by the annual change in the position of the earth's axis relatively to the sun.

²⁰Earth's tilt $23.5^\circ \times 2 = 47^\circ$.

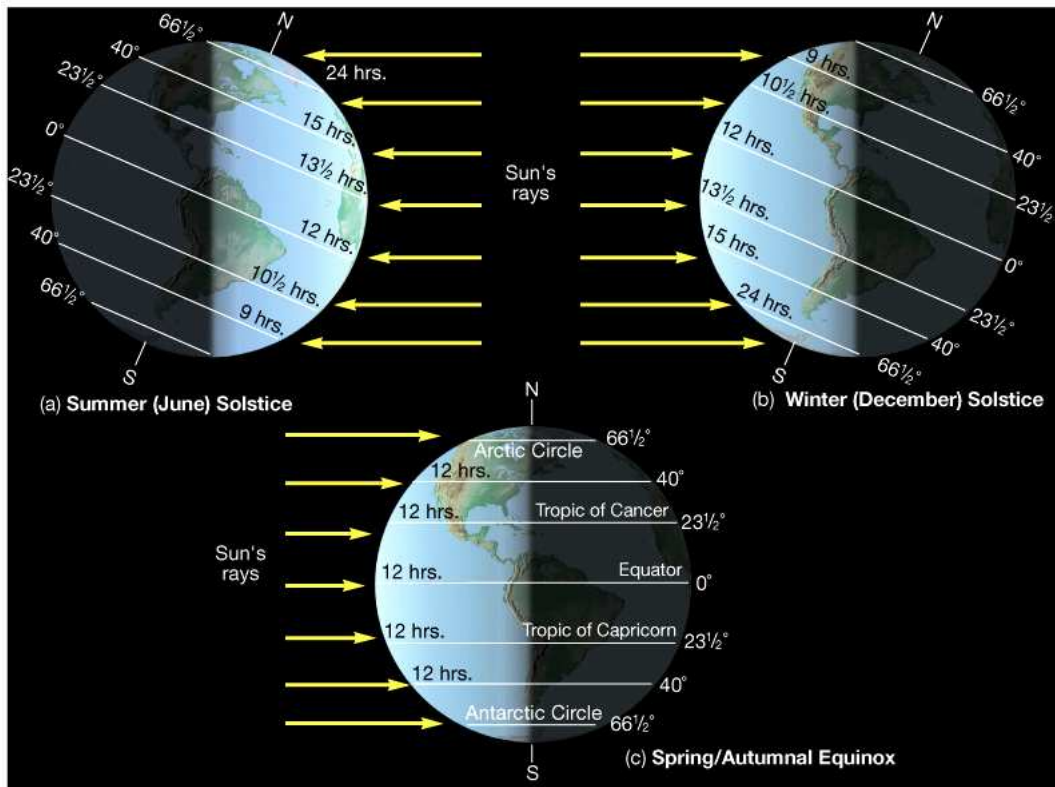


Figure 2.11: Relationship of maximum sun height to latitude for equinoxes and solstices.

Yearly changes in the position of the earth's axis cause the location of the sun to wander 47° across the sky, and changes in the location of the sun have a direct effect on the intensity of solar radiation.

The intensity of solar radiation is largely a function of the *angle of incidence*, the angle at which the sun's rays strike the earth's surface. If the sun is positioned directly overhead or 90° from the horizon, the incoming insolation strikes the surface of the earth at right angle and is most intense; differently, if the sun is 45° above the horizon, the incoming insolation strikes the earth's surface at an angle that is minor of 90° .

This causes the rays to be spread out over a larger surface area reducing the intensity of the radiation. The lower sun angle (45°) causes the radiation to be received over a much larger surface area. This surface area is approximately 40% greater than the area covered by an angle of 90° . The lower angle also reduces the intensity of the incoming rays by 30%.

The effect the angle of incidence has on insolation intensity can be modeled with the following simple equation:

$$\text{Intensity} = \sin(A)$$

where A is the angle of incidence.

Using this equation it can be determined that an angle of 90° gives a value of 1.00 or 100% (1.00×100). Comparing this maximum value with others determined for other

angles of incidence the values of the table below, that are a percentage of the potential maximum value, are obtained.

$\sin (80^\circ) = 0.98$ or 98%
$\sin (70^\circ) = 0.94$ or 94%
$\sin (60^\circ) = 0.87$ or 87%
$\sin (50^\circ) = 0.77$ or 77%
$\sin (40^\circ) = 0.64$ or 64%
$\sin (30^\circ) = 0.50$ or 50%
$\sin (20^\circ) = 0.34$ or 34%
$\sin (10^\circ) = 0.17$ or 17%
$\sin (0^\circ) = 0.0$ or 0%

Table 2.1: Percentages of intensity of solar radiation in relation with intensity of 90° 's solar radiation.

The yearly changes in the position of the Earth's axis relatively to the plane of the ecliptic also causes seasonal variations in day length to all locations outside of the equator. Longest days occur during the June solstice for locations north of the equator and on the December solstice for locations in the Southern Hemisphere.

Figure 2.12 describes the change in the length of day for locations at the equator, 10, 30, 50, 60, and 70 degrees North over a one-year period.

Also the potential insolation vary over a one-year period, as it can be seen in Figure 2.13. The values plotted on this graph take into account the combined effects of angle of incidence and day length duration. Locations at the equator show the least amount of variation in insolation over a one-year period. These slight changes in insolation result only from the annual changes in the altitude of the sun above the horizon, as the duration of daylight at the equator is always 12 hours. The peaks in insolation intensity correspond to the two equinoxes when the sun is directly overhead. The two annual minimums of insolation occur on the solstices when the maximum height of the sun above the horizon reaches an angle of 66.5° .

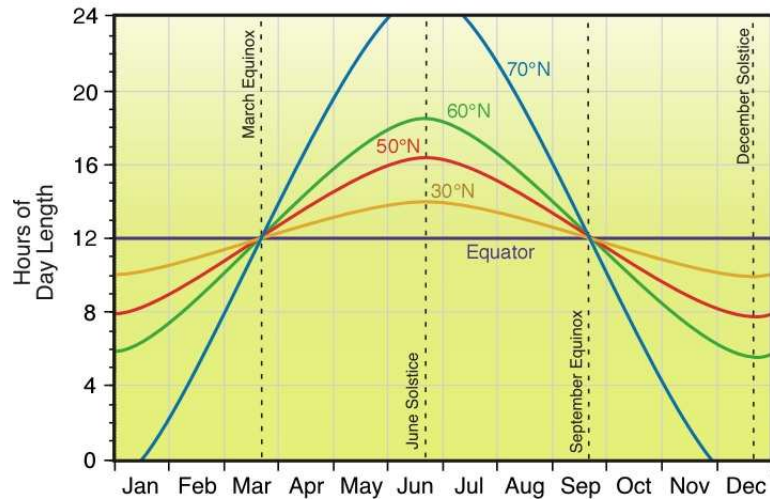


Figure 2.12: Daily length variation during a year. The illustration suggests that days are longer than nights in the northern hemisphere from the March equinox to the September equinox. Between the September to March equinox days are shorter than nights in the northern hemisphere. The opposite is true in the southern hemisphere. The graph also shows that the seasonal (winter to summer) variation in day length increases with increasing latitude.

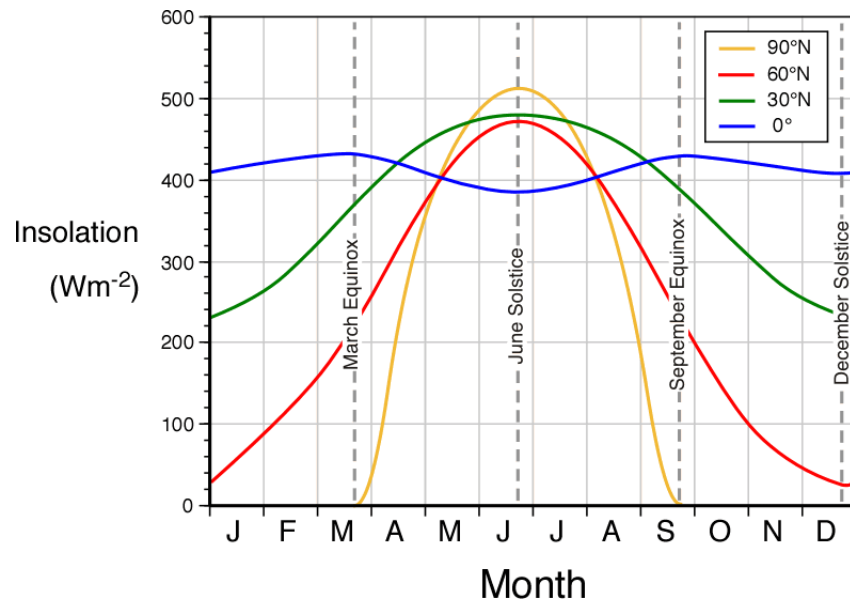


Figure 2.13: Monthly values of available insolation in W/m^2 for the equator, 30° , 60° , and 90° north.

Chapter 3

Solar Plant of Seville's University

The solar plant that has been analyzed and modeled is the thermosolar plant situated in the Seville's Engineering College, on the top of laboratories' building.

In this plant, the solar energy collected by a Linear Fresnel collector field is used by an absorption machine to provide at cooling the College.

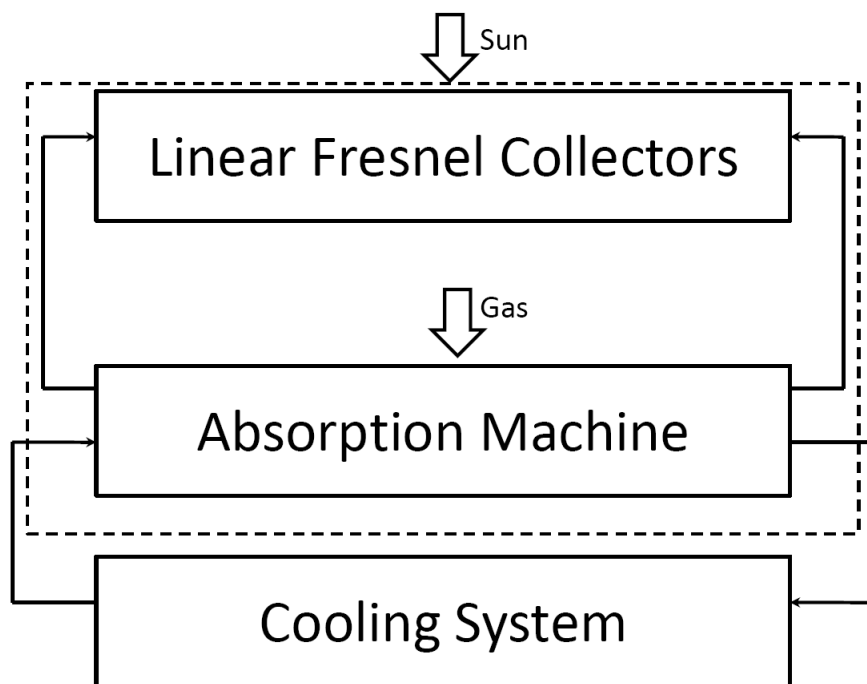


Figure 3.1: Solar Plant's Scheme: Linear Fresnel Collector and Absorption Machine in coupling with Cooling System. Gas is provided as energy source when solar energy is not enough alone.

The energy needed by the absorption machine to work can come from solar energy only, or from both solar energy and natural gas, when solar energy is not adequate alone. Therefore the plant exhibits two principal working modes: one based on solar energy only and one relying on a combination of solar energy and gas. In fact, there would be a third way of working, i.e. only gas, but this last mode is never utilized because of Seville's

good weather¹ and the most rainy days are in December and January, when the need for cooling is very low.

The way of working of the solar plant can be schematically divided into three phases:

1. Sun's rays beat on collector reflective mirrors' surface that reflect sunlight to an absorber pipe situated on a plane parallel to that of collector, but over it.
2. A heat-transport fluid (water) flows through the pipe, absorbing heat from the walls of the duct to warm up, increasing its own temperature.
3. The hot fluid enters in the absorption machine, that exploits water's heat to produce cold to refrigerate the buildings of Seville Engineering's College.

In this section a detailed description of the Linear Fresnel solar system and the absorption machine is given, explaining the way of working of the plant and the operating nominal condition.

3.1 Linear Fresnel Collector Field

Linear Fresnel Collectors for building thermal applications with medium temperature working point² are still in an experimental phase, even if there are already solar collectors prototypes in an advanced development phase that should become, in a near future, commercially available.

Solar collectors of Seville's Engineering College are prototypes of those just described and form, together with absorption machine, a thermosolar refrigeration plant.

The thermosolar part of the plant consists of

- Fresnel flat collectors³
- A receptor, formed by a single pipe, with covering. The receptor is situated on a plane parallel to flat collectors, over them. Inside the pipe flows the heat transport (or heat-carrier) fluid.
- A receptor carrying structure.
- A solar tracking collector mechanism. In this collector typology, each collector moves in an independent way.

On Figure 3.2 all the different elements that form a collector field, like the one of Seville's University, are indicated.

This Fresnel collector field, as described above, is a prototype that takes advantage of the latest developed technology, and it has been preferred to parabolic trough systems to test and improve the advantages of Fresnel technology in comparison with parabolic

¹The average Seville's annual precipitation is 534 mm, with only 54 rainy day for year.

²Thermal application with a duct's working point temperature between 100 and 250 Celsius degrees are said to have a working point of medium temperature.

³In fact, they are not completely flat, but slightly curved, with a curvature obtained by a process of cold bending.

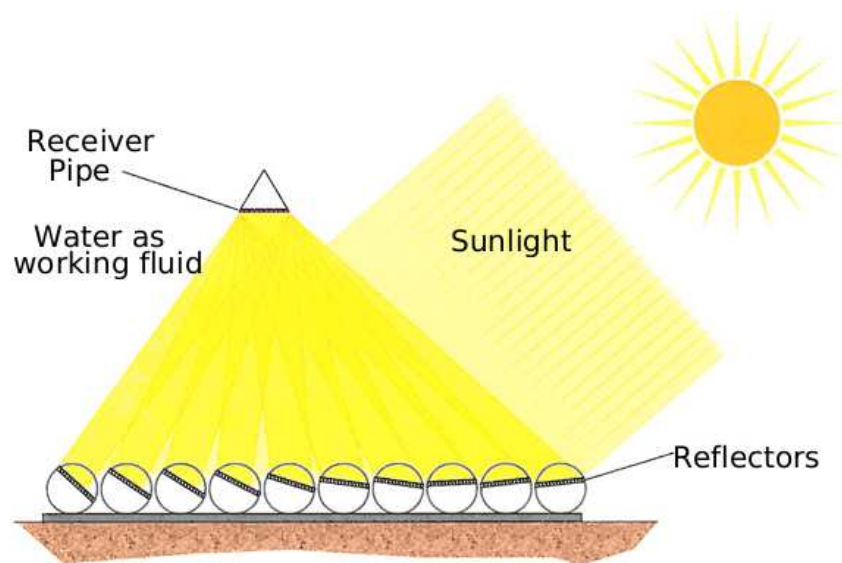


Figure 3.2: Linear Fresnel Collector Scheme.

through and to analyze the performance in forecast to make this technology available on the market.

The main advantages of a collector field of this type are:

- ◆ Mirrors and tracking system's low cost;
- ◆ Fixed absorber pipe, high pressure seals⁴ are not necessary;
- ◆ Expansion elbows are not necessary (the pipe has a free end to expand);
- ◆ Flat collectors collocated next to the ground, so that wind loads are reduced;
- ◆ Efficient ground use because collector rows can be placed side by side;
- ◆ Easy access to mechanic moving parts and surfaces⁵.

It is expected that the cost reduction due to the use of Fresnel technology, in comparison to cilindric/parabolic collectors, will be around 50% when the technology development will be sufficiently advanced.

3.2 Plant's Technical Data

Two elements that are fundamental in the construction and evaluation of a solar plant are its collocation and orientation, not only for efficiency valuation, but also for a correct plant model that needs a precise estimate of the solar position over the plant.

The Geographical Coordinates of the plant are 37.41° north-latitude and 6° west-longitude.

⁴Usually, in the parabolic trough, high pressure seals are needed because the collector tube is attached to the parabolic trough reflector, which rotates.

⁵For maintenance and cleaning.

The solar plant is situated over the top of the Seville Engineering College's Laboratories building, and it is quite parallel to the south front of laboratories building, with an angle of $12^{\circ} 3' 1''$ between the perpendicular to collector axis orientation and north-south direction.

In Table 3.1 technical data and the principal rating values of the elements that constitute the solar plant are reported.

The last table's value, optical concentration ratio, is a magnitude typical of concentrating solar plants, and it is the ratio between the radiation intensity with the collectors and the radiation intensity without them. It represents a sort of radiation amplification coefficient.

Now the various part of solar plant will be analyzed and described, focusing, in particular, on the constructive shrewdness utilized.

Steel Structure



Figure 3.3: Global view of solar plant (on the left); a particular of steel structure (on the right).

The steel structure supports reflective mirrors, their bearings and drive actuators, absorption pipe and secondary reflector.

This structure defines the boundary of the reflective mirrors area.

Because of its structural constitution, the structure has been painted with a solar reflective varnish. This particular varnish is oil-based and designed with glass micro-balls specifically treated to increase the reflectivity.

A special treatment like this has been made to limit the reduction of mirrors reflective area caused by the reflection of the steel structure on them⁶.

Unfortunately, mirrors area reduction due to pipe's reflection and shadows can not be avoided, because the pipe cannot be painted with the varnish, in order to not affect pipe's thermal properties.

TECHNICAL DATA	
Occupied Ground Extension	480 m^2
Total Reflecting Surface	352 m^2
Plant Orientation	East-West
Number of Receptor (Number of pipe)	1
Receptor's Length	64 m
Receptor Typology	Cavity receptor with secondary reflector and glass cover
Receptor Plane's Height	4 m over collectors plane
Receptor width	0.3 m
Absorber Typology	Steel pipe DNI 1.4541(AISI 321): stabilized austenitic stainless steel
Heat-Transfer Fluid	Water
Steam Generation	No
Duct Nominal Pressure	13 bar
Reflecting Mirror Rows Number	11, each one divided into 2 middle row
Single Reflective Mirror Length	4 m
Single Reflective Mirror Width	0.5 m
Total Number Of Reflective Mirrors	176
Mirror Nominal Reflectivity	0.92
Optical Concentration Ratio	25

Table 3.1: Principal technical data of the solar plant.



Figure 3.4: Reflective mirrors in operation (on the left) and in guard position (on the right).

Reflective Mirrors

Reflective mirrors⁷ are made of solar glass, slightly curved elastically with a radius of curvature of 9.6 meters. Being the radius of curvature so large, construction costs are reduced and at first sight mirrors seem to be flat.

The solar glass that constitutes reflective mirrors is made of a glass substrate and a reflective layer.

The reflective layer is designed to reflect the maximum amount of solar energy incident upon it and it comprises a highly reflective layer of thin silver plating. The use of silver as reflective layer leads to higher efficiency levels, because it is the most reflective metal.

Each mirror is attached to the load-bearing structure by ten steel supports and it is moved by a drive actuator, that allows for solar-tracking. Each mirrors' row moves independently of the adjacent ones.

In Figure 3.4 reflective mirrors on solar-tracking position and in guard position are illustrated.

Drive Actuator

The drive actuator is an electrical engine that rotates mirrors of an angle that permits at each row to reflect sunlight and concentrate it on the receptor.

Engine rotation is transmitted to mirrors through a transmission belt with a ratio speed reduction of $2.8 : 1$ on the output pulley.

Each drive actuator moves only four mirrors for row, in order to obtain an accurate mirror positioning, by minimizing output position error. This error, in absence of backlash, is of the order of a tenth of prime degree.

Solar tracking, therefore, is possible for the use of independent drive actuator for each single row.

⁶In this way it is estimated that the reflective area is reduced only of 3% instead of 7%, as it is the case without varnish.

⁷Produced by Mirrox, Germany.



Figure 3.5: A particular of drive actuator mechanism.

The position of a mirror is described by an angle that can be positive or negative with respect to the zero starting point, which is the position in which each mirror is parallel to the ground plane, with its reflective surface upwards.

Starting from this position and with direction east-west, a rotation toward right is considered positive, toward left a negative one.

The mechanism does not permit a complete rotation (360°) of the mirror, but the movement is limited to an arc from -100° to 100° .

There are three operative conditions for each mirrors's row: *operating*, *guard* and *dull*. In operating condition the mirror is normally moved for solar tracking; guard (90°) and dull ($-100^\circ/100^\circ$) are instead two special positions.

Guard position (perpendicular to the ground), also called stand-by, is the position in which mirrors are in the morning, when solar tracking begins, and that they assume in the evening, when the sun sets.

Finally, "dull" is an alert position: mirrors reach 100° (or -100°) when water temperature surpasses 180° ⁸ or when there is something wrong in the plant. In this latter case, the alert position is accompanied by an alarm signal.

Secondary Reflector

The secondary reflector (on the left of Figure 3.6) is formed by an aluminium thin envelop covered with a reflective mirror (with nominal reflectivity 0.77) mounted inside.

This structure has the function of reflecting the solar radiation that does not affect directly the absorber pipe, optimizing the plant total optical efficiency. Moreover, it also

⁸The reason of this way of working will be explained in the next chapter.

acts as pipe protection.



Figure 3.6: Secondary reflector (on the left) and receptor pipe (on the right).

In Table 3.2 dimensions and property of secondary reflector are reported.

Regarding the values reported, *absorptivity* is the fraction of radiation absorbed by the pipe, the *emissivity* of a material is the relative ability of its surface to emit energy by radiation and *conductivity* is an intrinsic property of a material that indicates its ability to conduct heat.

SECONDARY REFLECTOR	
Absorptivity	0.1
Emissivity	0.1
Conductivity	$20 \text{ W/m} \cdot \text{K}$
Receptor's Length	64 m
Outer Reflective Mirror Diameter	165 mm
Thickness	5 mm

Table 3.2: Technical data of secondary reflector.

Receptor

The receptor is formed by an absorber pipe and a glass cover.

The absorber pipe is a welded pipe, model SCHOTT PTR 70, with a nominal absorptivity of 0.94.

In both ends of the pipe there are flanges, model DN 50(DIN⁹ 2633, PN 16), to connect it with the hydraulic circuit.

The temperature in the hydraulic circuit is limited to a maximum of 200° Celsius and the pressure to a maximum value of 16 bar.

However, not to force the entire system and in order to respect the limits of each component, the operating standard conditions are a temperature of 180° Celsius and a pressure of 13 bar, with the pressure release valve limited to 16 bar.

Nominal caudal is of 13 m^3/h that, considered the pipe section, corresponds to a water speed of about 1.2 m/s.

The absorber pipe is surrounded by a glass cover, to ensure the vacuum between them, to minimize thermal losses.

An image of the receptor pipe can be seen on the right side of Figure 3.6, while in Table 3.3 are reported its dimensions and property. In reference to table's values, *transmissivity* is the fraction of incident radiation that is transmitted through a particular material.

RECEPTOR PIPE		
PROPERTY	Absorber Pipe	Glass Cover
Absorptivity	0.94	0.06
Emissivity	0.14	0.1
Transmissivity	-	0.96
Thermal Conductivity	16.3 $W/m \cdot K$	0.8 $W/m \cdot K$
Length	64 m	64 m
Outer Diameter	70 mm	125 mm
Thickness	2.1 mm	3 mm

Table 3.3: Technical data of receptor pipe.

Sensors

In the plant there are three different typologies of sensor: potentiometer, solar sensor and temperature sensor.

⁹*Deutsches Institut für Normung*, in English "German Institute for Standardization": it is the German national organization for standardization. DIN establishes uniform engineering or technical specifications, criteria, methods, processes or practices.

Potentiometer

Each reflective mirror row is equipped with a potentiometer, to determine the current position of the mirrors. These sensors are collocated in the drive actuator and thus there is a sensor every four mirrors.

Sensor readings are transmitted by a CAN bus (CANopen¹⁰) to the control system, through an interface analog/CAN.

Solar Sensor

Solar sensors are collocated on the top of the receiver at a distance of about 16 meters one from the other, for the optional automatic calibration of the mirrors' row.

These sensors detect any focal line of thereflective mirrors which is not centered. Each sensor is composed by a photovoltaic module sealed in an aluminium case.

A four-channels CAN interface transmits the measured value (in volts) to the control system in the switch cabinet.

Sensors are collocated out of absorber pipe (left side of Figure 3.7) to avoid overheating.

Temperature Sensor

To monitor duct temperature, there are two temperature sensors collocated at the entry and exit of the absorption pipe (right side of Figure 3.7).

The model of the sensor is PT100, a temperature sensor that exploits the predictable change in electrical resistance with changing temperature. Made of platinum, it has been preferred to the use of a thermocouple, due to its higher accuracy and reliability.

If the temperature exceeds the defined maximum value (fixed at 180° Celsius), the control system begins to blur mirrors' rows to obtain lower temperature value.

Again, the sensor is connected to the control system by a CAN bus.

3.3 Absorption Machine

The absorption cooling differs from most of the cooling systems because the cool effect is obtained by an heat flow, instead of by mechanical work as in steam compression system.

The absorption machine operational scheme is represented in Figure 3.8.

Unlike steam compression cooling systems, absorption systems utilize an absorber tank where an absorber substance (usually ammonia or lithium salt) retains water steam coming from the evaporator.

Water vapor is forwarded by a pump to a generator, where the refrigerant re-vaporizes using a waste steam heat source and the refrigerant-depleted solution then returns to the absorber tank.

¹⁰Controller Area Network (CAN) is a vehicle bus standard designed to allow microcontrollers and devices to communicate with each other within a vehicle without a host computer. In particular, CANopen is a communication protocol and device profile specification for embedded systems used in automation.



Figure 3.7: Solar sensor (on the left) and temperature sensor (on the right).

The main advantage of an absorption machine is the low power consumption in the driven pump of water-absorbent blend compared to the driven pump of cooler steam in the steam compression.

This power consumption subsists because moving a liquid caudal is much less expensive than moving a gaseous one.

As it can be seen in Figure 3.8, three energy flows can be distinguished in the absorption machine:

- Q_{evap} : is the cooling power to get cold a fluid in the evaporator;
- Q_{gen} : is the power introduced into absorber machine's generator;
- Q_{cond} : is the power dissipated in the condenser.

The hot water heated by solar energy is accumulated in the water storage tank and it is then supplied to the generator to boil off water vapor from a solution of lithium bromide-water.

The water vapor is cooled down in the condenser and then passed to the evaporator, where it again is evaporated at low pressure, thereby providing cooling to the required space.

In the absorber, the strong solution absorbs the water vapor leaving the evaporator; cooling water removes the heat by mixing and condensation.

Since the temperature of the absorber has a higher influence on the efficiency of the system than the condensing temperature, the heat-rejection (cooling water) fluid is allowed to flow through the absorber first and then to the condenser.

An auxiliary energy source is provided, so that the hot water is supplied to the generator when the solar energy is not sufficient to heat the water to the temperature level required by the generator.

Being cooling power the useful effect, a coefficient of useful power is defined, called COP¹¹, given by the following relationship:

¹¹Coefficient Of Performance.

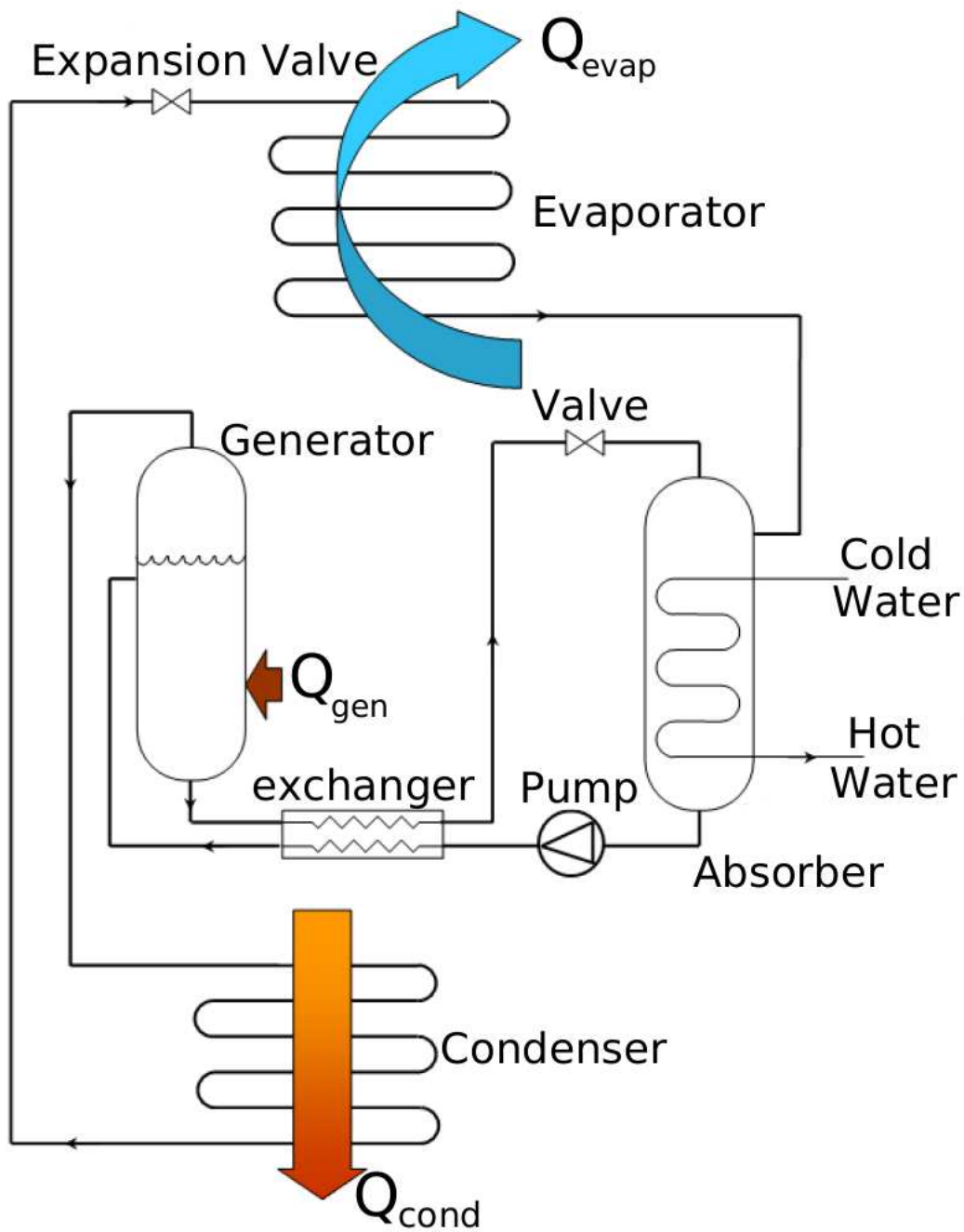


Figure 3.8: Absorption Machine Operational Scheme.

$$\text{COP} = \frac{Q_{\text{evap}}}{Q_{\text{gen}}}$$

To improve COP reducing the value of Q_{gen} , an heat exchanger is placed from hot blend flow effluent from generator to cold flow coming from absorber tank.

If there is only one heat exchanger, the system is called *simple effect*, if instead there are two heat exchangers, as in the one of the plants considered, is called *double effect*.

In double effect systems¹² a second heat exchanger is utilized and consequently also another generator, that operates at a lower temperature.

A simple effect absorption machine operates with generator temperature of 60-90 °C, reaching COP of 0.6; on the other hand, double effect absorption machines require a generator temperature of 120-140 °C, but reach COP values of 1.3-1.5.

Seville Engineering College's absorption machine is a BROAD BZH15¹³.

ABSORPTION MACHINE	
Maximum Power	174 kW
Chilled Water Inlet Temp.	12 °C
Chilled Water Outlet Temp.	7 °C
Chilled Water Flow Rate	30 m ³ /h
Cooling Water Outlet Temp.	37 °C
Cooling Water Inlet Temp.	30 °C
Cooling Water Flow Rate	36.6 m ³ /h
Energy Source	Solar Energy and Natural Gas

Table 3.4: Technical data of absorption machine.

Absorption machine's maximum power is 174 kW with a COP of 1.3 and a generator temperature (High Generator Temperature) of at least 145 °C.

The absorption system's objective is to reach 145 °C and maintain it as stable as possible.

In Table 3.4 the principal characteristics of absorption machine, given by the producer, are reported.

Lastly, the conjunct operation of a solar collector field and an absorption machine is described in Figure 3.9, where

- $E_{sol,i}$ is the solar energy affecting solar collector fields;
- $E_{sol,a}$ is the solar energy absorbed;
- $E_{sol,l}$ is the solar energy loss in the solar collectors;
- $E_{sol,p}$ is the solar energy loss in the pipe;

¹²The double effect absorption machine way of working scheme can be seen in Appendix F.

¹³BROAD is a Chinese firm, leader in refrigeration system.

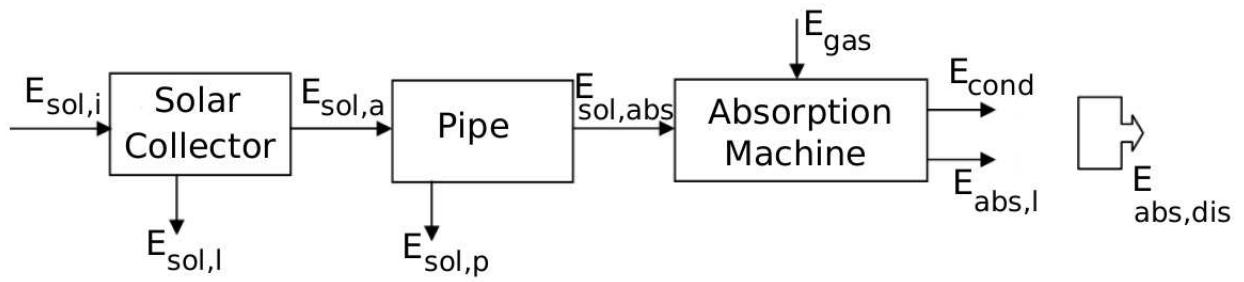


Figure 3.9: Energy transformation from solar collectors to absorption machine.

- $E_{sol,abs}$ is the solar energy transferred to absorption machine;
- E_{gas} is the energy provided by natural gas;
- $E_{abs,l}$ is the energy loss in fumes and unburned of absorption machine;
- E_{cond} is the condensation energy of the absorption machine;
- $E_{abs,dis}$ is the total energy dissipated by the absorption machine.

Chapter 4

Optical Model of The Solar Plant

In this chapter a description of the Fresnel collectors' optical model that has been used to describe the university solar plant is given: this model has a general validity and so it can be applied to any solar plant of that typology.

In the optical model, reflective mirrors are supposed to be flat, because of their high radius of curvature, and the origin of the reference system is placed at the beginning of the mirrors' middle row, as explained in detail later.

MATLAB¹ is the program utilized to model the solar plant, and it is a numerical computing environment and fourth-generation programming language that allows matrix manipulations, plotting of functions and data, implementation of algorithms, creation of user interfaces and interfacing with programs written in other languages, including C, C++, and Fortran.

The optical model is the result of two models combination: a two-dimensional one and a three-dimensional one.

The resulting final model has as its inputs:

1. Current date, in the format "day/month/year" ;
2. Local time, in the format "hour, minute" ;
3. Direct solar radiation (W/m^2) ;
4. Collector² field axis orientation, with the relative angle between the perpendicular to axis orientation and north-south direction.

The elaboration of all input data provides all the magnitudes necessary to monitor the plant's functioning and also for the thermal model's setting. These magnitudes, or model outputs, are:

1. Solar position;
2. Solar time ("hour, minute");

¹MATLAB is the acronym that stands for "MATrix LABoratory". Developed by The MathWorks, MATLAB is intended primarily for numerical computing, but it includes also optional packages, like Simulink, that adds graphical multi-domain simulation and model-based design for dynamic and embedded systems.

²In the following, we will refer to the collector simply as to the mirror, being the collector the reflective surface of the sunlight.

3. Mirrors rows' tilt (radians);
4. Mirrors proper shadow (m^2);
5. Unlit absorber pipe section (% of pipe length);
6. Optical losses factor;
7. Theoretical Reflected Radiation (W/m^2);
8. Real Reflected Radiation (W/m^2) .

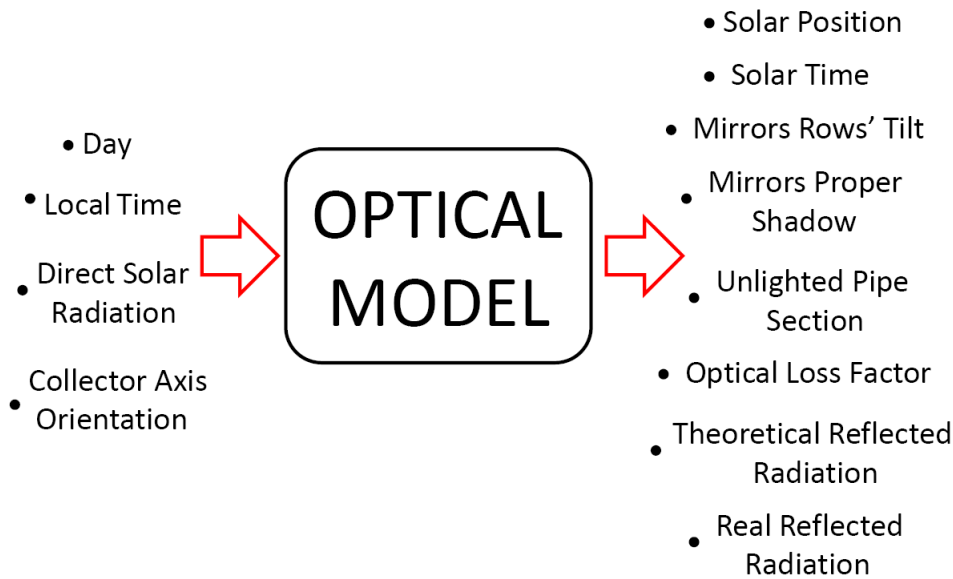


Figure 4.1: Optical Model Scheme, with in details inputs and outputs.

Before defining the optical model, a description of the principal quantities needed to determine the solar position with respect to plant throughout the day is made.

4.1 Solar Quantities Definition

First of all, the position of the reference system adopted with respect to the plant's placement is defined.

As described in the previous section, the geographical coordinates of the plant are 37.41° north-latitude and 6° west-longitude. The plant is parallel to the south front of the laboratories building, with an angle of $12^\circ 3' 1''$ between the perpendicular to the collector axis orientation and the north-south direction.

In Figure 4.2 an aerial vision of Seville engineering laboratories building can be seen, with a graphical representation of the meridian that passes through the center of the collector field and the inclination angle of plant in relation to geographical coordinates.

The origin of the reference system has been placed at the beginning of the farthest east mirrors rows, in the middle, where:

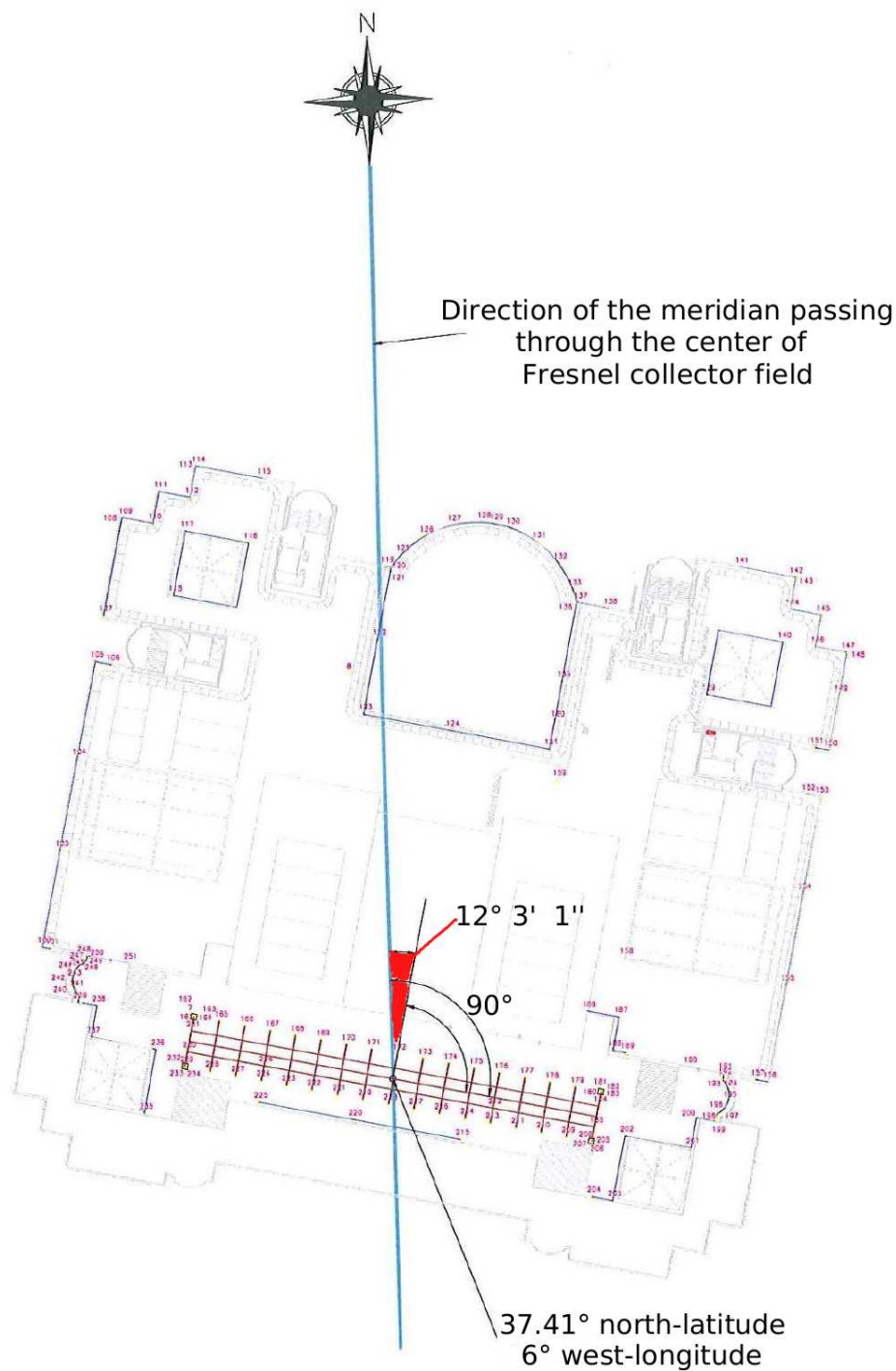


Figure 4.2: Aerial vision of Seville engineering laboratories building. In particular, the angle between collector axes orientation and north-south direction (in red) and plant geographical coordinates are highlighted.

- the x axis is parallel to the mirror short side³, with direction north-south and positive sense toward south;

³Remember that each mirror measures (0.5 x 4) meters.

- the z axis is parallel to the mirror long side, with direction east-west and positive sense toward west;
- the y axis is perpendicular to the xz-plane, with positive sense toward the receptor height.

According to this reference system, rows are numerated increasingly along the x axis, from left to right, with positive integer ranging from one to eleven.

The origin of the reference system has been placed in the center of sixth farthest east mirror row, just below the receptor, in order to simplify the model. Indeed, in this way, the coordinates of the receptor are $(0,4,z)$, being the receptor 4 meters above the mirrors and parallel to the z axis.

Mirrors' rotational axis positions along the x axis are expressed with respect to the origin, i.e. the sixth mirror rotation axis, knowing that each mirror is 0.5 meters wide and the distance from one mirror to the one(s) nearby is 0.2 meters.

In Figure 4.3 there is a visual representation of the reference system utilized and a particular of the front view, on the xy plane.

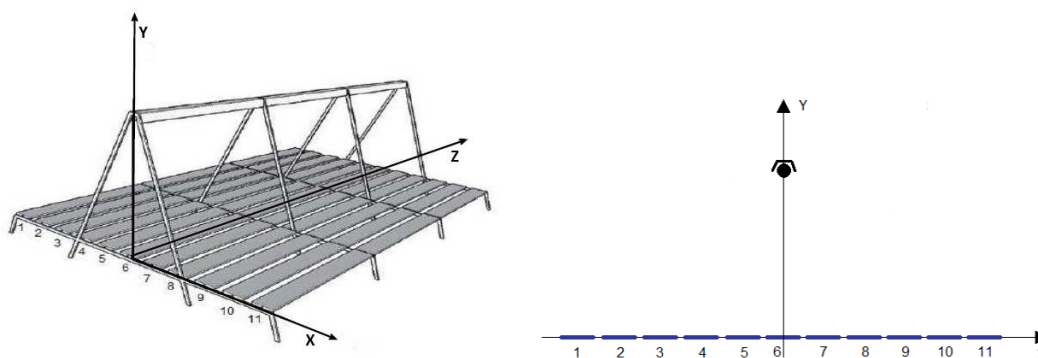


Figure 4.3: Model reference system: three-dimensions representation (on the left) and a front view of the xy plane (on the right).

A single mirror is represented in Figure 4.4, with all the parameters necessary to perform calculations on the model.

Referring to this Figure, *ori* is the orientation angle between the x axis and the north-south direction: turning counterclockwise the axes of the plane xz by an angle of $12^\circ 3' 1''$, the x and z axes coincide with the geographical axes.

The vector \vec{i} is the *solar incidence* vector that defines the way the sunrays affect each mirror, and its components depend on the values of *solar altitude*, *azimuth* and *orientation*.

Azimuth is an angular measurement of the position of a star in the sky. In particular it is the angle between the real north/south point and the perpendicular projection of the star down onto the horizontal plane.

In the model azimuth is the angle between the projection of incidence vector \vec{i} in the xz plane and the real south direction. Azimuth angle ranges between -180° and 180° , being positive in the south to east to north halfplane, negative in the south to west to north halfplane, and null when the projection coincides with the south axis.

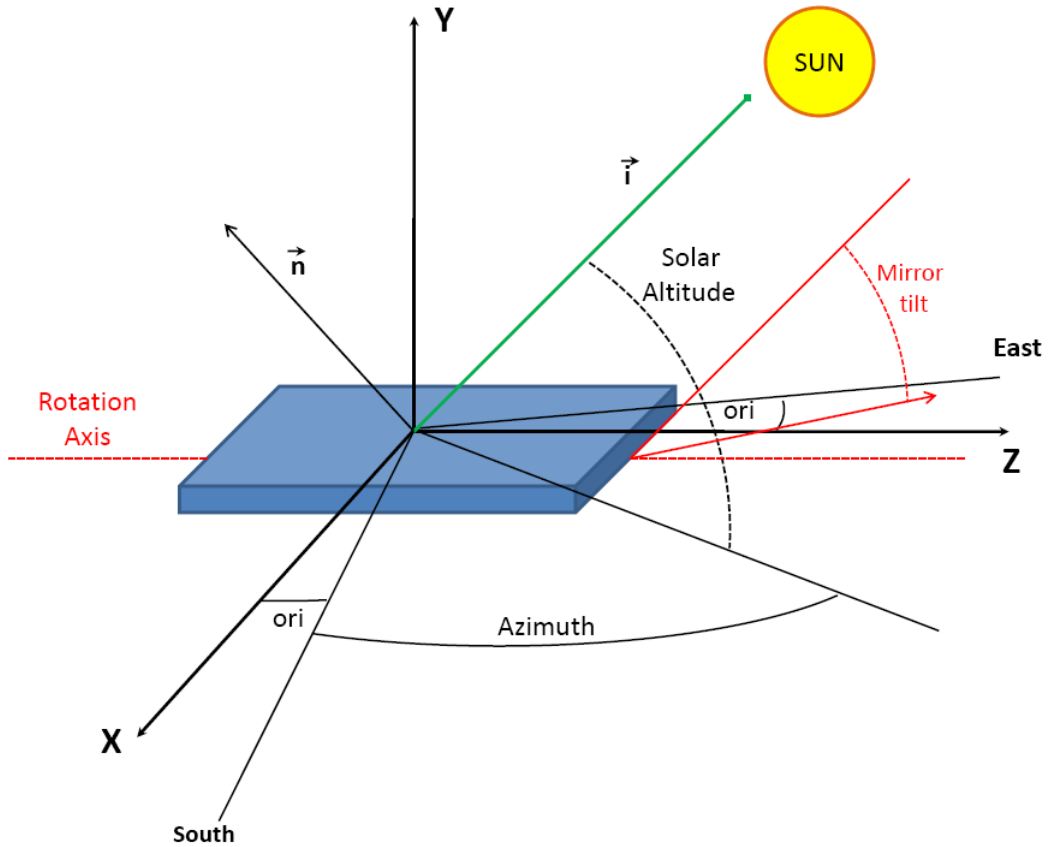


Figure 4.4: Reference system applied to a single mirror, with in evidence all quantities necessary to determine solar position and mirror tilt.

Solar altitude (also called solar elevation) is the elevation angle of the sun, i.e. the vertical angle between the line connecting the sun and its projection on the horizontal plane. At sunset/sunrise the altitude is 0° , and it is 90° when the sun is at the zenith. The altitude relates to the latitude of the site, the declination angle and the hour angle⁴.

Lastly, *mirror tilt* is the angle that each mirror creates with the x axis, as explained in detail in the next section, and \vec{n} is the vector normal to the mirror surface.

Depending on the value of the azimuth, the solar incidence vector can be calculated according to the following mathematical expressions:

1. **Azimuth ≥ 0**

$$\vec{i} = \begin{bmatrix} \cos(\text{elevation}) \cdot \cos(\text{orientation} + \text{azimuth}) \\ \sin(\text{elevation}) \\ \cos(\text{elevation}) \cdot \sin(\text{orientation} + \text{azimuth}) \end{bmatrix}$$

2. **Azimuth < 0 e $|\text{Azimuth}| \leq \text{orientation}$**

⁴These quantities will be defined later in this section.

$$\vec{\mathbf{i}} = \begin{bmatrix} \cos(\textit{elevation}) \cdot \cos(\textit{orientation} - |\textit{azimuth}|) \\ \sin(\textit{elevation}) \\ \cos(\textit{elevation}) \cdot \sin(\textit{orientation} - |\textit{azimuth}|) \end{bmatrix}$$

3. Azimuth < 0 e |Azimuth| > orientation

$$\vec{\mathbf{i}} = \begin{bmatrix} \cos(\textit{elevation}) \cdot \cos(|\textit{azimuth}| - \textit{orientation}) \\ \sin(\textit{elevation}) \\ \cos(\textit{elevation}) \cdot \sin(|\textit{azimuth}| - \textit{orientation}) \end{bmatrix}$$

Before describing in detail the optical model, all astronomical magnitudes needed for internal numerical computing are defined, with all angles converted to radians.

Julian Day

Julian day is used in the Julian date system of time measurement for scientific use by the astronomy community. Julian date is the number of days past from the first day of the year. Julian day for January 1 is 1, for December 31 is 365, except in leap years that is 366.

Therefore Julian day number JD can be calculated associating to each day of the year the number of days passed since the first of January (including the day itself).

Solar Declination

Solar declination, δ_s , is the angle between the equatorial celestial plane and the straight line joining the centers of the earth and the sun. Solar declination varies with the seasons and its period is one year. The maximum declination is on summer solstices, the minimum on winter solstices, and is equal to 0 during the two equinoxes⁵.

In Figure 4.5 it is represented the variation of the declination angle throughout a year, in the Northern hemisphere.

The declination of the sun, in radians, varies daily and is calculated through the following Spencer⁶ equation:

$$\delta_s = \frac{180}{\pi} \cdot (0.006918 - 0.399912 \cos \gamma + 0.070257 \sin \gamma - 0.006758 \cos 2\gamma \\ + 0.000907 \sin 2\gamma - 0.002697 \cos 3\gamma + 0.00148 \sin 3\gamma)$$

where

$$\gamma = \frac{2\pi}{365}(JD - 1)$$

is the fractional year in radians.

⁵For more details see Chapter 2.3.

⁶This equation has a maximum error of 0.0006 radians.

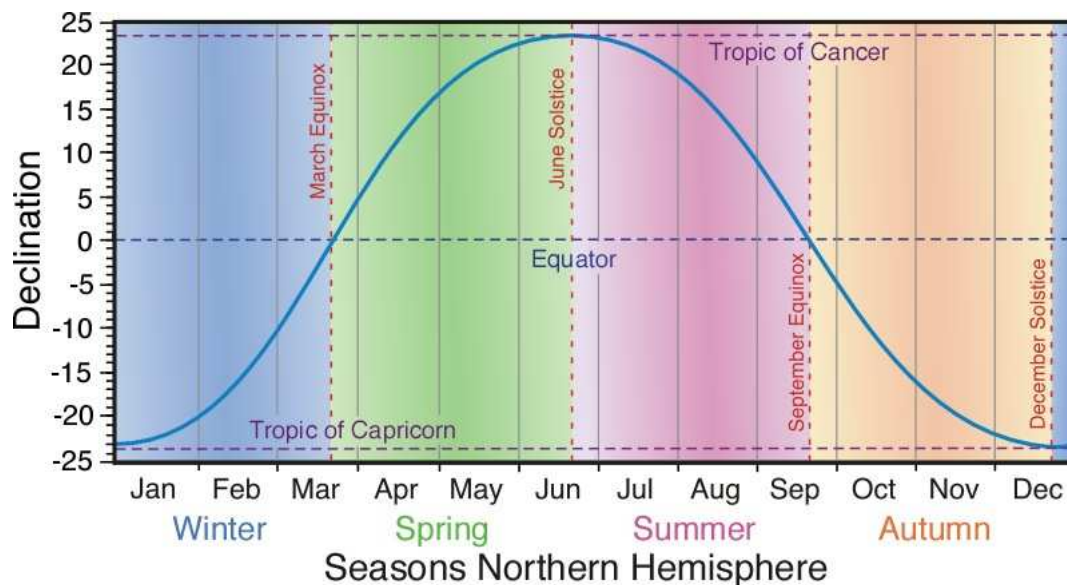


Figure 4.5: Declination variation (in degrees) throughout a year in the Northern hemisphere.

Time Equation

The equation of time is the difference between the *apparent solar time* and the *mean solar time*, both taken at a place with the same geographical longitude at the same instant of time.

The apparent solar time, or true solar time, is given by the daily apparent motion of the sun. It is based on the apparent solar day, which is the interval between two successive returns of the sun to the local meridian. Solar time can also be measured, clearly to a limited precision, by a sundial.

The mean solar time, instead, is the day time based on the motion of the “mean sun”, an imaginary sun moving uniformly along the celestial equator, assuming the earth rotates at a constant rate. Though the amount of daylight varies significantly, the length of a mean solar day does not change on a seasonal basis. In effect, the length of a mean solar day increases at a rate of approximately 1.4 milliseconds each century.

The equation of time results mainly from two different superposed astronomical causes, each causing a different non-uniformity in the apparent daily motion of the sun⁷ relative to the stars, and partly contributing to the global effect.

- *the obliquity of the ecliptic*, which is inclined relatively to the earth’s equator plane;
- *the eccentricity and elliptical form of the earth’s orbit* around the sun.

The equation of time values for each day of the year are plotted in Figure 4.6, and are obtained by means of the following equation, where the equation of time e_t is expressed in minutes:

⁷Naturally also other planets have an equation of time too. On Mars, for example, the difference between solar time and clock time can be as much as 50 minutes, due to the considerably greater eccentricity of its orbit.

$$\mathbf{e}_t = 229.18 \cdot (0.000075 + 0.001868 \cos \gamma - 0.032077 \sin \gamma - 0.014615 \cos 2\gamma - 0.04089 \sin 2\gamma)$$

where

$$\gamma = \frac{2\pi}{365}(JD - 1)$$

is the fractional year in radians.

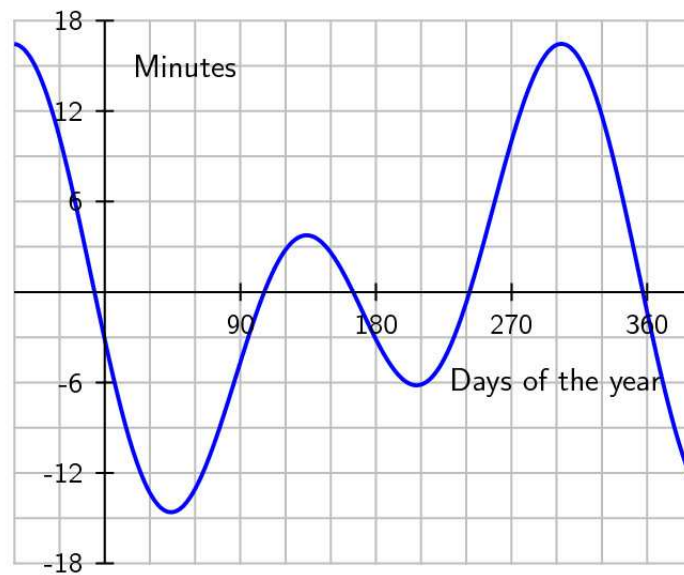


Figure 4.6: Time equation's minutes variation throughout the year.

Solar Time

Solar time, or real solar time, is the time measured with respect to the sun, and is given by the equation:

$$\mathbf{H}_{\text{sun}} = H_{loc} - H_{light} + 4 \cdot (L_{ref} - L_{loc}) + e_t$$

where

- H_{loc} is the local time, or mean local time;
- H_{light} is the hour correction due to jet lag, the local time difference with respect to the standard meridian. For Seville, H_{light} has value 2 from April to October and value 1 from November to March.
- L_{ref} is the Longitude of reference meridian, i.e. Greenwich meridian, that has the value of 0 degrees.
- L_{loc} is the local Longitude, in Seville it is 6 degrees west.
- e_t is time equation, previously defined.

Hour Angle

The hour angle, h_a , is the angular distance that the earth has rotated in a day. It is the expression in degree of solar time, based on the nominal time, 24 hours, required for the earth to rotate once (360 degrees) and it is equal to 15 degrees multiplied by the number of hours from the local solar noon.

Morning values are positive, while evening values are negative. The hour angle is defined by:

$$\mathbf{h_a} = 15 \cdot (12 - H_{sun})$$

where H_{sun} is the solar time.

Solar Altitude (Elevation)

Solar altitude (indicated usually with θ_s) is the elevation angle of the sun, that is the angle between the direction of the geometric center of the sun and the horizontal plane.

It can be calculated using the following formula:

$$\theta_s = \arcsin [\sin \delta_s \cdot \sin \lambda + \cos \delta_s \cdot \cos \lambda \cdot \cos h_a]$$

where δ_s is solar declination, h_a hour angle and λ is local latitude, that in Seville is 37.41° north.

Day Length

Day length is the theoretical number of hours from sunrise to sunset ⁸ and is a function of the solar elevation.

Sunrise and sunset occur when the solar elevation angle is zero. A daylight time factor ω_s is computed to calculate the solar day length for any latitude located between the two polar circles, based on the equation

$$\omega_s = \arccos [- \tan \lambda \cdot \tan \delta_s]$$

where λ is the latitude in radians and δ_s is solar declination in radians.

ω_s represents the time in hour angle at either sunrise (when a negative value is taken) or sunset (when a positive value is taken).

Azimuth

As previously stated, the azimuth is the angle α between the solar inclination projected vector and a reference vector on the horizon plane.

This angle is positive in the South-East-North direction (S-E-N) and negative in South-West-North direction (S-W-N), ranging between -180° and 180° .

The following expression is used to calculate the magnitude of the azimuth, while the sign depends on the value of hour angle, as explained below:

⁸The real number of day light hours would be less than this theoretical value due to cloudiness and other atmospheric factors.

$$\alpha = \arccos \left[\frac{\sin \theta_s \cdot \sin \lambda - \sin \delta_s}{\cos \theta_s \cdot \cos \lambda} \right].$$

Depending on the reference system, the final value of the azimuth is positive or negative, basing on the hour angle value. If h_a is positive, the azimuth changes sign, i.e.

$$\alpha = \begin{cases} \alpha & \text{if } h_a \leq 0, \\ -\alpha & \text{if } h_a > 0. \end{cases}$$

Zenith

The zenith angle, indicated as ψ , is the angle between the sun's direct rays and a line perpendicular to the horizontal surface at a given point. It is computed on a hourly basis as:

$$\psi = \arccos(\sin(\lambda) \cdot \sin(\delta_s) + \cos(\lambda) \cdot \sin(\delta_s) \cdot \cos[h_a \cdot (h_r - h_{r0})])$$

where h_r is the solar hour of the day, h_{r0} is hour corresponding to the solar noon (and hence equal to 12) and the others values have been previously defined.

The sun elevation angle γ and the zenith angle are complementary with respect to $\pi/2$:

$$\gamma = \frac{\pi}{2} - \psi \implies \sin \gamma = \cos \psi$$

The lower the elevation angle, the more unit area of beam is spread out on the ground, so its flux density on a unit area basis is reduced. Sunlight flux density is maximum (equal to one) when the sun is directly overhead and is null when the sun is aligned with the horizon.

4.2 2D-Model

After defining all astronomic variables of interest, the optical model of the plant is described.

As previously stated, the optical model is the result of two models combination, one two-dimensional and the other three-dimensional.

A 2D-Model (Figure 4.7) is developed in order to calculate the inclination of each mirror row, since each row has the same tilt throughout its length.

The model is then used to calculate shadows effects connected with mirrors' tilt and it is the basis for a 3D-Model.

4.2.1 Mirror Rows Inclination

First, the position of each mirror row in an ordinary day at any time has to be calculated.

Each row of mirrors has an independent sun-tracking system that rotates along the z axis, varying its inclination according to the solar altitude, or elevation.

The solar incidence vector is projected on the xy-plane to define its position with respect to the mirrors' tilt.

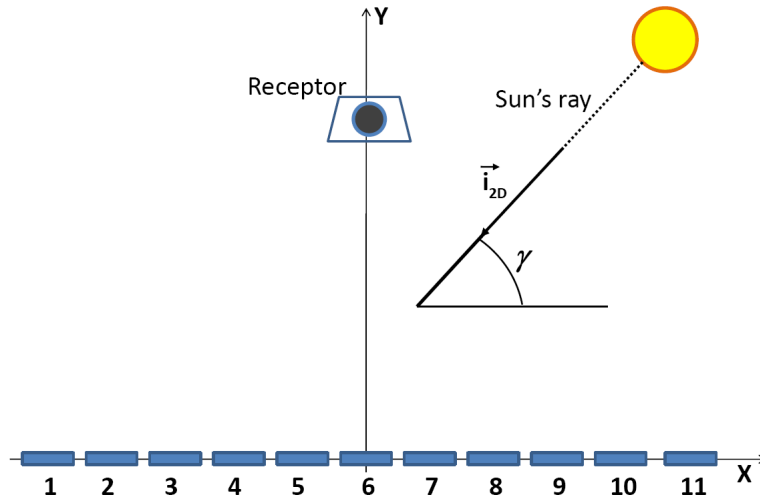


Figure 4.7: Reference system of the 2D-model. Rows of mirrors are numerated from 1 to 11 along the x axis, with reference system origin in the middle of the sixth row and the receptor located 4 meters above it. γ is the angle that the solar incidence vector form with the x axis.

The projection is again a vector, indicated as \vec{i}_{2D} , which still depends on the azimuth value α . The expression for the two-dimensional vector is the following one, where ϕ and θ_s indicate orientation angle and elevation, respectively⁹:

1. $\alpha \geq 0$

$$\vec{i}_{2D} = \begin{bmatrix} \cos \theta_s \cdot \cos (\phi + \alpha) \\ \sin \theta_s \end{bmatrix}$$

2. $\alpha < 0$ e $|\alpha| \leq \phi$

$$\vec{i}_{2D} = \begin{bmatrix} \cos \theta_s \cdot \cos (\phi - |\alpha|) \\ \sin \theta_s \end{bmatrix}$$

3. $\alpha < 0$ e $|\alpha| > \phi$

$$\vec{i}_{2D} = \begin{bmatrix} \cos \theta_s \cdot \cos (|\alpha| - \phi) \\ \sin \theta_s \end{bmatrix}$$

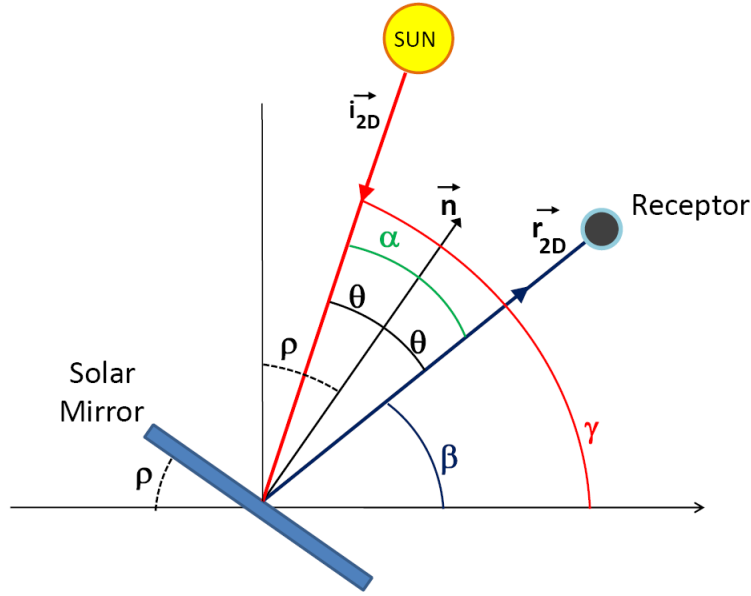


Figure 4.8: Schematic representation of sunlight reflection on mirror surface. Sunlight, with an elevation angle equal to γ , is reflected by the mirror surface to the receptor, with an angle equal to β .

In Figure 4.8 there is a schematic representation of the process of light reflection on a singular solar collector, and all the related magnitudes are reported.

The vector \vec{i}_{2D} , that has just been calculated, represents the sunlight that affects the mirror while the vector \vec{r}_{2D} denotes the light reflection on it.

Once the incidence vector is determined, the direction of \vec{r}_{2D} is forced to be the same as the receptor's, to warm it. Clearly the value of the reflection vector is calculated for each mirror row.

According to the reference system of the two-dimensional model, the receptor coordinates are $(X_R, Y_R) = (0, 4)$, because the absorber pipe is 4 meters above the sixth mirrors row, where the reference system origin is situated.

The value of the reflection vector is different for each mirrors row and so \vec{r}_{2D} is calculated for each one, taking as a reference point the solar collector midpoint, where the rotational axis is located.

With this choice, the coordinates of each row are expressed as $(X_M, Y_M) = (x_m, 0)$, where x_m is the row position on the x axis.

The values of x_m for each row are reported in the table below¹⁰

The reflection vector is obtained through the formula:

$$\vec{r}_{2D} = \begin{bmatrix} r_{2D_x} \\ r_{2D_y} \end{bmatrix} = \begin{bmatrix} \frac{X_R - x_m}{\sqrt{(X_R - x_m)^2 + (Y_R - y_m)^2}} \\ \frac{Y_R - y_m}{\sqrt{(X_R - x_m)^2 + (Y_R - y_m)^2}} \end{bmatrix}$$

⁹For a visual representation see Figure 4.4.

¹⁰The values take into account that the mirror width is 0.5 meters and the space between two consecutive mirrors is 0.2 meters.

Row	1	2	3	4	5	6	7	8	9	10	11
\mathbf{x}_m (meters)	-3.5	-2.8	-2.1	-1.4	-0.7	0.0	0.7	1.4	2.1	2.8	3.5

in which \vec{r}_{2D} is defined as a unit vector and each component is calculated as the difference between the endpoint and the initial point divided by the distance magnitude.

Once the components of the reflection vector are known, the angle formed by \vec{r}_{2D} and the horizontal x-axis, indicated by β , can also be calculated:

$$\beta = \arctan\left(\frac{r_{2D_y}}{\text{abs}(r_{2D_x})}\right).$$

The only two magnitudes that are still to be determined are the angles α and θ : geometrical relations of vectors and laws of reflection can be used to calculate them.

Angles α and θ are the only two magnitudes that are still to be determined: geometrical relations of vectors and laws of reflection can be used to calculate them.

The vector scalar product is utilized to obtain α . The scalar product of two vectors is equal to the product of the two vectors magnitudes multiplied by the angle between them. The reflected vector \vec{r}_{2D} is a unit vector and so its magnitude is unitary; the incidence vector \vec{i}_{2D} is a unit vector in the three dimensions space, but not in the two dimensional plane where it is projected, therefore α is equal to:

$$\vec{i}_{2D} \cdot \vec{r}_{2D} = |\vec{i}_{2D}| \cdot |\vec{r}_{2D}| \cdot \cos \alpha \quad \implies \quad \alpha = \arccos\left(\frac{\vec{i}_{2D} \cdot \vec{r}_{2D}}{|\vec{i}_{2D}| \cdot |\vec{r}_{2D}|}\right).$$

The laws of reflection are instead exploited to calculate γ . If the reflecting surface is very smooth, the reflection of light that occurs is called specular or regular reflection. The laws of specular reflection are the following:

1. The incident ray, the reflected ray and the normal to the reflection surface at the point of the incidence lie in the same plane.
2. The angle between the incident ray and the normal to the plane is equal to the angle between the reflected ray and the same normal.
3. Light paths are reversible.

So, according to the reflection laws, the reflection angle θ is half of the angle α , as it can be seen in Figure 4.8:

$$\theta = \frac{\alpha}{2}.$$

All necessary magnitudes have been obtained, so mirrors row inclination can be computed, differentiating the calculation based on the various possible cases.

The solar plant's geographical coordinates and its z axis orientation along east-west direction motivates the different ways of calculating mirrors row inclination, based on

solar elevation. In fact, the inclination vector's elevation remains always below 90° ¹¹ and so the inclination's computing is different depending on whether x_m takes a positive or a negative value (on the x axis).

1. $x_m < 0$ (Row 1-5)

a. $\gamma \geq \beta$

If the solar elevation γ is greater than the angle β that the reflection vector forms with positive x semiaxis (Figure 4.9 on the left), mirrors row inclination ρ ¹² is equal to

$$\rho = \frac{\pi}{2} - \beta - \theta.$$

This is the most typical situation, from middle of the morning, noon and until the central part of the afternoon, when the sun is high in the sky and so the angle γ is greater than β .

In particular, the first two rows have a quite elevated inclination, of about¹³ 30° .

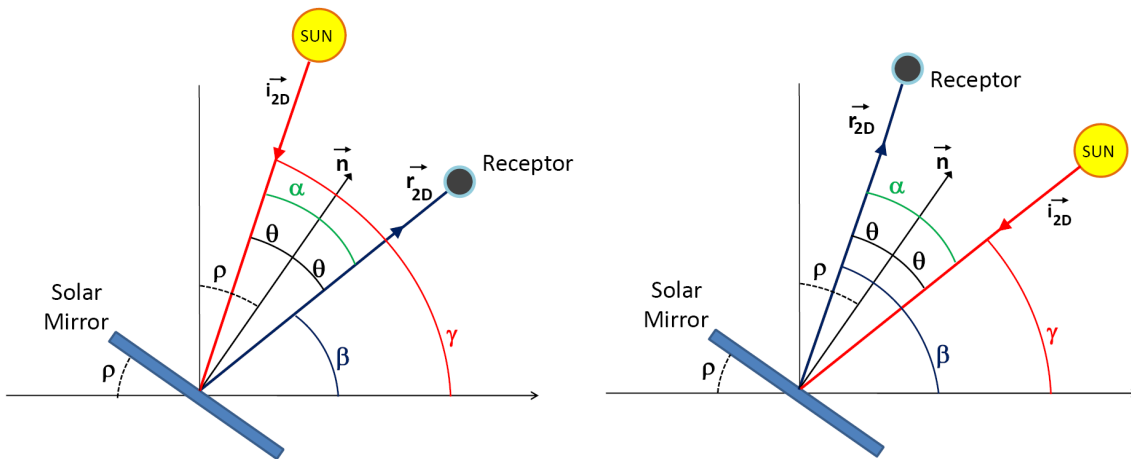


Figure 4.9: Representation of mirrors row inclination for first 5 rows, in case 1-a (on the left) and 1-b (on the right).

b. $\gamma < \beta$

If the solar elevation γ is less than the angle β (Figure 4.9 on the right), mirrors row inclination ρ is equal to

¹¹This statement is true in relation to the particular reference system adopted, with elevation angle measured in the xy plane, positive if counterclockwise.

¹²For a trigonometric explanation of ρ angles equivalence and angle positive sense definition see Appendix G.

¹³This will be proved in Chapter 6, where some mirrors rows inclination data will be reported to compare real data with model data.

$$\rho = \frac{\pi}{2} - \beta + \theta.$$

This happens in the early hours after sunrise and before sunset, when the sun has a small elevation angle and so its position, viewed from the mirrors, appears below the receptor's one.

2. $x_m = 0$ (Row 6)

In this case, the reflection vector is perpendicular to the x axis, being the receptor just above of mirror center (Figure 4.10 on the left), and so the inclination can be easily calculated as:

$$\rho = \theta.$$

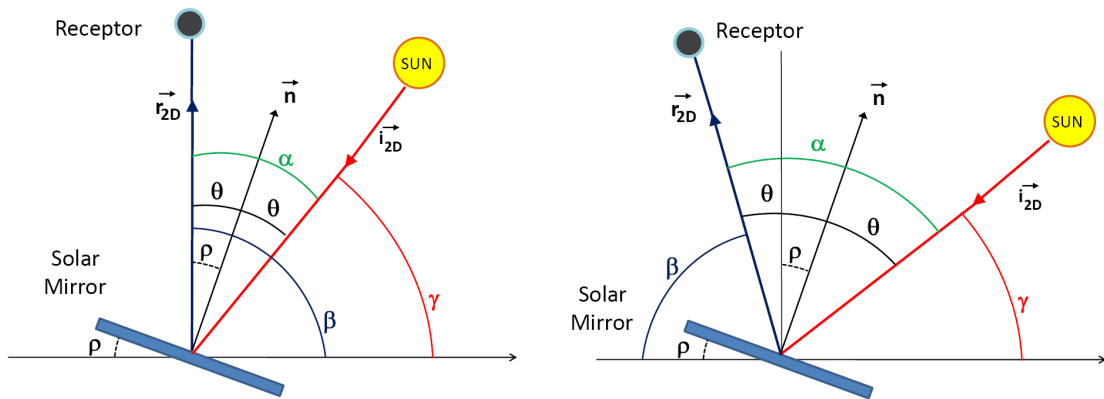


Figure 4.10: Representation of mirrors row inclination for row 6 (on the left) and for rows from 7 to 11 (on the right).

3. $x_m > 0$ (Row 7-11)

Mirrors rows from 7 to 11 are never affected by the receptor's shadow¹⁴ and have a reflection angle β that always lies in the second quadrant of the reference system.

As it can be seen in the right side of Figure 4.10, the mirror inclination angle is given by

$$\rho = \beta + \theta - \frac{\pi}{2}.$$

With this calculation procedure, the inclination value of each mirrors row, at every hour of every day, can be determined.

¹⁴This statement will be justified in section 4.3

4.2.2 Mirrors Shadows

A 2D-model is utilized also to calculate the total shadows on the collectors surface area.

Total shadows that affect mirrors area are the sum of two different components:

- shadows projected by each mirror row on the previous one;
- shadow produced by the receptor on the total collectors area.

For the particular path of the sun above the plant¹⁵, the shadow produced by each mirror on the near ones can only be from a mirror on the previous one, according to the increasing numeration along x axis.

The shadow projected by the receptor on the collector's surface is usually less in percentage than the mirrors' total shadow and it affects only the negative x semiaxis.

Once the total shadow in the 2D-model has been calculated, the total shadow surface is computed by multiplying the shadow width value along the x axis by the z axis length, taking into account the orientation of the z axis with respect to the south and the mirrors current inclination¹⁶.

Then, knowing the two different shadow components, *proper shadow factor*, *receptor shadow factor* and *total shadow factor* will be determined. These magnitudes indicate the reduction of mirrors reflective surface due to shadows.

Proper Mirror Shadows

The proper mirror shadow is the sum of the shadows that each mirror projects on the previous one.

In fact, being the solar elevation always smaller than 90°, a mirror can not projected shadow on following one.

The possible projected shadow depends not only on the sun elevation, but above all on the corresponding tilt of the adjacent mirror axes.

Therefore formulas for proper mirrors shadow calculation are differentiated according to mirror positive or negative inclination, excluding the case in which there is a mirror with negative inclination and the following one with positive inclination, a situation that can never happen¹⁷.

The following equations describe the case when mirror j project its shadow on mirror i , and ρ_i and ρ_j indicate their axes inclination.

- $\rho_i > 0$, $\rho_j > 0$

In this case, both mirrors have positive inclinations. As it can be seen in Figure 4.11, three critical points are defined: **D** and **E** are, respectively, the left extreme of mirror j and the right extreme of mirror i , and **F** is the projection of D-point on the mirror i due to sunlight.

¹⁵Mirrors can not have an inclination greater than 45° (both positive and negative) because of the sun position throughout the day above the plant and because they have to reflect sunlight on receptor by respecting laws of reflection.

¹⁶In order to consider blanks variation between mirrors.

¹⁷Clearly this only could happen in a plant where there are two or more receptors on opposite sides, with different points of sunlight reflection.

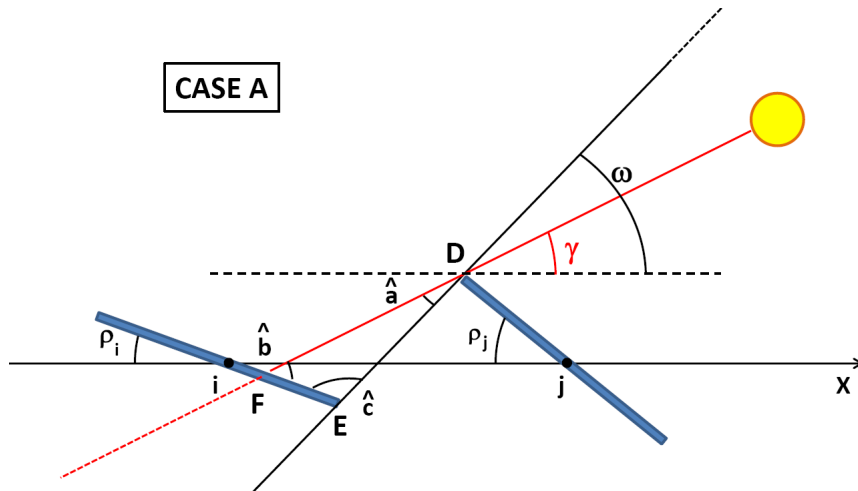


Figure 4.11: Shadow projection from mirror j onto mirror i in the case of positive inclination for both mirrors.

According to the previous definitions, segment \overline{FE} represents the shadow cast by mirror j on mirror i . Angles ω and γ represent the angle formed by \overline{ED} with the horizontal line and the solar elevation on the plane xy , respectively.

To calculate the shadow, the law of sines, applied to the triangle $\triangle DEF$, is used.

The law of sines is an equation relating the lengths of the sides of an arbitrary triangle to the sines of their opposite angles, in the following form:

$$\frac{a}{\sin \hat{a}} = \frac{b}{\sin \hat{b}} = \frac{c}{\sin \hat{c}}$$

where a , b , and c are the triangle sides' lengths, while \hat{a} , \hat{b} , and \hat{c} are their opposite angles.

Coordinates of points D and E are:

$$\mathbf{D} = \begin{bmatrix} x_D \\ y_D \end{bmatrix} = \begin{bmatrix} x_m(j) - \frac{mw}{2} \cdot \cos \rho_j \\ \frac{mw}{2} \cdot \sin \rho_j \end{bmatrix},$$

$$\mathbf{E} = \begin{bmatrix} x_E \\ y_E \end{bmatrix} = \begin{bmatrix} x_m(i) + \frac{mw}{2} \cdot \cos \rho_i \\ -\frac{mw}{2} \cdot \sin \rho_i \end{bmatrix}.$$

where mw is the mirror's width, equal to 0.5 meters.

\overline{FE} represents the shaded part of mirror i and so at least one side and two angles are needed to apply the law of sines to the triangle $\triangle DEF$. \overline{ED} can be computed

as the magnitude of the vector \overrightarrow{ED} , being E the initial point and D the final one. Angles \hat{a} and \hat{b} are equal to¹⁸:

$$\hat{a} = \omega - \gamma$$

$$\hat{b} = \rho_i + \gamma.$$

$$\omega = \arctan \left[\frac{|y_D - y_E|}{|x_D - x_E|} \right].$$

If γ is greater than ω , mirror j will not cast shadow on mirror i , in the opposite case there will be shadow.

In the case of shadow production, the law of sines can finally be applied to calculate the shadow \overline{FE} :

$$\frac{\overline{FE}}{\sin \hat{a}} = \frac{\overline{DE}}{\sin \hat{b}} \implies \overline{FE} = \overline{DE} \cdot \frac{\sin \hat{a}}{\sin \hat{b}}.$$

- $\rho_i > 0$, $\rho_j < 0$

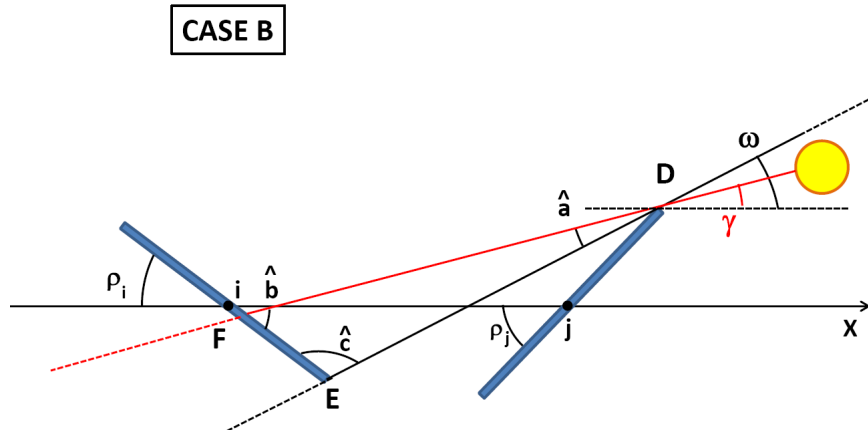


Figure 4.12: Shadow projection from mirror j to mirror i in case of positive inclination for mirror i and negative inclination for mirror j .

In this case, points **E** and **F** are the same as before, while **D** is now the right extreme of mirror i , and so:

¹⁸The following geometric angle relation has been used to calculate \hat{b} :

$$\pi - \hat{b} = \pi - (\gamma + \rho_i)$$

$$\mathbf{D} = \begin{bmatrix} x_D \\ y_D \end{bmatrix} = \begin{bmatrix} x_m(j) + \frac{mw}{2} \cdot \cos \rho_j \\ -\frac{mw}{2} \cdot \sin \rho_j \end{bmatrix},$$

$$\mathbf{E} = \begin{bmatrix} x_E \\ y_E \end{bmatrix} = \begin{bmatrix} x_m(i) + \frac{mw}{2} \cdot \cos \rho_i \\ -\frac{mw}{2} \cdot \sin \rho_i \end{bmatrix}.$$

There will be shadow only if γ is less than ω , and in this case one proceeds as it was previously done for shadow computation.

- $\rho_i < 0$, $\rho_j < 0$

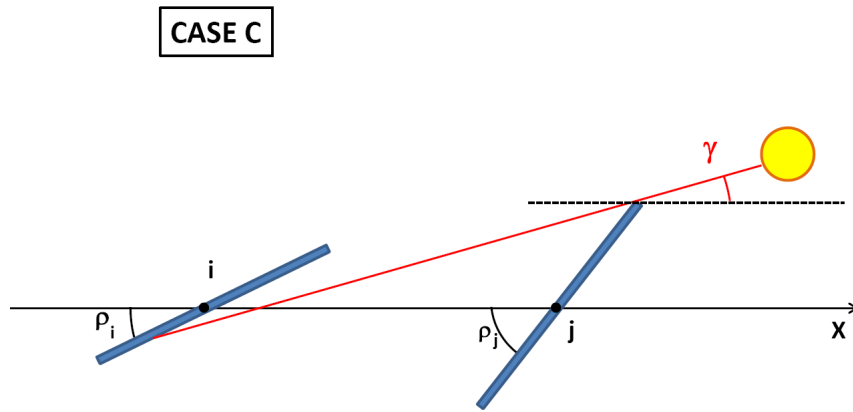


Figure 4.13: Absence of shadow projection between mirrors in the case of negative inclination for both ones.

In this case, as it can be seen in Figure 4.12, for considerations previously made, mirror j never produces shadow on mirror i .

The only way for this to happen would be if mirror j had a high inclination, but this could not happen because otherwise the mirror would not reflect any more sunlight on the receptor.

Clearly, the computation is made for all mirrors excluding the eleventh, since, being the last one, it does not have a following mirror which could project shadow on it.

After the calculation is performed for all mirrors, proper mirrors shaded area is obtained by multiplying each mirror's shadow for the z axis length, taking into account the plant's orientation angle.

Then *proper shadow proportion* \mathbf{p}_{ps} and *proper shadow factor* \mathbf{f}_{ps} are defined. \mathbf{p}_{ps} is the ratio between the proper mirrors shaded area and the total collector area (352 m^2), while \mathbf{f}_{ps} is the percentage of mirrors' available reflective area, after removing proper mirrors shadow:

$$p_{ps} = \frac{\text{Proper Mirrors Shaded Area}}{\text{Total Reflective Area}}$$

$$f_{ps} = 1 - p_{ps}$$

Receptor Shadow on Mirrors

In this section the shadow produced by the receptor on the mirror's reflective surface is analyzed.

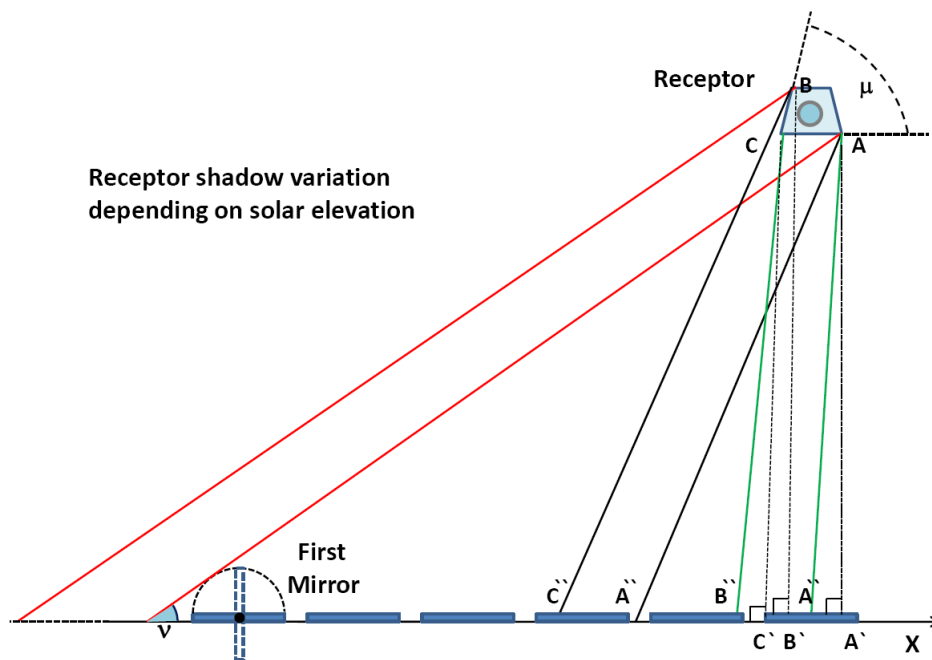


Figure 4.14: Receptor shadow variation depending on solar elevation. Red denotes the shadow out of mirrors reflective surface, while black and green represent the two possible different typologies of receptor shadow on the collector's surface.

In Figure 4.14 the variation of the receptor's shadow, depending on solar elevation, is represented.

μ is the inclination angle of the trapezoidal receptor¹⁹, while ν is the angle that defines the minimum value of the solar inclination (in the 2D-Model) that brings shadow on the mirrors' reflective surface. This angle is calculated taking into account the rotation of the first mirrors row and the distance vector between this row and the receptor.

Calculation of shadow extremes A'', B'', C'' is based on the values of ν and γ_s , where this latter is the shadow's inclination angle in the 2D-Model, depending on solar inclination:

¹⁹This angle for the plant is equal to 63°.

- $\gamma_s < \nu$

Receptor shadow out of mirrors reflective surface;

- $\gamma_s > \nu$, $\gamma_s < \mu$

Receptor shadow inside collector surface, with extremes A" and B";

- $\gamma_s > \nu$, $\gamma_s > \mu$

Receptor shadow inside collector surface, with extremes A" and C".

Clearly, if γ_s is less than ν , the receptor's shadow is out of the reflective surface; differently, if γ_s is greater than ν , two situations are possible, depending on the value of μ .

As it can be seen in Figure 4.14, the right shadow extreme is always A", while the left one varies: if γ_s is less than μ , the left extreme is the projection of vertex B, else is the projection of vertex C.

A rectangle triangle property is utilized to calculate the shadow extremes, namely cathetus determination given hypotenuse and an angle. Indicating with i , c_1 , c_2 hypotenuse and two catheti, respectively, and with θ_1 , θ_2 the angles opposite to catheti, the equations for catheti calculation are

$$c_1 = i \cdot \sin \theta_1 = i \cdot \cos \theta_2$$

$$c_2 = i \cdot \sin \theta_2 = i \cdot \cos \theta_1.$$

As segments $\overline{AA'}$, $\overline{BB'}$ and $\overline{CC'}$ are set²⁰, they can be considered as catheti to calculate, together with the angle γ_s , the coordinates of shadow extremes on the x axis.

So, $\overline{A'A''}$, $\overline{B'B''}$ and $\overline{C'C''}$ can be computed as:

$$\overline{A'A''} = \sqrt{\frac{\overline{AA'}^2}{\sin^2 \gamma_s} - \overline{AA'}^2}$$

$$\overline{B'B''} = \sqrt{\frac{\overline{AA'}^2}{\sin^2 \gamma_s} - \overline{AA'}^2}$$

$$\overline{C'C''} = \sqrt{\frac{\overline{AA'}^2}{\sin^2 \gamma_s} - \overline{AA'}^2}$$

and then, by adding or subtracting these quantities at the points of the receptor's projections on the x axis previously defined, the shadow coordinates along the x axis can be obtained.

For classification of possible case studies, the center of the mirror rotation axis is taken as reference point. Shadow extremes are thus compared to the center of each mirrors row²¹, with three possible situations:

²⁰These segments are set because they are the orthogonal projections of the receptor's structure on the x axis.

²¹In the following, we will refer to mirrors row simply as mirror, without loss of meaning because associated to the 2D-Model.

1. mirror center out of the shade zone, on the left side;
2. mirror center in the shadow area;
3. mirror center out of the shade zone, on the right side.

Before analyzing the cases study, three quantities are calculated in advance for each mirror, in order to facilitate the location of the receptor's shadow on the reflective area:

- distance from the mirror center to the receptor's shadow left extreme;
- distance from the mirror center to the receptor's shadow right extreme;
- the distance between the mirror rotation axis and the projection of the extreme of the mirror shadow in the x axis (depending on the specific sunlight orientation).

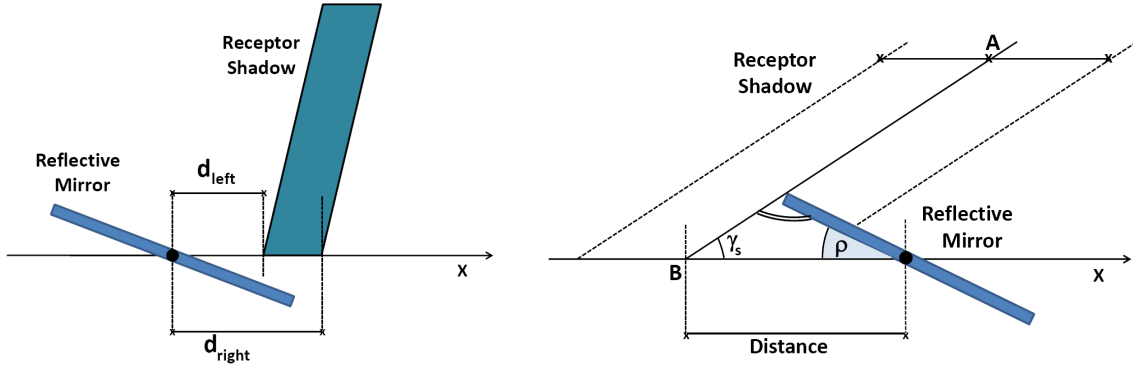


Figure 4.15: Distance of the mirror center from the left and right shadow's extremes (on the left) and definition of the distance between the mirror rotation axis and the projection of the extreme of the mirror shadow in the x axis (on the right).

In Figure 4.15, the three magnitudes just defined are illustrated.

The distance defined at the third point of the list above is the maximum distance value from the mirror center to the right/left²² shadow extreme.

Clearly, this value depends on the mirror's inclination ρ and the shadow's inclination γ_s . By applying law of sines, the maximum amplitude value d_{MAX} is

$$d_{MAX} = \frac{0.25 \cdot \sin(\pi - \rho - \gamma_s)}{\sin \gamma_s}$$

where 0.25 is half the width of the mirror, expressed in meters.

Now, each possible case listed above is analyzed, with all its sub-cases.

The analysis is performed by taking into account the maximum shadow's width, excluding situations that can not arise²³.

²²The choice of the left or right extreme depends on the receptor's shadow shape. With reference to the right side of Figure 4.15, if the shadow is on the left of \overline{AB} , the distance is from the center to the shadow right extreme, if the shadow is on the right of \overline{AB} , the distance is from the center to the shadow left extreme.

²³Specifically, the shadow's width is such that it can not fully cover a mirror.

Case 1 - Mirror's center out of the shade zone on the left side

The maximum amplitude value is compared to the shadows' extremes, and based on the result of this comparison, there are three possible sub-cases.

A *Mirror completely out of the shade zone*

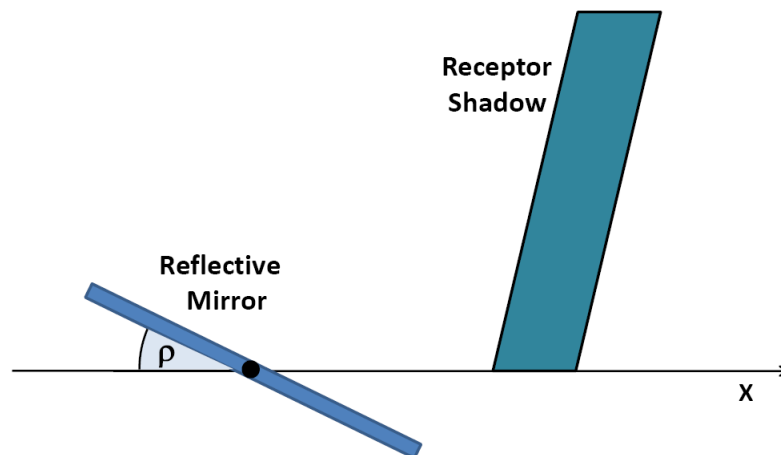


Figure 4.16: Case 1-A: receptor's shadow out of the mirror's reflective surface, on the left side.

In this case, the entire reflective surface of the mirror is available.

B *Shadow contains the mirror's right extreme*

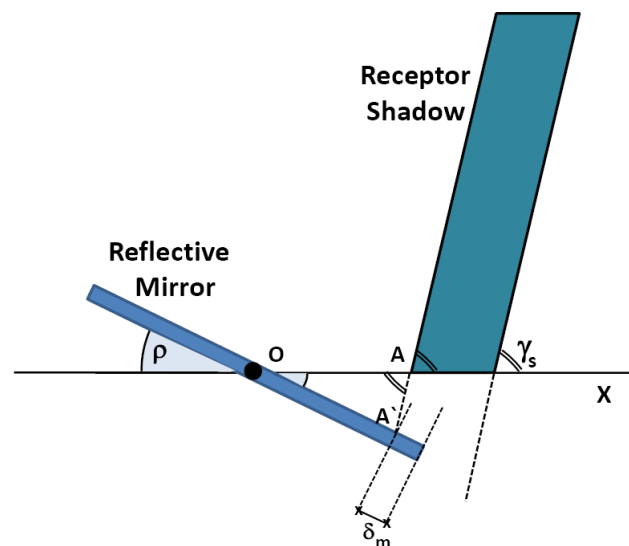


Figure 4.17: Case 1-B: receptor's shadow contains the mirror's right extreme, but not the mirror's center.

In this case, only a small part of the receptor's shadow affects the mirror, containing its right extreme.

The mirror's shaded part, δ_m , is calculated using the sines law²⁴ applied to $\triangle A'OA$, where A is the coordinate of the receptor shadow's left extreme on the x axis, A' its point of incidence on the mirror and O the mirror center coordinate (on the x axis).

Angles $A'\hat{O}A$ and $O\hat{A}A'$ are equal to, respectively, ρ and γ_S , and so the segment $\overline{OA'}$ is given by

$$\overline{OA'} = \frac{\overline{OA} \cdot \sin \gamma_S}{\sin (\pi - \rho - \gamma_S)}.$$

δ_m is then equal to

$$\delta_m = 0.25 - \overline{OA'}$$

where 0.25 is half the width of the mirror.

C *Shadow affects part of a mirror, without containing its right extreme*

The receptor's shadow in this situation affects the mirror without containing neither its center nor its right extreme.

Again, the sines law can be applied, using the angles ρ and γ_S , the receptor's shadow coordinates of both extremes and their points of incidence on the mirror.

Considering the triangles $\triangle A'OA$ and $\triangle B'OB$, $\overline{OB'}$ and $\overline{OA'}$ are obtained as

$$\overline{OA'} = \frac{\overline{OA} \cdot \sin \gamma_S}{\sin (\pi - \rho - \gamma_S)}.$$

$$\overline{OB'} = \frac{\overline{OB} \cdot \sin \gamma_S}{\sin (\pi - \rho - \gamma_S)}.$$

and δ_m is equal to

$$\delta_m = \overline{OB'} - \overline{OA'}.$$

Case 2 - Mirror's center located inside the shadow area

If the center is inside the shadow, the only possible situation is that of Figure 4.19.

In fact, possible receptor's shadow has never such an extension to cover more than half of the width of the mirror, due to receptor's width and the sun's path over the plant.

The mirror's shaded part δ_m is the sum of $\overline{OB'}$ and $\overline{A'O}$.

²⁴It is worthwhile noting that the sign of ρ affects on the values of the quantities derived using this law. However, due to the immediate correspondence between the two cases and in order to not complicate the treatment too much, only the case when ρ is positive is considered.

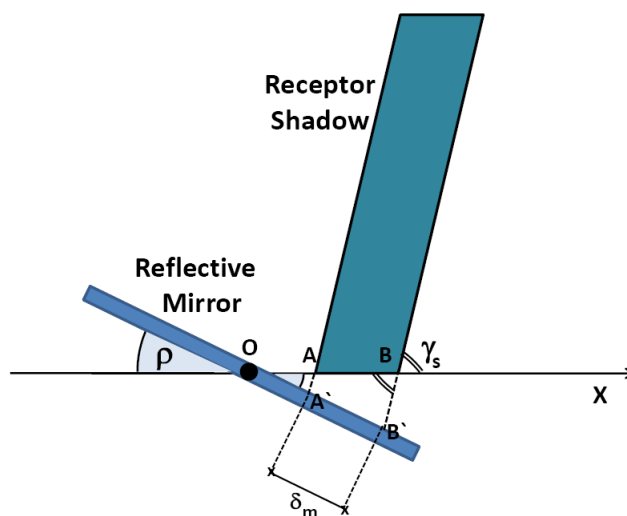


Figure 4.18: Case 1-C: receptor's shadow affects a part of the mirror, without containing its center nor its right extreme.

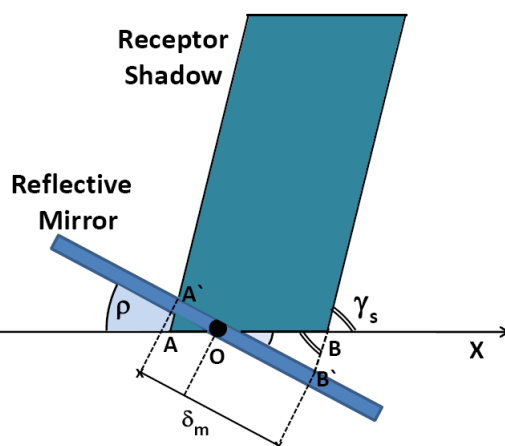


Figure 4.19: Case 2: receptor's shadow affects a part of possible mirror, containing its center.

To calculate $\overline{OB'}$ one has to proceed similarly to what was done in case 1-B so that

$$\overline{OB'} = \frac{\overline{OB} \cdot \sin \gamma_s}{\sin (\pi - \rho - \gamma_s)}.$$

By applying the sines law to the triangle, $\triangle AOA'$ is obtained

$$\overline{A'O} = \frac{\overline{AO} \cdot \sin \gamma_s}{\sin (\pi - \rho - \gamma_s)}$$

and so δ_m is equal to

$$\delta_m = \overline{OB'} + \overline{A'O}.$$

Case 3 - Mirror's center out of the shade zone on the right side

As in Case 1, there are three subcases and the approach is the same.

A *Mirror completely out of the shade zone*

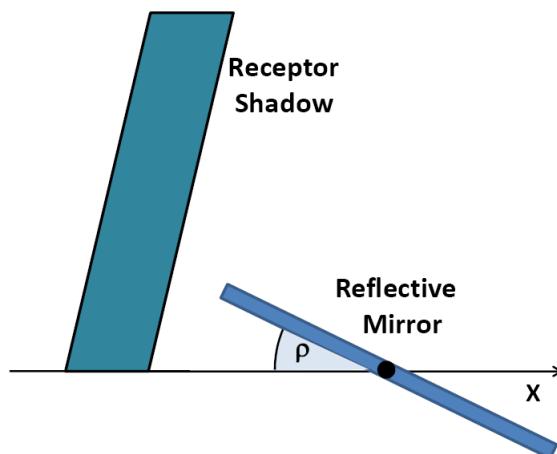


Figure 4.20: Case 3-A: receptor's shadow out of the mirror's reflective surface, on the right side.

In this case, the entire reflective surface of the mirror is available.

B *Shadow contains mirror right extreme*

By applying sines law to the triangle $\triangle AOA'$, $\overline{OA'}$ is equal to

$$\overline{OA'} = \frac{\overline{OA} \cdot \sin \gamma_S}{\sin (\pi - \rho - \gamma_S)}.$$

and δ_m has the following value

$$\delta_m = 0.25 - \overline{OA'}$$

where 0.25 is half the width of the mirror.

C *Shadow affects a part of the mirror, without containing its left extreme*

Again, by applying sines law to triangles $\triangle BOB'$ and $\triangle AOA'$, one obtains

$$\overline{OA'} = \frac{\overline{OA} \cdot \sin \gamma_S}{\sin (\pi - \rho - \gamma_S)}.$$

$$\overline{OB'} = \frac{\overline{OB} \cdot \sin \gamma_S}{\sin (\pi - \rho - \gamma_S)}.$$

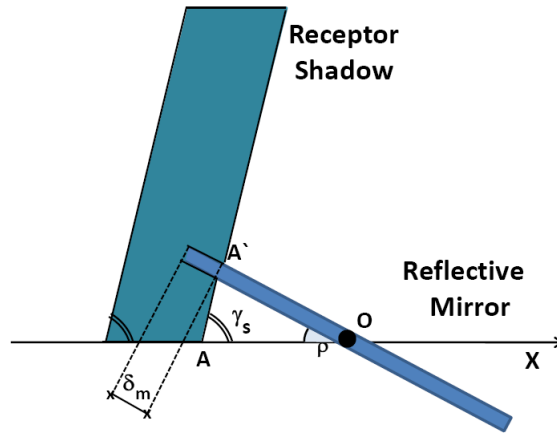


Figure 4.21: Case 3-B: receptor's shadow contains the mirror's left extreme, but not the mirror's center.

and δ_m is equal to

$$\delta_m = \overline{OA'} - \overline{OB'}.$$

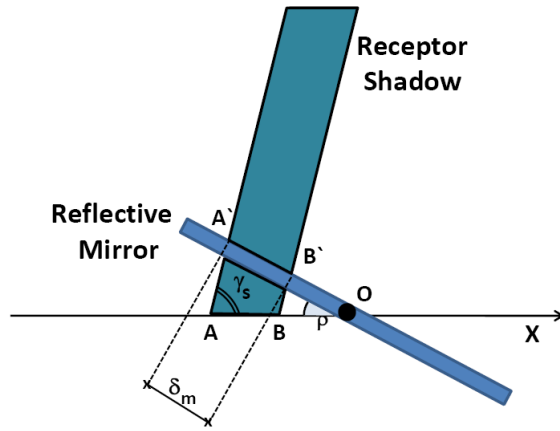


Figure 4.22: Case 3-C: receptor's shadow affects a part of the mirror, without containing its center nor its left extreme.

Once that the calculation has been performed, receptor's shadow on the reflective area of the mirrors is computed multiplying δ_m for the z axis length, taking into account the plant's orientation angle.

Similarly to proper mirrors shadow, two quantities are defined: *receptor shadow proportion*, p_{rs} , and *receptor shadow factor*, f_{rs} . p_{rs} is the ratio between the area of the receptor's shadow and the total collector's area (352 m^2) and f_{rs} is the percentage of the available reflective area of the mirrors, after removing receptor shadow:

$$p_{rs} = \frac{\text{Receptor Shadow Area}}{\text{Total Reflective Area}}$$

$$f_{rs} = 1 - p_{rs}$$

Then, sum proper mirrors shadow and receptor shadow, the total shaded zone on the reflective surface is obtained.

The *total shadow proportion*, p_{tot} , is thus the ratio between the total shaded area and the total reflective area and the *total shadow factor*, f_{tot} , is the percentage of reflective area of the mirrors that is available after removing the shaded area:

$$p_{tot} = \frac{p_{ps} + p_{rs}}{352}$$

$$f_{tot} = 1 - p_{tot}$$

4.2.3 Optical Losses

The real radiation that reaches the receptor's pipe is not the same one that affects the reflective mirrors, because of optical losses.

The incident solar radiation is fully exploited only if its direction is perpendicular to the reflective mirror's surface, but this never happens because mirrors are tilted to reflect solar radiation on the absorber's pipe.

Thus, there is always a loss of direct radiation that depends on the angle κ that a single mirror forms with the perpendicular to the direction of the solar inclination.

The angle κ is determined in two different ways, depending on the mirror's inclination value ρ .

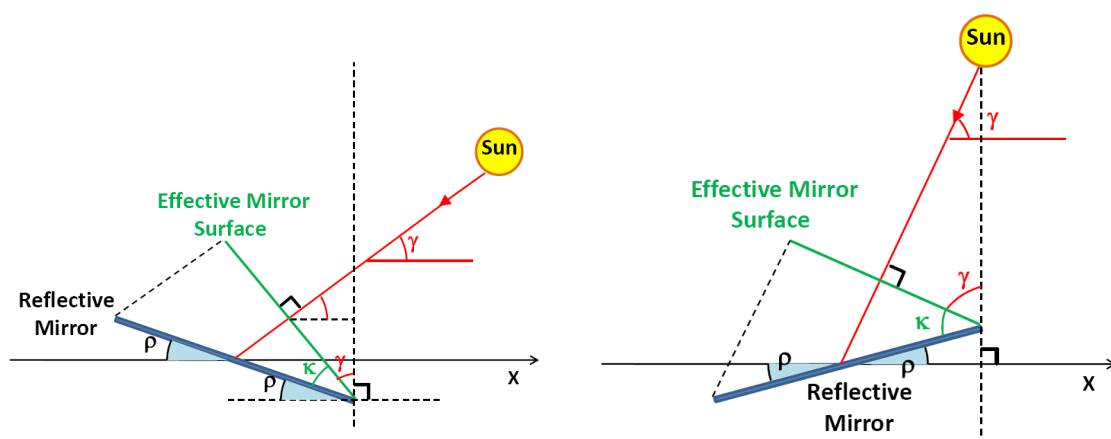


Figure 4.23: Angle of optical losses in the case of positive (on the left) or negative (on the right) mirror's axis tilt. In particular, mirror's effective reflective surface is indicated in green and it depends on κ , that is the angle that the mirror forms with the perpendicular to the sunlight direction.

- **Case 1** $\rho > 0$

As it can be seen on the left side of Figure 4.23, if the inclination has a positive value, κ is equal to

$$\kappa = \frac{\pi}{2} - \gamma - \rho$$

where γ is the angle of the solar incidence vector.

- **Case 2** $\rho < 0$

In this case, to compute the value of κ the following formula is utilized:

$$\kappa = \pi - \left(\frac{\pi}{2} - \rho \right) - \gamma = \frac{\pi}{2} + \rho - \gamma.$$

Optical losses factor, that is different for each mirrors row, is defined as:

$$f_{ol_i} = \cos \kappa_i$$

where κ_i is the angle of optical loss relative to the i th row. Optical losses factor will be utilized in section 4.3.1 to calculate the real solar radiation that affects the receptor's pipe.

4.3 3D-Model

Mirrors' inclination and total shadow on the reflective surface have been determined with the 2D-Model, and now the 3D-Model is used to calculate the real solar radiation affecting the receptor's pipe.

In order to compute this magnitude, the receptor's unlit part has to be ascertained.

The unlit part depends on the azimuthal solar component, which influences solar radiation affecting receptor, therefore a 3D-Model has to be utilized²⁵. In Figure 4.24 there is an example of a receptor unlit part, which is the unlit part in the east extreme before solar noon.

All three components of the solar incidence vector are considered, with the z component varying between 0 and 64 meters, which is the z axis length.

In the reference system adopted, the components of the normal vector \vec{n} , for each mirror, are:

$$\vec{n} = \begin{bmatrix} \sin \rho \\ \cos \rho \\ 0 \end{bmatrix}$$

where ρ is the inclination of the mirror axis.

²⁵The 3D-reference system is shown in Figure 4.3 of section 4.1.



Figure 4.24: Example of receptor unlit part on the east extreme before solar noon.

According to the laws of reflection²⁶, the angle of incidence is equal to the angle of reflection, and the incident ray, the normal and the reflected ray are coplanar, so in the 3D-Model the following equation appears:

$$\vec{i}_{3D} \times \vec{n} = \vec{n} \times \vec{r}_{3D}$$

where \vec{r}_{3D} is the vector of reflected sunray from mirror to the receptor's pipe.

\vec{r}_{3D} is calculated as the difference between the point where the sunlight is reflected and the center of mirror, divided by the distance, in order to obtain a unit vector.

The expression for \vec{r}_{3D} is

$$\vec{r}_{3D} = \begin{bmatrix} \frac{x_R - x_m}{\sqrt{(x_R - x_m)^2 + (y_R - y_m)^2 + (z_R - z_m)^2}} \\ \frac{y_R - y_m}{\sqrt{(x_R - x_m)^2 + (y_R - y_m)^2 + (z_R - z_m)^2}} \\ \frac{z_R - z_m}{\sqrt{(x_R - x_m)^2 + (y_R - y_m)^2 + (z_R - z_m)^2}} \end{bmatrix}$$

where (x_R, y_R, z_R) are the coordinates of the point of the reflected sunlight onto the receptor and (x_m, y_m, z_m) are the axes coordinates for a single mirror.

Due to the adopted reference system, y_m is always null and x_m has the values reported in table of section 4.2.1.

²⁶For more details see section 4.2.1.

z_m ranges between 0 and 64, but the calculation is performed only for two values, corresponding to the east ($z_m = 64$) and west ($z_m = 0$) receptor's extremes, because the unlit part of the absorber tube is located at the extremes.

(x_R, y_R) are known and equal to $(0, 4)$, while z_R has to be computed.

The value of z_R is obtained by exploiting the previous relation for the reflective vectors and it is then used to determine the unlit part δ_{up} caused by each mirror row.

When the shaded zone is at the east extreme ($z_m = 64$), δ_{up} is equal to

$$\delta_{up} = 64 - z_R$$

where 64 is the receptor's length, while when the shadow is at the west extreme ($z_m = 0$)

$$\delta_{up} = z_R.$$

The calculation is performed for each mirror row, and hence 11 different values are obtained, though they differ very little one from the other.

So, the value of unlit part δ_{upA} is the average of the 11 values:

$$\delta_{upA} = \frac{1}{11} \sum_{i=1}^{11} \delta_{upi}.$$

The receptor unlit part factor f_{up} , that represents a correction factor used in the following calculation of real radiation, is given by

$$f_{up} = \frac{64 - \delta_{upA}}{64}.$$

Notice that all the calculations performed in this section have been derived by assuming that the total sunlight reflected by the mirrors affects the absorber's pipe or secondary reflector. This is guaranteed by the large mirror's radius of curvature, that is 8.6 meters for rows from 4 to 8, and 10.6 for the others.

In fact, due to high mirror's radius of curvature²⁷, there are no reflected radiation losses.

In the final part of chapter 6 a study of the radius of curvature sensitivity will be provided, demonstrating that if the mirrors were totally plane, there would be large radiation losses.

4.3.1 Real Radiation Computation

The real solar radiation that affects the receptor is different from the theoretical one, because it takes into account all the losses and correction factors obtained in the previous section of this chapter.

The contribution that each mirror gives to the solar radiation that affects the receptor (in Watts / m^2) is computed according to the following equation, under the assumption that the solar radiation reflected by mirrors affects entirely the secondary reflector and is then reflected on the absorber's pipe:

²⁷Also the autocalibration mechanism described in section 3.2 has an impact, though.

$$rad_{real_i} = dr \cdot A_i \cdot \cos \kappa_i \cdot f_{up} \cdot \rho_m \cdot \rho_{sr}$$

where

- dr is direct solar radiation (W / m^2);
- A_i is i-row collectors area, equals to $32 m^2$;
- $\cos \kappa_i$ is optical losses factor for i-row;
- f_{up} is receptor unlit part factor;
- ρ_m is mirror nominal reflectivity, equals to 0.92;
- ρ_{sr} is secondary reflector nominal reflectivity, equals to 0.77.

The total real solar radiation that affects the receptor is the sum of the real reflected solar radiation of all rows, multiplied by the total shadow factor f_{tot} :

$$rad_{real_{TOT}} = \sum_{j=1}^{11} rad_{real_j} \cdot f_{tot} \cdot$$

The theoretical solar radiation (W/m^2) can be easily computed without taking into account the optical loss factor $\cos \kappa$ and the total shadow factor f_{tot} , and hence

$$rad_{theotot} = dr \cdot A_{tot} \cdot \rho_m \cdot \rho_{sr}$$

where A_{tot} is the total reflective surface, equal to $352 m^2$ (Watts / m^2).

The comparison between the real and the theoretical solar radiation is useful to give an index of optical efficiency of the plant and to understand and quantify the potential of real solar radiation in order to make changes to increase its exploitation.

Chapter 5

Thermal Model of The Solar Plant

In this chapter, a thermal model of the solar plant is developed, and the realization of an algorithm based on this model is explained.

The thermal model of the plant focuses on heat exchanges in the receptor.

The receptor is formed by an absorber pipe, model SCHOTT PTR 70¹, made of stabilized austenitic stainless steel, with a nominal absorptivity of 0.94, and a borosilicate glass cover² that surrounds the absorber's pipe.

All geometrical and structural data (like length, exterior diameter, thickness) of the absorber's pipe, glass cover and secondary reflector are known, as well as the thermal parameters necessary to calculate heat flow, absorptivity and emissivity.

In the thermal model, the quantities that have been considered as inputs are:

- Environment temperature ($^{\circ}$ C);
- Inlet water temperature ($^{\circ}$ C);
- Water flow (m^3/s);
- Real solar radiation, obtained with the optical model of chapter 4 (W/m^2).

The thermal model allows to know the temperature distribution in the absorption pipe and in the heat-transfer fluid (water) along the pipe at a given moment, as well as the temporary variation of the temperature at certain points of the pipe.

The following hypotheses have been made:

- The properties of the heat-transfer fluid are considered as functions of the temperature;
- The flow in each section is presumed to be circumferentially uniform and equal to the average value;

¹For more details see section 3.2, on the receptor.

²Borosilicate glass is a type of glass, with the main glass-forming constituents silica and boron oxide. Borosilicate glasses are known for having very low coefficients of thermal expansion making them resistant to thermal shock, more so than any other common glass. One of the most common use for borosilicate glass is as vacuum tube.

- Variations in the radial temperature of the pipe walling are not taken into account. This assumption is reasonable in the case of a thin wall with good thermal conductivity, as in the case of the plant considered;
- Water flow and irradiance are considered as time functions and are always the same for each element;
- Water is supposed to be an incompressible fluid³.
- Losses caused by the conduction of axial heat on both sides of the wall and from the fluid are negligible.

The heat axial conduction in the tube should be negligible, given that the walls are thin, having a high heat resistance. The heat axial conduction in the fluid is relatively small, as the water conductivity is poor⁴;

- Specific heat capacity at constant pressure and volume is considered a constant quantity. This assumption is reasonable for steel and water, due to the range of values of pressure and temperature of the thermal process of the plant.

Using the above hypotheses and applying the conservation of the energy to the metal pipe of a volume $d\mathbf{x}$ over a time interval $d\mathbf{t}$, the energy balance for each infinitesimal volume is obtained.

The time variation of the internal energy on each volume can be expressed as:

$$\frac{\partial U}{\partial t} = \rho_m C_m A_m \frac{\partial T_m}{\partial t} d\mathbf{x}$$

This variation of internal energy is equal to the difference between the energy of the solar radiation incident on the absorber pipe and the sum of the energy released by the pipe to the ambient and the energy transferred to the fluid.

The energy that affects the absorber's pipe is the energy due to the real solar radiation⁵ reflected by the collectors. As explained in the previous chapter, real radiation takes into account optical losses and the reflectivity of collectors and of the secondary reflector.

The expression for the solar radiation energy is:

$$E_{rad} = \omega_r \cdot B \cdot d\mathbf{x}$$

where ω_r is the real solar radiation and B is the total collector's aperture.

In fact, the solar radiation is expressed in W/m^2 and the area taken as reference surface is the one given by the total collector's aperture, i.e. the overall width of eleven rows of mirrors, multiplied by the infinitesimal length $d\mathbf{x}$.

The energy released by the absorber's pipe to the ambient and the energy transferred to the fluid have a similar expression:

$$E_{amb} = H_l(T_m - T_a)B d\mathbf{x}$$

³This assumption is reasonable because tests performed showed that water has small compressibility variations up to 10000 bar.

⁴Water conductivity is in the range of $5 \cdot 10^{-2} \div 10^{-4}$

⁵For more details about the calculation of the real solar radiation see section 4.3.

Energy Balance of Absorber Pipe

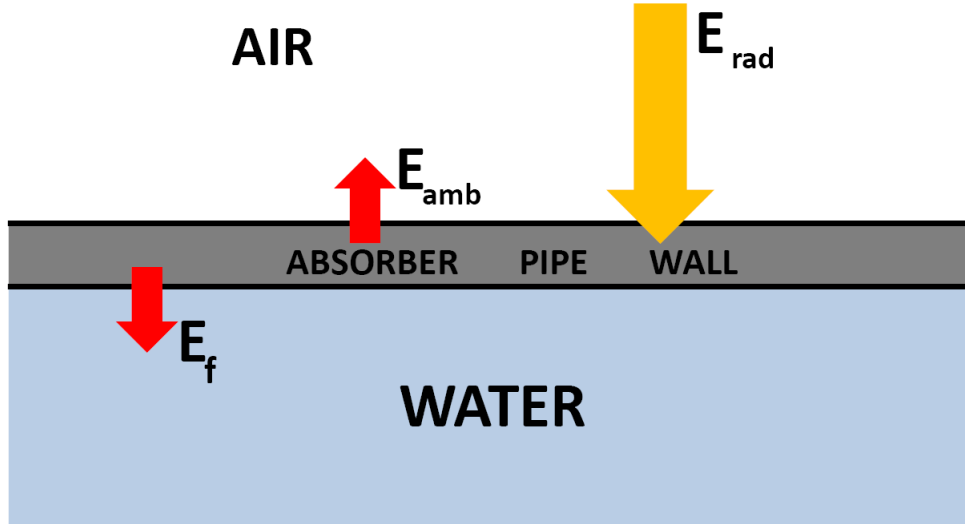


Figure 5.1: Energy balance of absorber pipe: the energy of reflected solar radiation E_{rad} warms absorber pipe walls; a part of this energy, indicated with E_{amb} , is ceded to the ambient while an other part, E_f , is transferred to the fluid. If the coefficient value of metal-fluid transmission is high and the coefficient value of global losses is small, E_{rad} is transferred quite entirely to the fluid.

$$E_f = H_t(T_m - T_f)L dx$$

where T_m , T_a , T_f are the temperatures of metal, ambient, fluid in Celsius degrees, respectively, L is the inner diameter of the absorber's pipe and H_l , H_t are the coefficient of the global thermal losses and the coefficient of the metal-fluid transmission, respectively, both expressed in $W/m^2 \text{ } ^\circ C$.

Therefore, the variation of the internal energy is equal to:

$$\begin{aligned} \frac{\partial U}{\partial t} &= E_{rad} - E_{amb} - E_f = \\ &= \omega_r \cdot B \cdot dx - H_l(T_m - T_a) \cdot B \cdot dx - H_t(T_m - T_f) \cdot L \cdot dx. \end{aligned}$$

The global coefficient of the thermal losses per unit of mirror area is considered, that is the power (in Watts) lost per mirror square meter and Celsius degree. The coefficient of the metal-fluid transmission corresponds to the thermal power lost through the contact surface between fluid and metal.

The energy balance in the metal can thus be expressed as:

$$\rho_m C_m A_m \frac{\partial T_m}{\partial t} = \omega_r B - H_l B (T_m - T_a) - L H_t (T_m - T_f).$$

In a similar manner, the first law of is considered thermodynamics can be applied to the considered volume of fluid:

$$\frac{\partial U}{\partial t} = H_t L(T_m - T_f)dx - \dot{m} (\bar{H}_{x+dx} - \bar{H}_x)$$

where \dot{m} is the infinitesimal fluid element mass variation, H_t is the coefficient of the metal-fluid transmission just described while $(\bar{H}_{x+dx} - \bar{H}_x)$ is the difference in enthalpy on the fluid element of base area A_f and length dx .

The enthalpy variation is equal to

$$\frac{\partial \bar{H}}{\partial x} dx = C_f \frac{\partial T_f}{\partial x} dx$$

under the assumption that the specific heat capacity at constant pressure does not vary in the fluid element considered.

Thus, the internal energy variation in the infinitesimal element can be indicated as:

$$\frac{\partial U}{\partial t} = H_t L(T_m - T_f)dx - \dot{q} \rho_f C_f \frac{\partial T_f}{\partial x} dx$$

where \dot{v} is⁶ the volume of the infinitesimal fluid element.

On the other hand, the internal energy variation in the fluid element can be expressed as a function of the fluid temperature:

$$\frac{\partial U}{\partial t} = \rho_f C_f A_f dx \frac{\partial T_f}{\partial t}$$

where $(A_f \cdot dx)$ is the fluid element volume.

Using this relation, the energy balance in the fluid element takes the following expression:

$$\rho_f C_f A_f \frac{\partial T_f}{\partial t} + \rho_f C_f \dot{q} \frac{\partial T_f}{\partial x} = H_t L (T_m - T_f).$$

The equations for the energy balance in the infinitesimal element are therefore the following, where the subscripts m and f refer to the metal and to the fluid, respectively:

$$\rho_m C_m A_m \frac{\partial T_m}{\partial t} = \omega_r B - H_l B (T_m - T_a) - H_t L (T_m - T_f)$$

$$\rho_f C_f A_f \frac{\partial T_f}{\partial t} + \rho_f C_f \dot{q} \frac{\partial T_f}{\partial x} = H_t L (T_m - T_f)$$

where

- ρ is the density (Kg/m^3)
- C is the specific heat capacity ($KJ/Kg \text{ } ^\circ C$)
- A is the section area (m^2)

⁶Remember that the relation between mass and volume is $m = \rho \cdot q$, where ρ is the density.

Energy Balance of the fluid

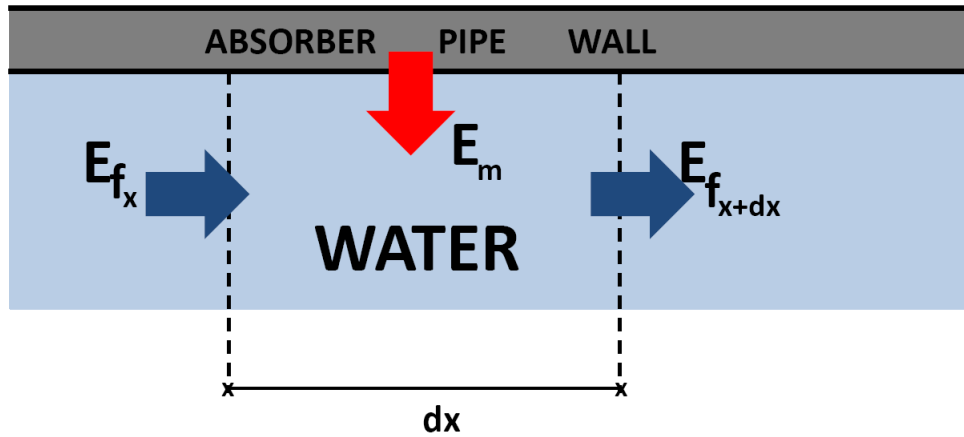


Figure 5.2: Energy balance in the fluid: the temperature of each infinitesimal volume of fluid depends on the energy E_m transferred by the metal, and on the energy of the previous infinitesimal volume. In fact, the fluid accumulates energy flowing along the absorber's tube and so in the tube section dx acquires the energy E_{x+dx} that cedes to the nearby fluid volume.

- T is the temperature ($^{\circ}\text{C}$)
- T_a is the ambient temperature ($^{\circ}\text{C}$)
- ω_r is the real solar radiation (W/m^2)
- H_l is the global losses coefficient ($\text{W}/\text{m}^2 \text{ }^{\circ}\text{C}$)
- H_t is the metal-fluid transmission coefficient ($\text{W}/\text{m}^2 \text{ }^{\circ}\text{C}$)
- B is the total collector's aperture (m)
- L is the inner diameter of the absorber's tube (m)
- \dot{q} is the water flow (m^3/s).

These equations are only applicable to active zones, that is, the parts of the absorber's pipe which receive the beam radiation. The equations which describe the performance in a passive element are similar, except that the solar energy input is nil.

Thus, the model for the complete field consists of a series of active and passive elements⁷.

The equations derived can be solved using an iterative process with finite differences. The temperature of the fluid and of the absorber's pipe are calculated for each time

⁷Passive elements are at the beginning of the absorber's pipe, when the unlit part is on the west side, and at the end, when unlit part is on the east side.

interval and for each element. For the plant considered, a value of 1 meter for $d\mathbf{x}$ length and a time integration interval of 0.5 seconds have been chosen.

A two stage algorithm has been implemented to solve the temperature equations.

In the first stage the temperatures of the fluid and of the metal are calculated supposing that the fluid is in a steady state.

In the second stage the fluid temperature is "corrected" in function of the net energy transported by the fluid.

1st Stage

$$T_m(\mathbf{n}, \mathbf{k}) = T_m(\mathbf{n}, \mathbf{k} - 1) + \frac{\Delta t}{\rho_m C_m A_m} (\omega_r B - H_t B (T_m(\mathbf{n}, \mathbf{k} - 1) - T_a(\mathbf{k})) - H_t L (T_m(\mathbf{n}, \mathbf{k} - 1) - T_f(\mathbf{n}, \mathbf{k} - 1)))$$

$$T_{f_p}(\mathbf{n}, \mathbf{k}) = T_{f_p}(\mathbf{n}, \mathbf{k} - 1) + \frac{H_t L \Delta t}{\rho_f C_f A_f} (T_m(\mathbf{n}, \mathbf{k} - 1) - T_f(\mathbf{n}, \mathbf{k} - 1))$$

2nd Stage

$$T_f(\mathbf{n}, \mathbf{k}) = T_{f_p}(\mathbf{n}, \mathbf{k}) - \frac{\dot{q} \Delta t}{A_f \Delta x} (T_{f_p}(\mathbf{n}, \mathbf{k}) - T_{f_p}(\mathbf{n} - 1, \mathbf{k}))$$

In these difference equations, $T_f(\mathbf{n}, \mathbf{k})$ and $T_m(\mathbf{n}, \mathbf{k})$ are the temperatures of the fluid and the metal in the segment \mathbf{n} during the \mathbf{k} -th time interval, while $T_a(\mathbf{k})$ is the ambient temperature during the \mathbf{k} -th time interval⁸.

Moreover T_{f_p} is the fluid partial temperature before the temperature correction, while T_f is the final fluid temperature.

Thus, the outputs of the model are:

- Metal temperature of each pipe segment (°C);
- Partial fluid temperature of each pipe segment (°C);
- Final fluid temperature of each pipe segment (°C).

5.1 Implementation of the Model

As said before, in the model, $d\mathbf{x}$ and $d\mathbf{t}$ take the values of 1 meter and 0.5 seconds, respectively. So, the absorber's pipe results to be divided into 64 segments of 1-meter length and the temperatures are calculated every 0.5 seconds⁹.

⁸Ambient temperature is supposed to be the same for each element in the $\mathbf{k} - \mathbf{th}$ time interval.

⁹The time interval is chosen as 0.5 seconds because the maximum value of the water speed in the pipe is about 1 m/s and so calculations can be well performed with this time interval value.

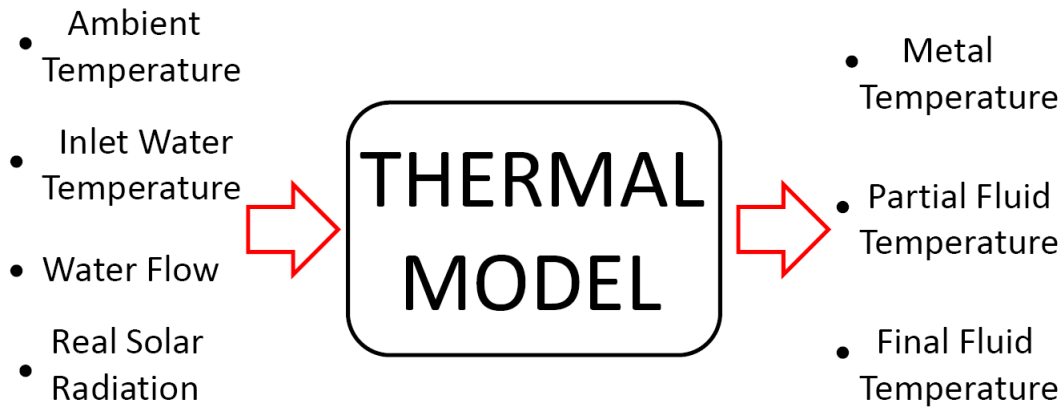


Figure 5.3: Thermal model scheme.

Although all the sizes are needed for a complete description of the process, the only output of the thermal model that can be utilized for a comparison with real data is the final temperature of the last segment of the absorber's pipe.

In fact, as described in section 3.2, there are only two temperature sensors, one at the beginning and the other at the end of absorber's pipe, and so is not possible to compare the temperatures of the model internal segments with the real ones, because these latter are not available.

Neither the metal temperatures of the pipe segments can be compared to the real ones, because there are not sensors to monitor them.

Thus, only the final temperature of the last pipe's segment, i.e. the 64-th, is utilized to set and evaluate the goodness of the model, comparing it to the real outlet water temperature.

As mentioned earlier, all geometrical and structural data of the plant are known and thus the constant values of the model can be determined.

The constant values for the metal¹⁰ are:

- ρ_m , equal to 8027 kg/m^3 ;
- C_m , equal to $0.5 \text{ kJ/kg } ^\circ\text{C}$;
- A_m , equal to 0.00045 m^2 ;
- B^{11} equal to 5.5 m ;
- L , equal to 0.0658 m .

Regarding the equations of the fluid, there are not constant values, except for A_f , whose value is 0.0034 m^2 . In fact, the value of the density and the specific heat capacity of water are not constant, but vary with temperature.

¹⁰Remember that the absorber's pipe is made of stabilized austenitic stainless steel, and has DIN 1.4541 and AISI 321, as explained in section 3.2.

¹¹The value of B is a constant because the effective reflective surface, depending on the inclination value of each row, is already taken into account in real solar radiation calculation (see section 4.3).

So, for each time interval, the following equations expressing the value of ρ_f and C_f in function of the temperature are utilized:

$$\rho_f = 1000 \left[1 - \frac{T + 288.9414}{(508929.2) \cdot (T + 68.12963)} \cdot (T - 3.9863)^2 \right]$$

$$\frac{C_f}{C_{15}} = 0.996185 + 0.0002874 \left(\frac{T + 100}{100} \right)^{5.26} + 0.011160 \cdot 10^{-0.036T}$$

where T is the temperature expressed in $^{\circ}\text{C}$ and C_{15} is the reference specific heat capacity of water at 15°C , equal to $4.1855 \text{ kJ/kg } ^{\circ}\text{C}$.¹²

In Appendix H the values of the density and the specific heat capacity for the temperature range of the plant, obtained with these equations, are reported.

Thus, the only magnitudes that are unknown are the global losses coefficient H_l and the metal-fluid transmission coefficient H_t . These coefficients are typical of the particular process, and so are valid only for the particular dynamics of the plant considered.

H_l and H_t have been expressed as polynomial functions¹³ of the temperature, as follows:

$$T_m(n, k) = T_m(n, k - 1) + \frac{\Delta t}{\rho_m C_m A_m} [a \cdot \omega_r B - B \cdot (b_1 (T_m(n, k - 1) - T_a(k)) + b_2 (T_m(n, k - 1) - T_a(k))^2) - L \cdot (c_1 (T_m(n, k - 1) - T_f(n, k - 1)) + c_2 (T_m(n, k - 1) - T_f(n, k - 1))^2)].$$

$$T_{f_p}(n, k) = T_{f_p}(n, k - 1) + \frac{L \Delta t}{\rho_f C_f A_f} [c_1 (T_m(n, k - 1) - T_f(n, k - 1)) + c_2 (T_m(n, k - 1) - T_f(n, k - 1))^2]$$

where parameters b_1 and b_2 refer to the global losses coefficient H_l , while parameters c_1 and c_2 refer to the metal-fluid transmission coefficient H_t , expressing the effects of H_l and H_t in the real system depending on the temperature.

In the last equations, the parameter a also appears. This parameter is a kind of mirror soiled factor, and takes into account the possible mirror reduction of reflectivity due to the accumulated dirt on the mirrors. The dirt can be caused by dust, sand transported by the wind, rain,....

In the determination of this parameter, weather station data can be considered. The value of a is equal to 1 when mirrors are perfectly clean, for example after a cleaning operation or after a sunny day without wind, otherwise its value is reduced depending

¹²These equations are taken from [20].

¹³Polynomial functions of second degree already give excellent results and therefore polynomials of higher order have not been utilized.



Figure 5.4: Examples of dirty mirror (on the left) and clean mirror (on the right). The parameter α of the model is a cleaning index for mirrors: it is equal to 1 when mirrors are clean and its value decreases as the dirt increases.

on the weather conditions of the previous days, with an experimental algorithm based on real data¹⁴.

The different parameters of the thermal model equations have been determined using real data from the plant, utilizing the least squares method.

5.2 Solving of the Model

The *Least Squares Method* is a standard approach to determine the values of a set of parameters based on squared errors minimization. The overall solution of the least squares method minimizes the sum of the squares of the errors made in solving every single equation.

Its most important application is in data fitting. The best fit in the least-squares sense minimizes the sum of the squared residuals, a residual being the difference between an observed value and the value provided by a model.¹⁵

There are two principal categories of least squares problems: linear least squares and nonlinear least squares, depending on whether or not the residuals are linear in all the parameters. The linear least-squares problem occurs in statistical regression analysis; it has a closed form solution. The non-linear problem has no closed solution and it is usually solved by iterative refinement; at each iteration the system is approximated by a linear one, thus the core calculation is similar in both cases.

As it can be seen from the previous equation, the model developed is linear in the parameters because it comprises a linear combination of the parameters.

So, a numerical algorithm for a linear model is utilized to solve it. This algorithm minimizes the sum of the squared distances between the observed responses in the dataset

¹⁴This parameter has not be included in the calculation of the real solar radiation for two reasons: the first one is the need to test the algorithm, still under development; the other is the possibility to set it always equal to 1 (and so to eliminate it) through daily cleaning

¹⁵For a more detailed description of the least squares method see Appendix I.

and the responses predicted by the linear model. A description of this algorithm is given below.

Each one of the parameterized equation can be written in a general form as a linear function of the parameters:

$$f(x) = \theta_1 f_1(x) + \theta_2 f_2(x) + \cdots + \theta_k f_k(x)$$

where $\theta_1, \dots, \theta_k$ are the k parameters and $k \ll n$, n being the number of known points.

Defining the matrix \mathbf{A} and the vectors $\boldsymbol{\theta}$ and \mathbf{y} as

$$\mathbf{A} = \begin{bmatrix} f_1(x_1) & \cdots & f_k(x_1) \\ \vdots & \ddots & \vdots \\ f_1(x_n) & \cdots & f_k(x_n) \end{bmatrix}, \quad \boldsymbol{\theta} = \begin{bmatrix} \theta_1 \\ \vdots \\ \theta_k \end{bmatrix}, \quad \mathbf{y} = \begin{bmatrix} y_1 \\ \vdots \\ y_n \end{bmatrix}$$

theoretically the model could be expressed in matrix form as

$$\mathbf{y} = \mathbf{A}\boldsymbol{\theta}.$$

But in fact there is always some measurement noise, and so the expression for the real system is

$$\mathbf{y} = \mathbf{A}\boldsymbol{\theta} + \boldsymbol{\epsilon}$$

where $\boldsymbol{\epsilon}$ is the vector of measurement errors.

The objective is to find the value of the parameters vector that best approximates the real data, i.e. the value of the parameters vector that minimizes the measurement error.

Defining the residue as the magnitude of the difference between the value predicted by the model and the real value

$$\|\mathbf{r}\| = \|\mathbf{A}\boldsymbol{\theta} - \mathbf{y}\| = \|\boldsymbol{\epsilon}\|,$$

the problem of minimization according to the least squares method is thus equivalent to the minimization of the sum of the absolute values of the squared residuals:

$$\|\mathbf{r}\|^2 = \|\mathbf{A}\boldsymbol{\theta} - \mathbf{y}\|^2 = ([\mathbf{A}\boldsymbol{\theta}]_1 - y_1)^2 + \cdots + ([\mathbf{A}\boldsymbol{\theta}]_n - y_n)^2 = \sum_{i=1}^n (f(x_i) - y_i)^2 = \mathcal{S}$$

where $[\mathbf{A}\boldsymbol{\theta}]_i$ is the i -th component of the vector obtained by multiplying \mathbf{A} and $\boldsymbol{\theta}$.

The minimum of $\|\mathbf{r}\|^2$ can be obtained by deriving $\|\mathbf{r}\|^2$ with respect to each component θ_m and by imposing that each derivative is equal to zero:

$$\frac{d\|\mathbf{r}\|^2}{d\theta_m} = \sum_{i=1}^n 2\left(\sum_{j=1}^k a_{ij}\theta_j - y_i\right)a_{im} = 0$$

where a_{ij} is the (i, j) th element of the matrix \mathbf{A} .

This last equation can be expressed in matrix form as

$$(\mathbf{A}\boldsymbol{\theta} - \mathbf{y})^T \mathbf{A} = \mathbf{0},$$

so the vector $\bar{\boldsymbol{\theta}}$ that minimizes the sum \mathbf{S} is the solution of the equation

$$\mathbf{A}^T \mathbf{A} \bar{\boldsymbol{\theta}} = \mathbf{A}^T \mathbf{y}.$$

This last equation is called *normal equation*. If \mathbf{A} is of full column rank, then $\mathbf{A}^T \mathbf{A}$ is invertible and so

$$\bar{\boldsymbol{\theta}} = (\mathbf{A}^T \mathbf{A})^{-1} \mathbf{A}^T \mathbf{y}$$

where $(\mathbf{A}^T \mathbf{A})^{-1} \mathbf{A}^T$ is the *pseudo inverse* of \mathbf{A} .

In the second section of the next chapter the results obtained with the thermal model will be reported and the real data will be compared to the values predicted by the model.

Chapter 6

Practical and Experimental Results

In this chapter the results of the plant's optical and thermal model are compared to the real data measured from the plant.

Thus the inclination angle of each mirror row, the proper shadow factor, the receptor shadow factor, the receptor unlit part, the real solar radiation and the water outlet temperature of the plant are confronted with the predictions of the optical and thermal model described in the previous two chapters.

6.1 Optical Model

Inclination of Mirrors Row

The following days of the year have been chosen to compare real data with model data for the inclination of the mirrors rows:

- 21-st of April 2010 (Julian Day 111)
- 27-th of May 2010 (Julian Day 147)

In these days there were no or almost no clouds during the day and so the measurements made were particularly good and reliable.

The measurements of the mirrors rows inclination have been taken for different days at different times and have been then compared to the ones calculated with the optical model.

The data reported refer to the time interval from 13:00 to 15:30 (local time).

The real data have been obtained by Metasys, the software installed in the control units of the plants that allows to control and set the inclination of each mirrors row.

The results of the comparison show that the inclinations calculated by the model¹ are practically equal to the real ones, with a maximum error of 0.3 degrees and a mean error of 0.16 degrees.

In the two tables and graphics below, a comparison between the real data and the prediction of the optical model is reported. The first ones refer to the 21-st April 2010, the second ones refer to the 27-th May 2010.

¹The precision of the inclination performed by the model is of 0.1 degrees.

The screenshot shows the Metasys software interface. On the left is a tree view of system elements, including 'ETSI', 'User Views', 'BACnet Protocol Eng', 'Eth IP Datalink', 'Bus N2', 'HORARIOS', 'PROGRAMAS', 'GRAFICOS', 'BACnet', and 'PSE'. The main window displays a table with columns for 'Estado', 'Elemento', 'Valor', and 'Descripción'. The table lists various mirror positions and setpoints with their corresponding values and descriptions.

Estado	Elemento	Valor	Descripción
Normal	Mirror Position 2.01	45,9 ° angul...	Posicionamiento Espejo 2.01
Normal	Mirror Position 1.11	4,7 ° angul...	Posicionamiento Espejo 1.11
Normal	Mirror Position 1.10	7,8 ° angul...	Posicionamiento Espejo 1.10
Normal	Mirror Position 1.09	11,5 ° angul...	Posicionamiento Espejo 1.09
Normal	Mirror Position 1.08	15,7 ° angul...	Posicionamiento Espejo 1.08
Normal	Mirror Position 1.07	20,3 ° angul...	Posicionamiento Espejo 1.07
Normal	Mirror Position 1.06	25,2 ° angul...	Posicionamiento Espejo 1.06
Normal	Mirror Position 1.05	30,2 ° angul...	Posicionamiento Espejo 1.05
Normal	Mirror Position 1.04	35,0 ° angul...	Posicionamiento Espejo 1.04
Normal	Mirror Position 1.03	39,1 ° angul...	Posicionamiento Espejo 1.03
Normal	Mirror Position 1.02	42,6 ° angul...	Posicionamiento Espejo 1.02
Normal	Mirror Position 1.01	45,9 ° angul...	Posicionamiento Espejo 1.01
Normal	Percentage Focus	1,0	Standby-Enfoque Espejos
Normal	AI Percentage Focus	9.976,0	0-10V Standby-Enfoque Espejos
Normal	Mirror Setpoint 1.06	25,2 ° angul...	Consigna Espejo 1.06
Normal	Mirror Setpoint 1.05	30,1 ° angul...	Consigna Espejo 1.05
Normal	Mirror Setpoint 1.04	34,8 ° angul...	Consigna Espejo 1.04
Normal	Mirror Setpoint 1.03	39,0 ° angul...	Consigna Espejo 1.03
Normal	Mirror Setpoint 1.02	42,7 ° angul...	Consigna Espejo 1.02
Normal	Mirror Setpoint 1.01	45,8 ° angul...	Consigna Espejo 1.01
Normal	Mirror Position 2.11	4,8 ° angul...	Posicionamiento Espejo 2.11
Normal	Mirror Position 2.10	7,9 ° angul...	Posicionamiento Espejo 2.10
Normal	Mirror Position 2.09	11,4 ° angul...	Posicionamiento Espejo 2.09
Normal	Mirror Position 2.08	15,7 ° angul...	Posicionamiento Espejo 2.08
Normal	Mirror Position 2.07	20,3 ° angul...	Posicionamiento Espejo 2.07
Normal	Mirror Position 2.06	25,2 ° angul...	Posicionamiento Espejo 2.06
Normal	Mirror Position 2.05	30,2 ° angul...	Posicionamiento Espejo 2.05
Normal	Mirror Position 2.04	34,9 ° angul...	Posicionamiento Espejo 2.04
Normal	Mirror Position 2.03	39,1 ° angul...	Posicionamiento Espejo 2.03
Normal	Mirror Position 2.02	42,7 ° angul...	Posicionamiento Espejo 2.02
Normal	Mirror Setpoint 2.11	4,7 ° angul...	Consigna Espejo 2.11
Normal	Mirror Setpoint 2.10	7,7 ° angul...	Consigna Espejo 2.10
Normal	Mirror Setpoint 2.09	11,4 ° angul...	Consigna Espejo 2.09
Normal	Mirror Setpoint 2.08	15,6 ° angul...	Consigna Espejo 2.08
Normal	Mirror Setpoint 2.07	20,2 ° angul...	Consigna Espejo 2.07
Normal	Mirror Setpoint 2.06	25,2 ° angul...	Consigna Espejo 2.06
Normal	Mirror Setpoint 2.05	30,1 ° angul...	Consigna Espejo 2.05
Normal	Mirror Setpoint 2.04	34,8 ° angul...	Consigna Espejo 2.04
Normal	Mirror Setpoint 2.03	39,0 ° angul...	Consigna Espejo 2.03
Normal	Mirror Setpoint 2.02	42,7 ° angul...	Consigna Espejo 2.02
Normal	Mirror Setpoint 2.01	45,8 ° angul...	Consigna Espejo 2.01
Normal	Mirror Setpoint 1.11	4,7 ° angul...	Consigna Espejo 1.11
Normal	Mirror Setpoint 1.10	7,8 ° angul...	Consigna Espejo 1.10
Normal	Mirror Setpoint 1.09	11,4 ° angul...	Consigna Espejo 1.09
Normal	Mirror Setpoint 1.08	15,6 ° angul...	Consigna Espejo 1.08
Normal	Mirror Setpoint 1.07	20,2 ° angul...	Consigna Espejo 1.07
Normal	T Collector Out	18,1 ° C	Temperatura Salida Colector

Figure 6.1: Visual representation of a Metasys screen, the software utilized by the plant to calculate the inclination of each mirrors row.

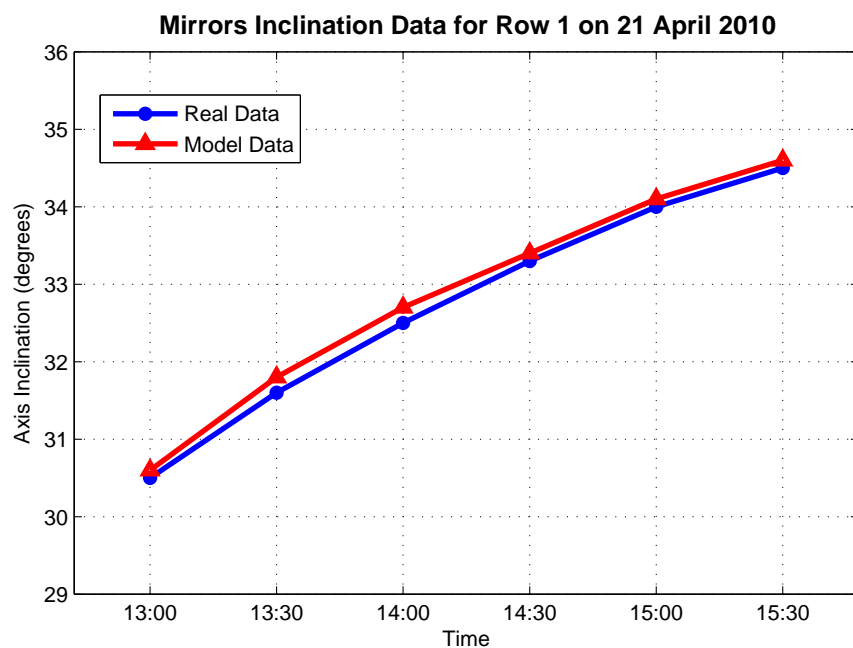
In the tables the values of the mirrors inclinations (in degrees) for each row from 13 to 15.30 are reported. For each row, the values in the column labeled with the letter M are the ones provided by the model while the values in the column labeled with the letter R are the real ones. Model and real values differ very little, as it can be inferred from the tables.

Each row of the tables gives a description of the time evolution of a particular mirrors row, while each column gives a global description of the inclination of all the mirrors rows, but for a particular instant of time. In the tables the local time and the solar time are also reported.

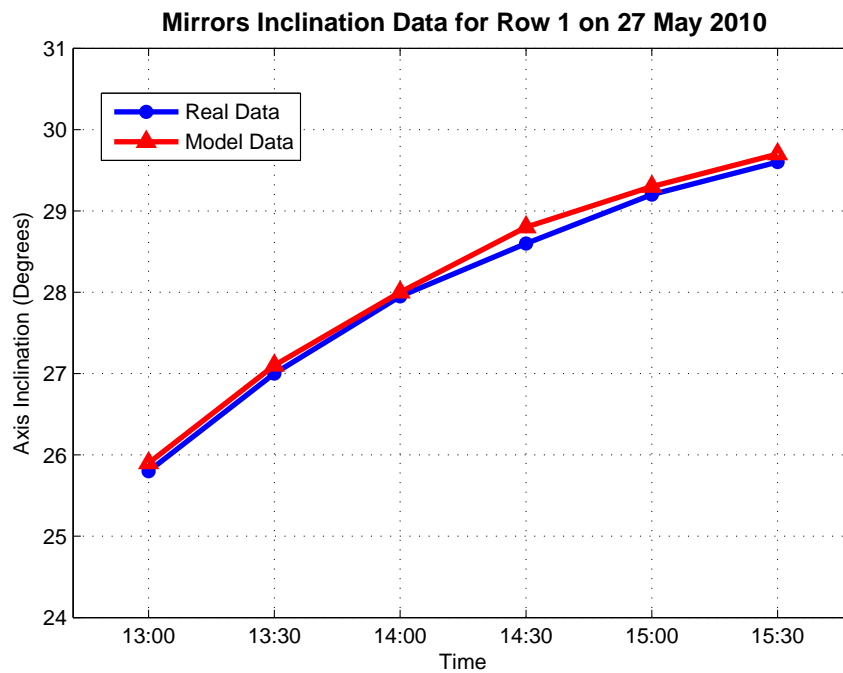
In the figures the graphs of the real and the model data, for the first mirrors row, are compared. In these figures the movement of the mirrors rotation in order to keep reflecting sunlight onto the absorber pipe can be appreciated. Furthermore from the graphics it can be seen that the values predicted by the model are always above the real ones. This happens because the calculation of the mirrors row inclination is made taken into account the solar elevation and other solar magnitudes, expressed by equations that are an approximation in excess of natural phenomena².

²Note that the approximation is excellent because the difference between real and model data is in the order of tenths of a degree.

MIRRORS INCLINATION DATA (degrees) FOR THE DAY 21 APRIL 2010												
Local Time	13:00		13:30		14:00		14:30		15:00		15:30	
Solar Time	10:37		11:07		11:37		12:07		12:37		13:07	
	M	R	M	R	M	R	M	R	M	R	M	R
Row 1	30.6	30.5	31.8	31.6	32.7	32.5	33.4	33.3	34.1	34.0	34.6	34.5
Row 2	27.7	27.5	28.7	28.5	29.6	29.5	30.1	30.1	31.0	30.9	31.5	31.3
Row 3	24.1	24.0	25.1	25.1	26.0	25.9	26.7	26.4	27.3	27.1	27.8	27.6
Row 4	19.9	19.7	20.9	20.8	21.8	21.6	22.5	22.4	23.1	22.9	23.6	23.4
Row 5	15.2	15.0	16.2	16.0	17.1	16.8	17.8	17.6	18.4	18.3	19.0	18.8
Row 6	10.2	10.0	11.3	11.1	12.1	12.0	12.8	12.6	13.5	13.4	14.0	13.9
Row 7	5.3	5.2	6.3	6.1	7.2	7.2	7.9	7.8	8.5	8.3	9.0	8.9
Row 8	0.6	0.4	1.6	1.5	2.5	2.4	3.2	3.2	3.8	3.8	4.3	4.1
Row 9	-3.6	-3.7	-2.6	-2.7	-1.7	-1.9	-1.0	-1.1	-0.4	-0.6	0.1	-0.1
Row 10	-7.3	-7.5	-6.2	-6.3	-5.4	-5.5	-4.7	-4.7	-4.0	-4.2	-3.5	-3.6
Row 11	-10.4	-10.5	-9.3	-9.3	-8.5	-8.6	-7.8	-7.9	-7.1	-7.3	-6.6	-6.7



MIRRORS INCLINATION DATA (degrees) FOR THE DAY 27 MAY 2010												
Local Time	13:00		13:30		14:00		14:30		15:00		15:30	
Solar Time	10:39		11:09		11:39		12:09		12:39		13:09	
	M	R	M	R	M	R	M	R	M	R	M	R
Row 1	25.9	25.8	27.1	27.0	28.0	28.0	28.8	28.6	29.3	29.2	29.7	29.6
Row 2	22.8	22.7	24.0	24.0	24.9	24.8	25.7	25.7	26.2	26.0	26.7	26.5
Row 3	19.2	19.2	20.4	20.2	21.3	21.3	22.0	21.8	22.6	22.5	23.1	22.9
Row 4	15.0	14.9	16.2	16.1	17.1	17.0	17.8	17.5	18.4	18.2	18.8	18.6
Row 5	10.3	10.2	11.5	11.3	12.4	12.3	13.1	13.1	13.7	13.5	14.1	14.0
Row 6	5.3	5.2	6.5	6.3	7.4	7.3	8.2	8.0	8.7	8.5	9.2	9.1
Row 7	0.4	0.2	1.5	1.3	2.5	2.3	3.2	3.1	3.8	3.6	4.2	4.1
Row 8	-4.3	-4.3	-3.1	-3.2	-2.2	-2.3	-1.5	-1.7	-0.9	-1.1	-0.5	-0.6
Row 9	-8.5	-8.6	-7.3	-7.5	-6.4	-6.5	-5.7	-5.9	-5.1	-5.2	-4.7	-4.8
Row 10	-12.1	-12.3	-11.0	-11.2	-10.1	-10.1	-9.3	-9.4	-8.7	-8.8	-8.3	-8.5
Row 11	-15.4	-15.5	-14.1	-14.2	-13.2	-13.4	-12.4	-12.5	-11.8	-12.0	-11.4	-11.6



Receptor Unlit Part

The same two days of the year utilized in the previous section have been chosen to compare the receptor real unlit part with the prediction of the model:

- 21-st of April 2010 (Julian Day 111)
- 27-th of May 2010 (Julian Day 147)

The measurements of the receptor unlit part have been taken in different days at different times, and have then been compared to the ones calculated with the optical model.

The measurements accuracy in this case is relatively low, of the order of centimeters, due to the difficult access to the receptor's tube.

In the following tables, the letters E and W on the right of the measurement indicate if the unlit part is on the East (E) or on the West (W) side of the plant³.

21 April 2010

In the following table, real and model data of the receptor's unlit part are reported, referred to the 21-st of April 2010.

Local Time	Solar Time	Receptor Unlit Part (m) <i>Model</i>	Receptor Unlit Part (m) <i>Real</i>
13:00	10:37	2.14 E	2.15 E
13:30	11:07	1.56 E	1.62 E
14:00	11:37	0.89 E	0.83 E
14:30	12:07	0.13 W	0.11 W
15:00	12:37	0.38 W	0.40 W
15:30	13:07	0.65 W	0.61 W

27 May 2010

In the following table, real and model data of the receptor's unlit part are reported, referred to the 27-th of May 2010.

Local Time	Solar Time	Receptor Unlit Part (m) <i>Model</i>	Receptor Unlit Part (m) <i>Real</i>
13:00	10:39	1.63 E	1.61 E
13:30	11:09	1.11 E	1.15 E
14:00	11:39	0.67 E	0.65 E
14:30	12:09	0.12 W	0.11 W
15:00	12:39	0.46 W	0.44 W
15:30	13:09	0.92 W	0.95 W

³For a detailed description of the receptor's unlit part see section 4.3.

As it can be inferred from the tables, the receptor's unlit part is on the east side of the plant before noon and on the west side after noon.

The difference between the real values and the ones calculated by the model is very small, with a maximum error value of 8 centimeters and a mean error of 3.7 centimeters.

The difference between real and model data is principally due to three factors:

- The calculations are made taken into account solar elevation and other solar magnitudes, expressed by equations that are an approximation of the natural phenomena;
- The possible advancement or delay of the clock taken as reference for the local time;
- The difficulty of taking an accurate measure of the real unlit part.

Proper Shadow Factor

In this section the calculation of the proper shadow factor is performed. In the days considered in the previous sections there was no mirrors proper shadow in the time interval considered, and so other two days have been chosen:

- 12-th of February 2010 (Julian Day 43)
- 16-th of March 2010 (Julian Day 75).

In the days considered mirrors cast shadows; in particular, these days have been chosen to highlight the different evolution of the shadow during the day.

However an important clarification has to be make.

It has been impossible to measure the real entity of the shadows, because the data available were not adequate to give a precise measurement of the shadow entity.

Thus, instead of utilizing and considering data with a high rate of inaccuracy, only optical model prediction data have been reported, unfortunately without the possibility of comparison with the real ones.

The time interval considered is wider than the one considered in the previous section, in order to better appreciate the variation and the evolution of the proper mirror shadow throughout the day.

12 February 2010

In the table at the top of Figure 6.2, the proper shadow proportion⁴, defined as the ratio between the proper mirror shaded area and the total collector area, and the proper shadow factor, defined as the complement to the unit for the proper shadow proportion, are reported.

As it can be seen from the graphic at the bottom of Figure 6.2, there is proper mirror shadow throughout the day. The curve has a trend that resembles a parable, with a maximum value at the 11:30, that corresponds to a minimum value for the shadow extension.

⁴For a more detailed description see section 4.2.2.

Local Time	Solar Time	Proper Shadow Proportion	Proper Shadow Factor
10:00	8:22	0.2012	0.7988
10:30	8:52	0.1774	0.8226
11:00	9:22	0.1680	0.8320
11:30	9:52	0.1673	0.8327
12:00	10:22	0.1725	0.8275
12:30	10:52	0.1823	0.8177
13:00	11:22	0.1960	0.8040
13:30	11:52	0.2134	0.7866
14:00	12:22	0.2348	0.7652
14:30	12:52	0.2604	0.7396
15:00	13:22	0.2910	0.7090
15:30	13:52	0.3277	0.6723
16:00	14:22	0.3720	0.6280
16:30	14:52	0.4264	0.5736
17:00	15:22	0.4941	0.5059
17:30	15:52	0.5802	0.4198

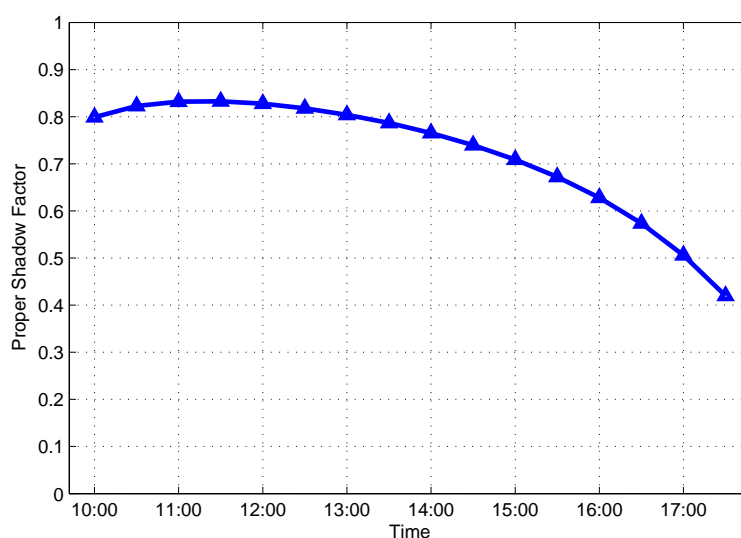


Figure 6.2: Proper shadow data for the day 21 April 2010: data table (on the top) and the graphic of the proper shadow factor trend throughout the day.

16 March 2010

In the table at the top of Figure 6.3, the proper shadow proportion and the proper shadow factor are reported.

As it can be inferred from the graphic at the bottom of Figure 6.3, the reflective surface is totally available until 12:30, when the proper mirrors shadow begins to be produced.

From this time, the shadow entity increases gradually during the day, but starting later than in the previous example, the shadow does not reach the same extension.

Local Time	Solar Time	Proper Shadow Proportion	Proper Shadow Factor
10:00	8:23	0.0000	1.0000
10:30	8:53	0.0000	1.0000
11:00	9:23	0.0000	1.0000
11:30	9:53	0.0000	1.0000
12:00	10:23	0.0000	1.0000
12:30	10:53	0.0033	0.9967
13:00	11:23	0.0098	0.9902
13:30	11:53	0.0187	0.9813
14:00	12:23	0.0296	0.9704
14:30	12:53	0.0429	0.9571
15:00	13:23	0.0595	0.9405
15:30	13:53	0.0811	0.9189
16:00	14:23	0.1109	0.8891
16:30	14:53	0.1520	0.8480
17:00	15:23	0.2021	0.7979
17:30	15:53	0.2663	0.7337

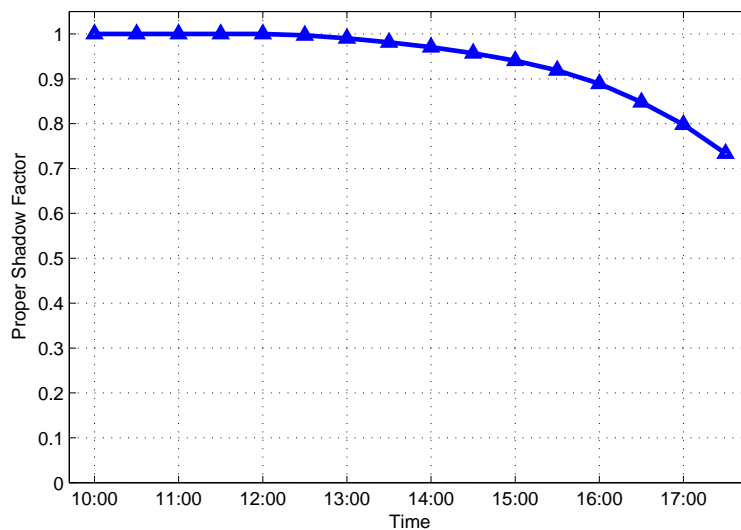


Figure 6.3: Proper shadow data for the day 27 May 2010: data table (on the top) and the graphic of the proper shadow factor trend throughout the day.

Thus, during this day, the mean of the available reflective surface is greater than in the previous example, allowing for a better exploitation of the plant.

By the studies made on the plant, based on data collected on the last two years, it can be inferred that the shadow entity has a decreasing trend from the beginning of the year until the middle of April. In fact, from the middle of April the shadow is null⁵ and it begins again starting from the last days of August.

⁵This statement is true in reference to daily operating time of the plant, that is from 10 to 19.

Receptor Shadow Factor

In this section the calculation of the receptor shadow factor is performed. The days considered for the calculation are the same as in the previous section, i.e.:

- 12-th of February 2010 (Julian Day 43)
- 16-th of March 2010 (Julian Day 75).

Also for the receptor shadow factor computation it has been impossible to measure the real entity of the shadow and so only optical model prediction data have been reported, without the possibility of a comparison with real data.

12 February 2010

In the table below, the receptor shadow proportion⁶, defined as the ratio between the area of the receptor shadow and the total collector area, and the receptor shadow factor, defined as the complement to the unit of the receptor shadow proportion, are reported.

Local Time	Solar Time	Receptor Shadow Proportion	Receptor Shadow Factor
10:00	8:22	0.0000	1.0000
10:30	8:52	0.0000	1.0000
11:00	9:22	0.0091	0.9909
11:30	9:52	0.0121	0.9879
12:00	10:22	0.0204	0.9796
12:30	10:52	0.0159	0.9841
13:00	11:22	0.0186	0.9814
13:30	11:52	0.0243	0.9757
14:00	12:22	0.0299	0.9701
14:30	12:52	0.0212	0.9788
15:00	13:22	0.0225	0.9775
15:30	13:52	0.0322	0.9678
16:00	14:22	0.0186	0.9814
16:30	14:52	0.0091	0.9909
17:00	15:22	0.0000	1.0000
17:30	15:52	0.0000	1.0000

In Figure 6.4, the different values of receptor shadow factor throughout the day are represented.

As it can be inferred by the graphic, the shadow produced by the receptor's pipe is very small, especially if compared to the total reflective area.

In fact, the shadow due to the receptor does not reach even 5% of the total reflective area, and so the receptor's shadow factor is usually greater than the proper shadow factor.

The trend of the curve is different from the one in the previous section, and seems a little more irregular. This is due mainly to two causes: the first is that the values of two consecutive samples differ very little, the second is that in the computation of the factor, the variations of the blank spaces between mirrors⁷ are taken into account.

⁶For more details see section 4.2.2.

⁷For more details see section 4.2.2.

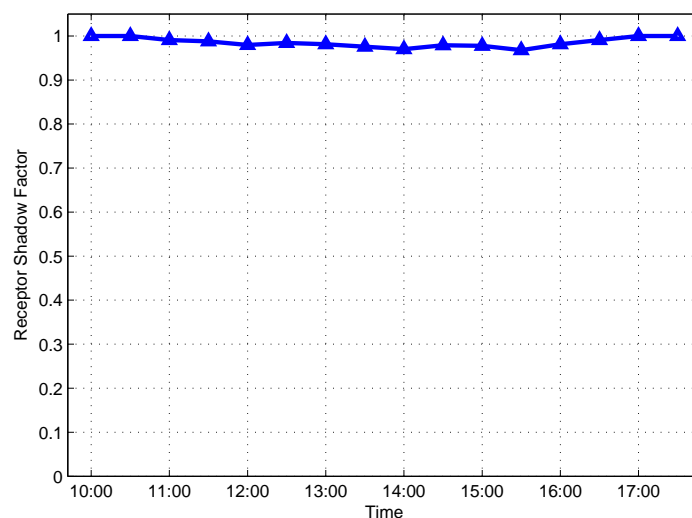


Figure 6.4: Graphic of proper shadow factor trend for the day 12 February 2010.

16 March 2010

In the table below, the receptor's shadow proportion and the receptor shadow factor are reported.

Local Time	Solar Time	Receptor Shadow Proportion	Receptor Shadow Factor
10:00	8:23	0.0000	1.0000
10:30	8:53	0.0053	0.9947
11:00	9:23	0.0111	0.9889
11:30	9:53	0.0163	0.9837
12:00	10:23	0.0101	0.9899
12:30	10:53	0.0232	0.9768
13:00	11:23	0.0266	0.9734
13:30	11:53	0.0211	0.9789
14:00	12:23	0.0283	0.9717
14:30	12:53	0.0321	0.9679
15:00	13:23	0.0354	0.9646
15:30	13:53	0.0298	0.9702
16:00	14:23	0.0244	0.9756
16:30	14:53	0.0169	0.9831
17:00	15:23	0.0073	0.9927
17:30	15:53	0.0013	0.9987

In Figure 6.5, the different values of the receptor's shadow factor during the day are represented.

The shadow produced by the receptor's pipe, as said before, is very small and not reach even the 5 % of the total reflective area.

In this case, the shadow affects the reflective area longer than the previous case one because the hours of sunlight increase approaching summer.

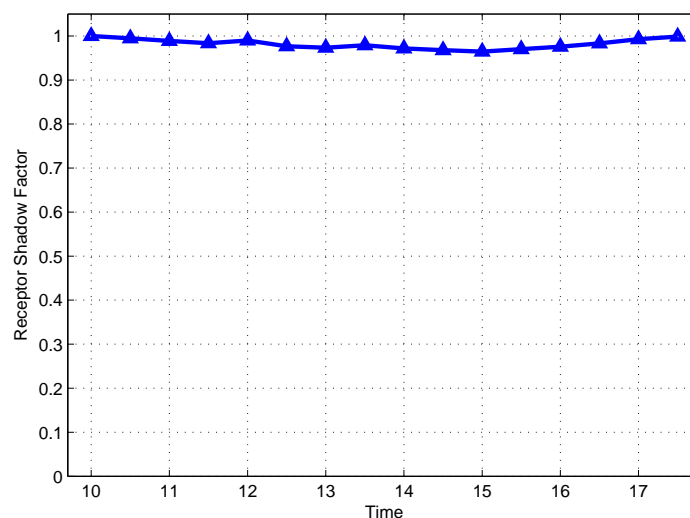


Figure 6.5: Graphic of proper shadow factor trend for the day 16 March 2010.

Thus the receptor's shadow has an opposite behavior with respect to the proper shadow one, due to the solar elevation and to the sun position throughout the day above the plant.

Solar Radiation

In this section the calculation of the real solar radiation is performed. The real solar radiation will be used in the thermal model and so the days chosen for the calculation of this section will be the same for the next section. The days considered for the computation are:

- 21-st of April 2010 (Julian Day 111)
- 27-th of May 2010 (Julian Day 147).

The real solar radiation is the percentage of the direct solar radiation, in Watt, that is reflected by the mirrors reflective surface onto the absorber's pipe.

As it was said in section 4.3, the level of cleanliness of the mirrors is not taken into account in the computation of the real solar radiation, but it is instead considered in the thermal model with the parameter α . Clearly, if the mirrors are dirty, the reflected radiation is reduced and furthermore the solar rays can be deviated without reaching the receptor.

In the following calculations a distinction between real solar radiation and effective solar radiation is made.

In fact, the real solar radiation computed by the optical model developed in chapter 4 has to be multiplied by the percentage of mirrors that are in operating state at each time instant to obtain the effective solar radiation that really reaches the receptor.

The percentage of operating mirrors is obtained by the Control and Supervision System of the plant, that provides these data in real-time.

The effective solar radiation data calculated in this section will be then utilized as input data for the thermal model in the next section, to compute the water outlet temperature.

21 April 2010

In the table below the direct radiation data, the real solar radiation data, the effective solar radiation data and the percentage of operating mirrors are reported.

Local Time	Solar Time	Direct Radiation (W/m^2)	Real Radiation (W)	Operating Mirrors (%)	Effective Radiation (W)
13:00	10:37	930.7	140680	100.0	140680
13:30	11:07	944.5	143570	52.5	75374
14:00	11:37	964.4	147290	49.5	72908
14:30	12:07	970.2	148850	42.7	63559
15:00	12:37	961.8	146870	42.5	62420
15:30	13:07	955.1	143940	45.3	65205

The direct radiation data are expressed in W/m^2 , while the real radiation data and the effective radiation data are expressed in W because they take into account the available reflective surface⁸.

As it can be inferred from the table, the percentage of operating mirrors affects significantly the effective radiation that reaches the absorber's pipe.

In this case, after the 14:00, the percentage of operating mirrors is stable below 50%, and this could lead to erroneously think that the system does not work well.

But one should remember that the plant has a control system that, monitoring the water temperature in the absorber's pipe, sets a percentage of mirrors in dull position⁹ when the water temperature is near to 180° C, not to permit the temperature to exceed it.

This means that, in the day considered, the plant is well functioning, and due to a particularly clear and warm day, the radiation reflected by only approximately 50 % of the mirrors is sufficient to maintain the optimal temperature.

27 May 2010

In the table below the direct radiation data, the real solar radiation data, the effective solar radiation data and the percentage of operating mirror are reported.

In this day, the percentage of operating mirrors during the day is greater than the in the previous case.

As it can be noted by comparing the two day direct radiation data, in the day considered the radiation intensity is on the average nearly 100 W/m^2 less than the one of the 21-th of April, and hence to maintain the optimal water temperature more reflective surface is needed.

But in this day, another factor that has to be considered is the wind.

⁸For more details see section 4.3.

⁹See section 3.2 on drive actuator.

Local Time	Solar Time	Direct Radiation (W/m^2)	Real Radiation (W)	Operating Mirrors (%)	Effective Radiation (W)
13:00	10:39	867.0	149900	100.0	149900
13:30	11:09	872.9	152300	100.0	152300
14:00	11:39	875.7	153930	96.7	148850
14:30	12:09	864.0	152910	83.6	127830
15:00	12:39	882.3	154990	57.1	88499
15:30	13:09	884.1	153680	68.6	105420

In fact, in case of wind, with the same radiation, more reflective surface is needed because the metal thermal losses increase¹⁰.

6.2 Thermal Model

In this section, the predictions of the thermal model and the real data are compared, in order to prove and test the goodness of the model.

The water outlet temperature is the only magnitude that can be compared with the real data. In fact, as explained in chapter 5, the water outlet temperature, together with the inlet one, are the only available temperatures for the plant.

In the distributed parameters model, the water outlet temperature corresponds to the temperature of the 64-th segment of the receptor's pipe.

The days that have been chosen for the comparison are the same utilized for the solar radiation calculation in the previous section, because the effective solar radiation is one of the inputs of the thermal model.

The selected days are:

- 21-st of April 2010 (Julian Day 111)
- 27-th of May 2010 (Julian Day 147).

21 April 2010

In the figure below, the trend of the water outlet temperature in °C is reported.

As it can be inferred from the figure, the model prediction data fit very well the real ones.

The reason of this optimal model behavior is that this day was particularly good, in the sense that there was almost no clouds nor wind.

This last natural element should not be underestimated: the effects of its presence will be seen in the next day data.

The fluctuations of the curve are due to the passage of clouds or to the dull position of the mirrors to prevent the water temperature rises, too. In fact, in a day like the one considered, the intensity of the radiation is so high that if all the mirrors were in

¹⁰The wind effect will be analyzed in details in the next section.

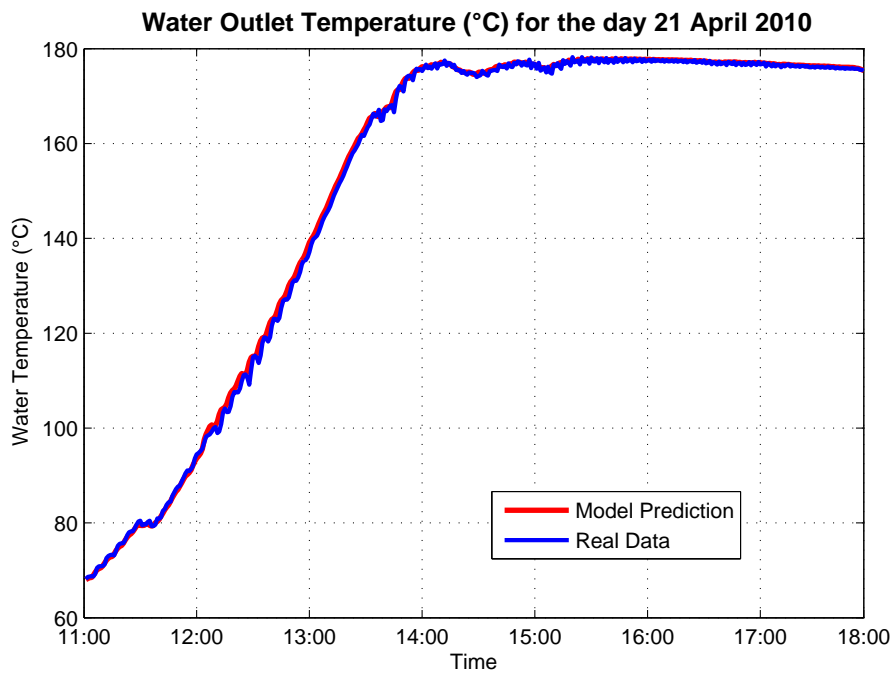


Figure 6.6: Comparison between the model prediction and the real data of water outlet temperature for the day 21 April 2010.

the operating position, the water temperature would increase up to exceed the maximum temperature allowed.

Anyway, the graphic has not to deceive, because the range of temperatures reported is very high, and so the difference between the model data and the real data appears smaller that it really is.

For this purpose, the two following particular images are reported.

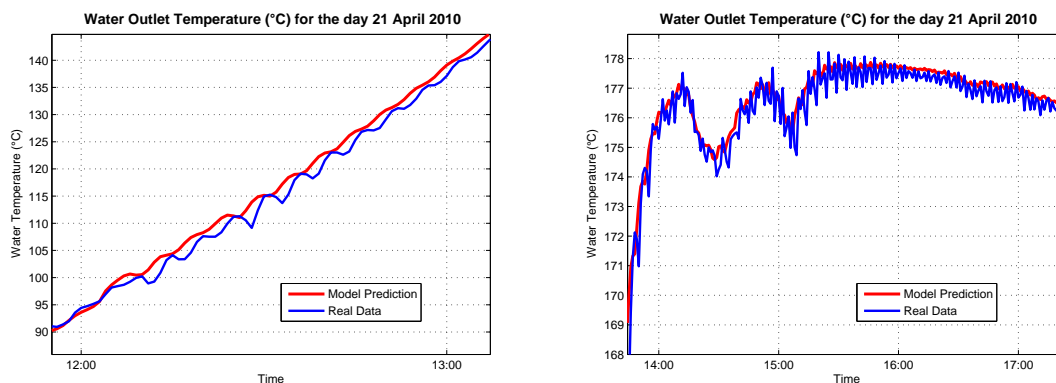


Figure 6.7: Particulars of the Figure 6.6. : on the left a particular of the transient; on the right a particular of the steady state with small fluctuations.

The graphic of the water outlet temperature is usually decomposed into two parts: the transient and the steady state.

The transient time is the time that the fluid takes to reach the 95 % of the maximum permitted value for the temperature. Clearly this time is not fixed, but it depends on the weather conditions, principally on the solar radiation's intensity.

The steady state is the part of the graphic in which the temperature of the fluid is at its operating point. The curve in this section should be as flat as possible, but in a solar plant this is very difficult because there is a factor that cannot be controlled: the weather.

In the transient section the maximum difference between the temperature of the model prediction and the real one is 5°C . The oscillatory behavior that can be seen on the left side of Figure 6.7 is partly due to the noise measurement and partly due to passage of small rarefied clouds.

On the right side of Figure 6.7, there is instead a particular of the temperature curve corresponding to the passage of two banks of clouds. The two oscillations of the curve are not only due to clouds, but also to the concomitant reduction of the operating mirrors caused by the elevated water temperature.

Again, the model curve is very similar to the real one.

27 May 2010

In the figure below, the trend of the water outlet temperature in $^{\circ}\text{C}$ is reported.

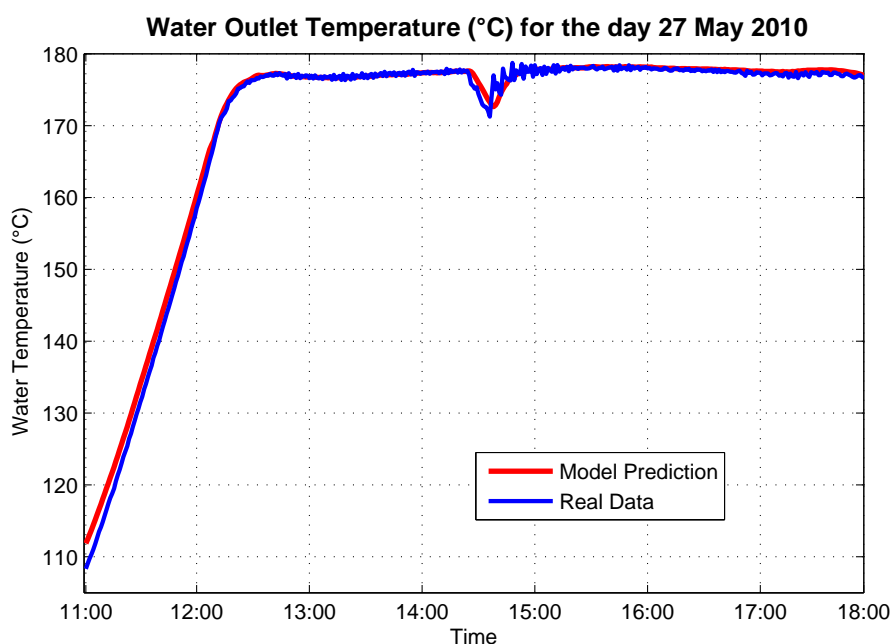


Figure 6.8: Comparison between the model prediction and the real data of water outlet temperature for the day 27 May 2010.

The model curve follows very well the real one, but compared to the previous day graphic, this time the difference between the real data and the model data is greater, especially in the first and in the last part of the curve.

This difference is principally due to the wind, that especially from the 9:00 to the 12:00 and from the 16:30 to the 19:00 blew incessantly and firmly.

Two different aspects and consequences of the wind presence are analyzed in the particulars reported in the following figure.

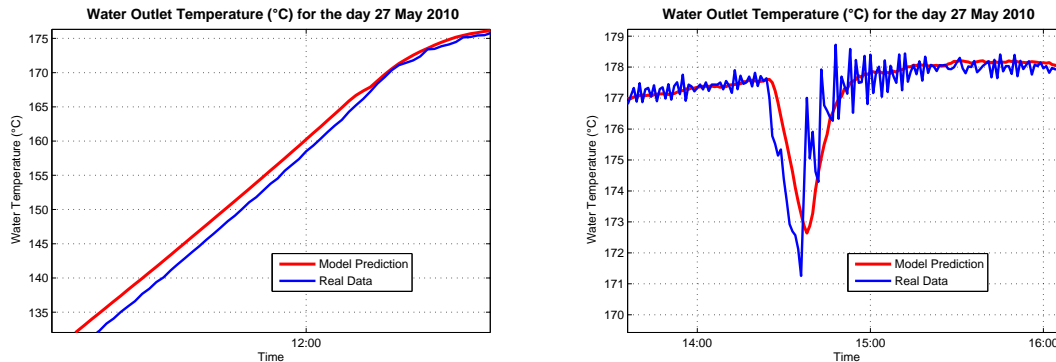


Figure 6.9: Particulars of the Figure 6.8: on the left a particular of the transient; on the right a particular of the steady state.

In the left side of Figure 6.9 a particular of the transient is reported. As it can be seen from the graphic, the curve of the model is above the curve of real data. This is due to the wind.

In fact, the presence of the wind, especially of strong wind, influences the thermal balance of the metal, increasing the thermal losses to the ambient and reducing the sunray capacity to heat the metal walls. Accordingly the model, that has not a parameter which takes into account the wind effect¹¹, has values that are greater than the real ones.

In the right side of Figure 6.9 there is a particular of the steady state, in which the graphic has a negative peak, due to the passage of a bank of clouds over the plant.

The model has a delay in following the unexpected and sudden changes. This delay is due again to the wind.

In fact, as it was said before, the wind presence alters the energy balance in the absorber's tube, accelerating the cooling of the walls, and so the model cannot follow this change so fast as in reality, accumulating delay.

A final clarification: the trend of the model curve is not as linear as expected, because among all inputs of the model there are the water inlet temperature and the caudal that are affected by the measurement noise.

The model, as it can be inferred from the graphics reported, follows very well the real trend, with the limits due to the unpredictability of the weather.

A further comparison between real and model data is made, for the day 17-th of November 2009. This day was a particularly bad day, with a lot of clouds and wind.

The comparison between real and model data for this day is reported in Figure 6.10.

The system, as can be seen in the Figure, has a transient until the 12:00, that well follows from the model, but then it does not reach a steady state.

In fact, the intensity of the solar radiation, due to the season, is not so elevated to allow the temperature to reach 180°C.

¹¹The wind dynamic is very complicated and it is not easy to express its effects on a solar plant. These effects depend not only on the wind force, but also on the wind direction and the air temperature. The wind dynamic and its relation with a solar plant are still under study.

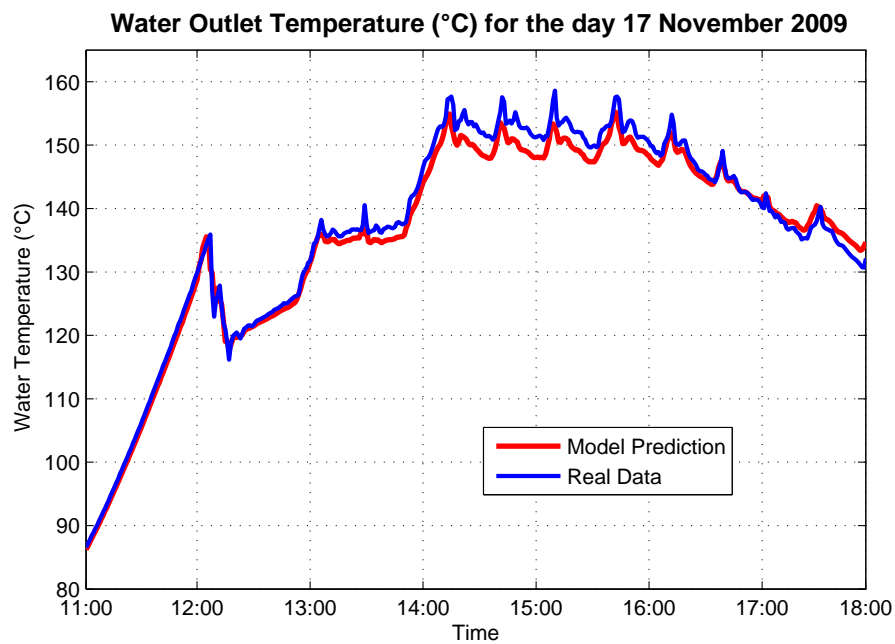


Figure 6.10: Comparison between the model prediction and the real data of water outlet temperature for the day 17 November 2009.

Moreover, the presence of banks of clouds hinders further temperature increase and results in a series of peaks that are still followed well enough by the model with a maximum difference between real and model data of about 8 °C.

This difference is not excessive, because the control systems, for installations of the type considered, have a tolerance of up to 10 degrees for it.

This ulterior test evidences the robustness of the distributed parameters model, that gives good results also in days with bad weather conditions.

Chapter 7

Conclusions and Future Developments

This Project has been realized in the solar plant of the “Escuela Superior de Ingenieros” of Seville’s University.

Two different models have been developed and realized: an *optical model* and a *thermal model*.

The optical model has been implemented in MATLAB and provides all the magnitudes and quantities necessary to optically characterize the reflective mirrors and the receptor.

The study and analysis performed on the data collected have highlighted the following facts:

- The small difference between real and model data is partly due to the possible advancement or delay of the clock taken as reference for the local time and partly due to the equations utilized to calculate the astronomical magnitudes, that cannot be exact because describe natural phenomena;
- The ray of curvature of mirrors is a fundamental factor for the efficiency of the system. In fact, the ray of curvature utilized is a compromise between a small one, excellent in performance but very expensive, and a flat one, very cheap but with poor performance.

The choice of a different ray of curvature for the internal and external mirrors row, with a ray of curvature of respectively 8.6 meters and 10.6 meters, further contributes to increase benefits in terms of reflectivity;

- The cleanness of the mirrors is not a fundamental factor to be taken into account. Clearly, if the mirrors are dirty, their reflectivity is reduced, but the problem can be eliminated with daily cleaning.

The thermal model has also been implemented in MATLAB and, exploiting the energy balance in the absorber’s tube, provides the water outlet temperature that can be compared with the real one.

The principal considerations arisen from the analysis performed on data are the following:

- ▼ The soiling factor of the glass cover is very difficult to estimate. The glass cover cannot be cleaned often because of its inaccessibility, so it gets dirtier every day and this leads to a reduction of its transmittance. From the data analyzed, the soiling factor for the glass cover has been estimated to range between 0.8 and 0.9;

- ▼ The mirrors transition from the operating state to the dull state influences the model. In fact, when the water temperature is near to the maximum set value, a percentage of mirrors is set in the dull state to prevent to exceed it. This transition can cause a delay in the model response or an excessive difference between real and model temperature;
- ▼ The wind is an important natural factor that should be taken into account. As seen in the last chapter, the presence of strong wind modifies the energy balance of the receptor, reducing the heating power of the solar radiation and accelerating the cooling of the metal.

The models developed are very good in terms of performance. The optical one is precise and well describe the dynamic of the reflection process of the solar radiation while the thermal one is robust and reliable even in the case of bad weather, as evidenced by the simulations of the previous chapter.

Clearly, these models are not definitive, but could be improved on the basis of the experimental results obtained and of the considerations made.

The main future developments and improvements that can be done are:

- ◆ Clean more frequently¹ the glass cover, in order to maintain its soiling factor near the unit value;
- ◆ Set the percentage of the operating mirrors based on the effective solar radiation intensity rather than on the water temperature, in order to avoid the continuous mirrors movement from operating position to dull position and vice versa;
- ◆ Set a different operation time for the plant, differentiating according to seasons. In particular, delay time of plant closure on spring and summer to exploit more hours of sunshine;
- ◆ Model the wind effect on the plant, or derive a wind factor from the data and simulations made, that takes into account the wind effects on the particular plant considered;
- ◆ In a plant of the same typology, a better solution could be to change the receptor's position.

In particular, change the receptor's pipe position by placing it in the north extreme rather than in the middle of the solar collectors.

In this way the receptor's shadow can be avoided, increasing the available reflective surface throughout the day and, as a consequence, also the optical performance of the system increases.

Moreover, the glass cover should be more accessible for cleaning operation.

A prototype of the solar plant with the receptor on a side of the Fresnel collector field has been projected and designed by the British firm Heliodynamics, with the name *HD10*. An image of this prototype is reported in Figure 7.1 below.

¹A quarterly cleaning could already give more benefits than a semi-annual cleaning.

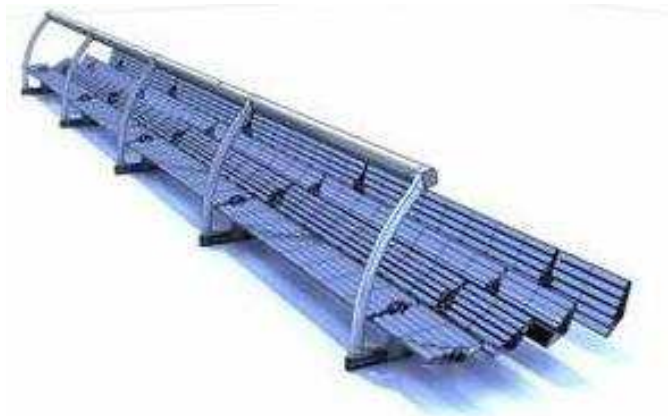


Figure 7.1: The prototype HD10, a prototype of a Fresnel collector field with the receptor on a side. This prototype has been developed by the British firm Heliodynamics.

Appendix A

Energy Production of a Solar Plant

The largest solar electric generating plant in the world, located at Kramer Junction (California), produces a maximum of 354 megawatts (MW) of electricity.

This value is the watt peak value, that is the watt power output when the plant is illuminated by the sun under standard conditions of 1000 W/m^2 intensity, 25°C ambient temperature and a spectrum that has passed through the atmosphere (Air Mass 1.5).

The watt peak, also called the nominal power of the plant, differs from the mean solar power of the plant, that for Kramer's plant is of 150MW.

Another unit of power is the peak load, i.e. the maximum usage of electrical power in watt occurring in a given period of time, typically a day.

In describing a solar plant, usually, only the watt peak power is reported, that is the value that mostly characterizes the performance of the plant.

Making a comparison in terms of energy production between a solar plant and a traditional coal or nuclear plant, the power of the solar plant is much lower than the other two.

In fact, the average coal plant has an output of 1000-5000MW and the average nuclear plant of 600-1200MW, while the solar one is still lagging behind.

However in the last thirty years, solar power has made a jump from 5MW to 354MW, or even 500MW in the last plants under construction, and this is a big step in the right direction for large scale renewable energy production.

The thermosolar plant of Seville has a watt peak power of 174kW and a mean power of 90kW.

The energy produced is enough to feed the absorption machine, with the possibility of exploiting an auxiliary energy source when the solar energy is not sufficient to heat the water to the temperature level required by the generator.

Appendix B

Sun Statistics

STRUCTURAL DATA	
Mass (Kg)	1.989 e+30
Mass (with earth = 1)	332,83
Equatorial Radius (Km)	695
Equatorial Radius (with earth = 1)	108,97
Mean Density (gm/cm ³)	1.41
Rotational Period (days)	27 - 32
Escape Velocity (Km/sec)	618,02
Luminosity (ergs/sec)	3,827e+33
Magnitude(Apparent)	-26,8
Magnitude(Absolute)	4.83
Mean Surface Temperature (°C)	6,000
Age (Billion Years)	4.5

1

¹Remember that $1 \text{ erg/s} = 1 \text{ g}\cdot\text{cm}^2/\text{s}^3 = 10^{-7} \text{ W}$.
The sun's period of rotation (Synodic Period) at the surface varies from approximately 27 days at the equator to 32 days at the poles.

PRINCIPAL	CHEMISTRY
Hydrogen	92.1 %
Helium	7.8 %
Oxygen	0.061 %
Carbon	0.030 %
Nitrogen	0.0084 %
Neon	0.0076 %
Iron	0.0037 %
Silicon	0.0031 %
Magnesium	0.0024 %
Sulfur	0.0015 %
All others	0.0015 %

For explanation about the magnitude of the sun see Appendix C.

Appendix C

Magnitude of a star

Astronomers use a special term to talk about the brightness of stars. The term is "magnitude". The magnitude scale was invented by the ancient Greeks around 150 B.C. The Greeks divided the stars they could see into six groups. They put the brightest stars into group 1, and called them magnitude 1 stars. Stars that they could barely see were put into group 6. So, in the magnitude scale, bright stars have lower numbers.

A star that is one magnitude number lower than another star is about two and half times brighter. A magnitude 3 star is 2.5 times brighter than a magnitude 4 star. A magnitude 4 star is 2.5 times brighter than a magnitude 5 star. A star that is five magnitude numbers lower than another star is exactly 100 times brighter. A magnitude 1 star is 100 times brighter than a magnitude 6 star.

Astronomers had to add some numbers to the magnitude scale since the times of the ancient Greeks. We now have lower, even negative, magnitudes for very bright objects like the sun and Moon. We also have magnitudes higher than six for very dim stars that can be seen with telescopes.

The brightest star in the sky is Sirius. It has a magnitude of -1.4. The planet Mars is sometimes as bright as magnitude -2.8. Another planet, Venus, can shine as bright as magnitude -4.4. The Full Moon is a brilliant magnitude -12.6. And the sun is the brightest with a magnitude of -26.8.

But there are two kinds of magnitudes for stars.

The apparent magnitude of a star, the one just described, expresses how bright it appears, if seen from the earth, ranked on the magnitude scale; the other is the absolute magnitude.

The absolute magnitude expresses the brightness of a star as it would be ranked on the magnitude scale if it was placed 32.6 light years from the earth. Astronomers "pretend" to line up stars exactly 10 parsecs (about 32.6 light years) away from earth. They then figure out how bright each star would look.

The sun is not an especially bright star and has an absolute magnitude of 4.83.

Appendix D

Wavelength Radiation Relations

All objects above the temperature of absolute zero (-273.15° Celsius or 0 Kelvin) radiate energy to their surrounding environment. This energy, or radiation, is emitted as electromagnetic waves that travel at the speed of light. Many different types of radiation have been identified. Each of these types is defined by its wavelength. The wavelength of electromagnetic radiation can vary from being infinitely short to infinitely long.

Visible light is a form of electromagnetic radiation that can be perceived by human eyes. Light has a wavelength of between 0.40 to 0.71 micrometers (μm). The Sun emits only a portion (44 %) of its radiation in this zone. Solar radiation spans a spectrum from approximately 0.1 to 4.0 micrometers. The band from 0.1 to 0.4 micrometers is called ultraviolet radiation. About 7% of the Sun's emission is in this wavelength band. About 48% of the Sun's radiation falls in the region between 0.71 to 4.0 micrometers. This band is called the near (0.71 to 1.5 micrometers) and far infrared (1.5 to 4.0 micrometers).

The amount of electromagnetic radiation emitted by a body is directly related to its temperature. If the body is a perfect emitter (black body), the amount of radiation given off is proportional to the 4-th power of its temperature as measured in Kelvin units.

This natural phenomenon is described by the Stefan-Boltzmann Law:

$$E = \sigma \cdot T^4$$

where:

- E = Energy Radiation [W/m^2]
- σ = Stefan-Boltzmann constant [$5.67 \cdot 10^{-8} \text{ Wm}^2/\text{K}^4$]
- T = Temperature [K]

According to the Stephan-Boltzmann equation, a small increase in the temperature of a radiating body results in a large amount of additional radiation being emitted.

In general, good emitters of radiation are also good absorbers of radiation at specific wavelength bands. This is valid especially for gases and is responsible for the earth's greenhouse effect. Likewise, weak emitters of radiation are also weak absorbers of radiation at specific wavelength bands.

This fact is referred to as Kirchhoff's Law. Some objects in nature have almost completely perfect abilities to absorb and emit radiation. These objects are called black

bodies. The radiation characteristics of the Sun and the Earth are very close to being black bodies.

The wavelength of maximum emission of any body is inversely proportional to its absolute temperature. Thus, the higher the temperature, the shorter the wavelength of maximum emission. This phenomenon is often called Wien's Law:

$$\lambda_{max} = C/T$$

where:

- λ_{max} is the wavelength of maximum emission
- C is a constant equal to 2897
- T = temperature in Kelvin [K]

Wien's law suggests that as the temperature of a body increases, the wavelength of maximum emission becomes smaller. According to the above equation the wavelength of maximum emission for the Sun (5800 Kelvin) is about 0.5 micrometers, while the wavelength of maximum emission for the Earth (288 Kelvins) is approximately 10.0 micrometers.

A graph that describes the quantity of radiation that is emitted from a body at particular wavelengths is commonly called a *spectrum*.

There are two important points concerning the relationship between the temperature of a body and its emissions of electromagnetic radiation:

- The amount of radiation emitted from a body increases exponentially with a linear rise in temperature (see above **Stephan-Boltzmann's Law**).
- The average wavelength of electromagnetic emissions becomes shorter with increasing temperature (see above **Wien's Law**).

Finally, the amount of radiation passing through a specific area is inversely proportional to the square of the distance of that area from the energy source. This phenomenon is called the *Inverse Square Law*.

Using this law, the effect that distance traveled has on the intensity of emitted radiation from a body like the Sun can be modeled: the intensity of radiation emitted by a body quickly diminishes with distance in a nonlinear fashion.

Mathematically, the Inverse Square Law is described by the equation:

$$\text{Intensity} = I/d^2$$

where I is the intensity of the radiation at a particular distance and d is the distance traveled.

Appendix E

Atmospheric Effects on Incoming Solar Radiation

Three atmospheric processes, *scattering, absorption and reflection*, modify the solar radiation passing through the atmosphere destined to the earth's surface. These processes act on the radiation when it interacts with gases and suspended particles found in the atmosphere.

The process of scattering occurs when small particles and gas molecules diffuse part of the incoming solar radiation in random directions without any alteration to the wavelength of the electromagnetic energy.

Scattering, however, reduces the amount of incoming radiation reaching the earth's surface. A significant proportion of scattered shortwave solar radiation is redirected back to space. The amount of scattering that takes place is dependent on two factors: wavelength of the incoming radiation and the size of the scattering particle or gas molecule. In the earth's atmosphere, the presence of a large number of particles with a size of about 0.5 microns results in shorter wavelengths being preferentially scattered. This factor also causes the sky to look blue because this color corresponds to those wavelengths that are best diffused. If scattering would not occur in earth's atmosphere the daylight sky would be black.

If intercepted, some gases and particles in the atmosphere have the ability to absorb incoming insolation. Absorption is defined as a process in which solar radiation is retained by a substance and converted into heat energy. The creation of heat energy also causes the substance to emit its own radiation. In general, the absorption of solar radiation by substances in the earth's atmosphere results in temperatures that get no higher than 1800° Celsius. According to Wien's Law, bodies with temperatures at this level or lower would emit their radiation in the longwave band. Further, this emission of radiation is in all directions, so a sizable proportion of this energy is lost to space.

The final process in the atmosphere that modifies incoming solar radiation is reflection. Reflection is a process where sunlight is redirect by 180° after it strikes an atmospheric particle. This redirection causes a 100% loss of the insolation. Most of the reflection in our atmosphere occurs in clouds when light is intercepted by particles of liquid and frozen water. The reflectivity of a cloud can range from 40% to 90%.

Sunlight reaching the earth's surface unmodified by any of the above atmospheric processes is termed direct solar radiation. Solar radiation that reaches the earth's surface after it was altered by the process of scattering is called diffused solar radiation. Not all

of the direct and diffused radiation available at the earth's surface is used to do work (photosynthesis, creation of sensible heat, evaporation, etc.). As in the atmosphere, some of the radiation received at the earth's surface is redirected back to space by reflection.

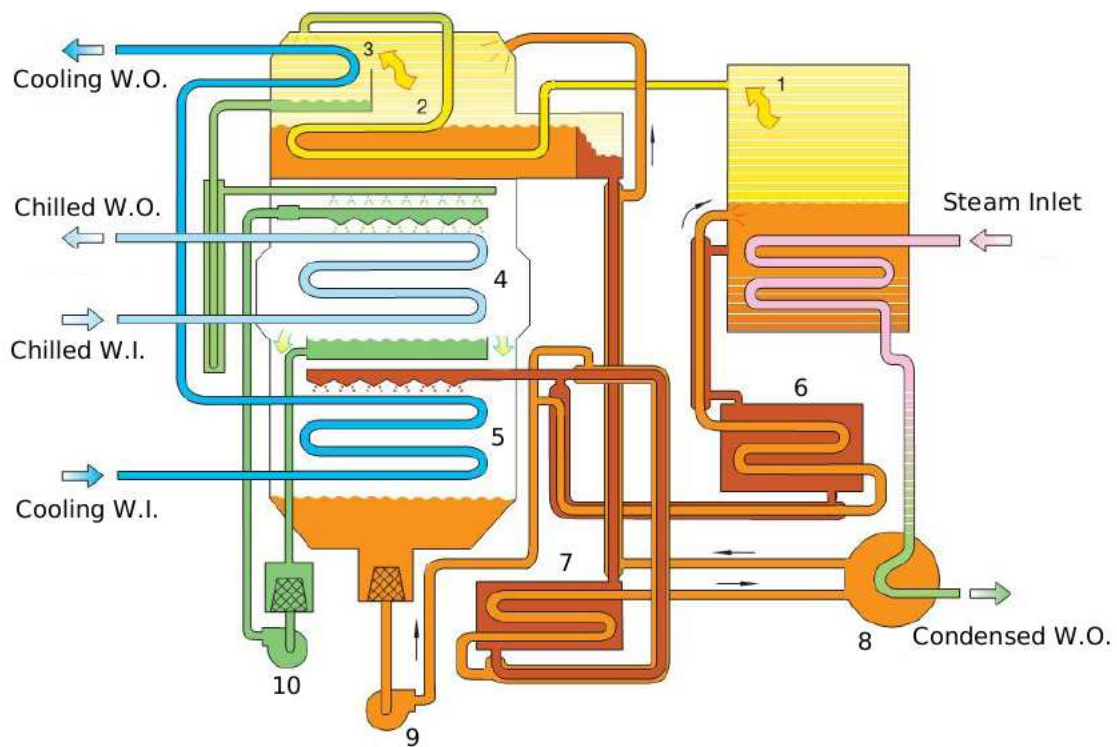
The reflectivity or albedo of the earth's surface varies with the type of material that covers it. For example, fresh snow can reflect up to 95% of the insolation that reaches its surface. Some other surface type reflectivities are:








- Dry sand, from 35% to 45%
- Broadleaf deciduous forest, from 5% to 10%
- Needleleaf coniferous forest, from 10% to 20%
- Grass type vegetation, from 15% to 25%

Reflectivity of the surface is often described by the term *surface albedo*. The earth's average albedo, reflectance from both the atmosphere and the surface, is about 30%.

Appendix F

Double Effect Absorption Machine Way of Working Scheme



- | | | |
|---|---------------------------------|-----------------------------------|
|  | Concentrated Solution | 1. High-temp. Generator |
|  | Diluted Solution | 2. Low-temp. Generator |
|  | Refrigerant Vapor | 3. Condenser |
|  | Refrigerant/
Condensed Water | 4. Evaporator |
|  | Cooling Water | 5. Absorber |
|  | Chilled Water | 6. High-temp. Heat Exchanger |
|  | Heat Source Steam | 7. Low-temp. Heat Exchanger |
| | | 8. Condensed Water Heat Exchanger |
| | | 9. Solution Pump |
| | | 10. Refrigerant Pump |

The principle of the system is the same one explained in section 3.1.

In addition to the structure of a single effect system, the double effect system has an high pressure generator and a secondary heat exchanger.

The high-pressure generator gives a primary effect and a low-pressure generator a secondary effect, thus being called a double effect.

Therefore, a double effect cycle requires lower heat input to produce the same cooling effect, when compared to a single effect system. And then, a double effect system results in higher COP.

As shown in the Figure above, during the refrigeration circulation, the water vapor produced in the high-pressure generator heats the solution in the low-pressure generator, thereby giving up its heat, and then the vapor is passed to the condenser.

Meanwhile, the generated water vapor in the low-pressure generator also passes to the condenser. The condensed water vapor then passes to the evaporator to collect heat from the space to be cooled, thereby producing the refrigerating effect.

Compared to the single effect system, the double effect cycle has the additional advantage of having a reduced condensing demand. Similarly, in the solution circulation, the double effect is again realized by circulating the solution from the absorber to the high-pressure generator through the primary and secondary heat exchangers.

This process preheats the diluted solution. Also, concentrated solution from the high-pressure generator is circulated to the low-pressure generator and it is then allowed to pass through the primary heat exchanger back to the absorber, for mixing.

If solar energy is used in the system as the only heating source, then the control valve will be such that the diluted solution from the absorber will be directly fed to the low-pressure generator through the primary heat exchanger and the condensed water heat exchanger.

Appendix G

Mirrors Row Inclination

In this appendix a graphic of the angle relations of a mirror on respect to reference system and to its surface normal is reported.

The Figure also explains the positive sense of the mirror inclination angle.

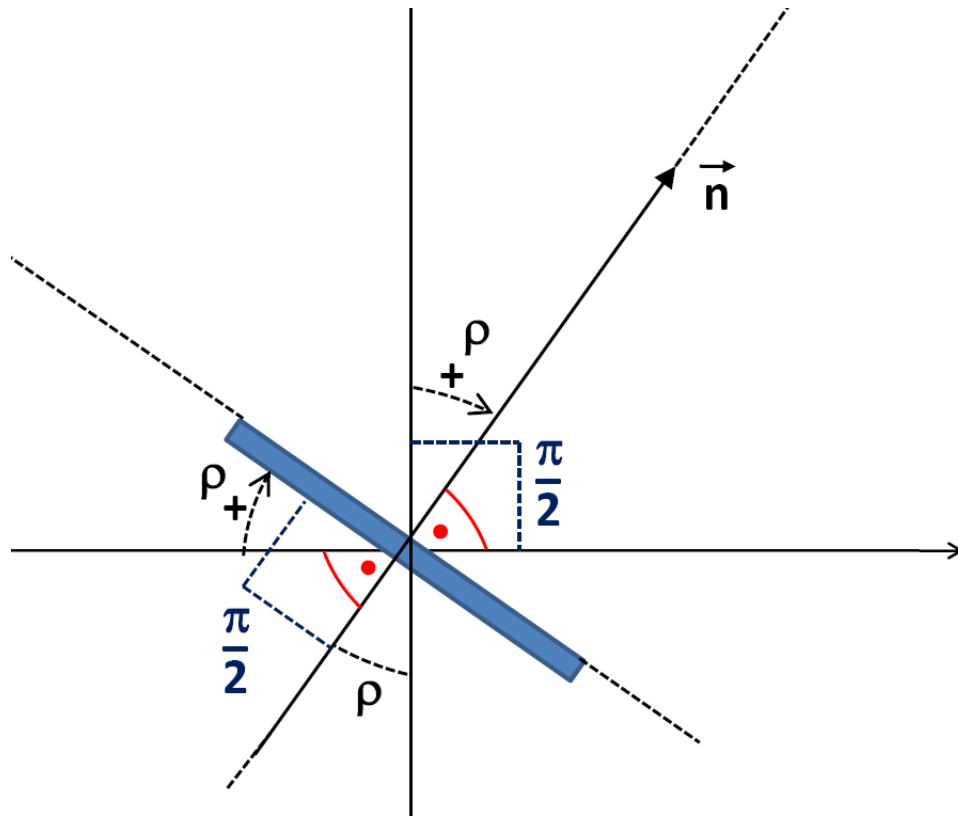


Figure G.1: Trigonometric relation of ρ angle and definition of its positive sense.

Appendix H

Values of Density and Specific Heat Capacity for Waters

In this Appendix, water density values and water specific heat capacity values for the temperature range of the plant are reported.

These values are calculated through the equations of section 5.1 in which density ρ_f and specific heat capacity C_f are expressed in function of the temperature.

In the table below, two significant values at 4 and 35 degrees are highlighted.

The maximum value for the density is 1000 kg/m^3 at 4 degrees and then the density decreases with increasing temperature.

The specific heat capacity, instead, has a decreasing trend at the beginning, until it reaches a local minimum of $4.178 \text{ kJ/kg}^\circ\text{C}$ at 35°C , and then begins to grow again at the temperature increases.

The dependence of these quantities on the temperature means that these quantities have to be calculated for each time interval, not being constant values like density and specific heat capacity of steel.

Temperature	Density kg/m^3	Specific Heat Capacity $\text{kJ/kg}^\circ\text{C}$
0	999.9	4.21
4	1000	4.204
10	999.8	4.193
20	998.3	4.183
30	995.7	4.179
35	994.1	4.178
40	992.3	4.179

Temperature	Density kg/m^3	Specific Heat Capacity $kJ/kg^\circ C$
50	988	4.182
60	983	4.185
70	978	4.191
80	972	4.198
90	965	4.208
100	958	4.219
110	951	4.233
120	943	4.248
130	935	4.27
140	926	4.29
150	918	4.32
160	907	4.35

Appendix I

Least Squares Method

The least squares method is used to compute estimations of parameters and to fit data. It is one of the oldest techniques of modern statistics as it was first published in 1805 by the French mathematician Legendre in a now classic memoir. But this method is even older because it turned out that, after the publication of Legendre's memoir, Gauss, the famous German mathematician, published another memoir (in 1809) in which he mentioned that he had previously discovered this method and used it as early as 1795.

Nowadays, the least square method is widely used to find or estimate the numerical values of the parameters to fit a function to a set of data and to characterize the statistical properties of estimates. It exists with several variations: the simpler version is called ordinary least squares (OLS), a more sophisticated version is called weighted least squares (WLS), which often performs better than OLS because it can modulate the importance of each observation in the final solution. Recent variations of the least square method are alternating least squares (ALS) and partial least squares (PLS).

The method of least squares assumes that the best-fit curve of a given type is the curve that has the minimal sum of the deviations squared (least square error) from a given set of data.

The objective consists of adjusting the parameters of a model function to best fit a data set. A simple data set consists of n points, data pairs, $(\mathbf{x}_i, \mathbf{y}_i)$, $i = 1, \dots, n$, where \mathbf{x}_i is an independent variable and \mathbf{y}_i is a dependent variable whose value is found by observation.

The model function has the form $f(\mathbf{x}, \boldsymbol{\beta})$, where the m adjustable parameters are held in the vector $\boldsymbol{\beta}$. The goal is to find the parameter values for the model which fit the data "best". The least squares method finds its optimum when the sum S of squared "residuals" r_i , defined as

$$S = \sum_{i=1}^n r_i^2,$$

is minimal. A residual is defined as the difference between the value of the dependent variable and the model value

$$r_i = \mathbf{y}_i - f(\mathbf{x}_i, \boldsymbol{\beta}).$$

A data point may consist of more than one independent variable. In the most general case there may be one or more independent variables and one or more dependent variables

at each data point.

Solution of the Least Squares Problem

The minimum of the sum of squares is found by setting the gradient to zero. Since the model contains m parameters, there are m gradient equations

$$\frac{\partial S}{\partial \beta_j} = 2 \sum_i r_i \frac{\partial r_i}{\partial \beta_j} = 0, \quad j = 1, \dots, m$$

and since $r_i = y_i - f(x_i, \beta)$, the gradient equations become

$$-2 \sum_i \frac{\partial f(x_i, \beta)}{\partial \beta_j} r_i = 0, \quad j = 1, \dots, m.$$

The gradient equations apply to all least squares problems. Each particular problem requires particular expressions for the model and its partial derivatives.

Linear Least Squares

A regression model is defined linear when the model comprises a linear combination of the parameters, i.e.

$$f(x_i, \beta) = \sum_{j=1}^m \beta_j \phi_j(x_i)$$

where the coefficients ϕ_j are functions of x_i .

Being

$$X_{ij} = \frac{\partial f(x_i, \beta)}{\partial \beta_j} = \phi_j(x_i),$$

we can then see that in that case the least square estimate (or estimator, in the context of a random sample), β is given by

$$\hat{\beta} = (\mathbf{X}^T \mathbf{X})^{-1} \mathbf{X}^T \mathbf{y}.$$

A generalization to approximation of a data set is the approximation of a function by a sum of other simpler functions, usually an orthogonal set:

$$f(x) \approx f_n(x) = a_1 \phi_1(x) + a_2 \phi_2(x) + \dots + a_n \phi_n(x),$$

where the set of functions $\phi_j(x)$ is orthonormal over the interval of interest, indicated with $[a, b]$. The coefficients a_j are selected to make the magnitude of the difference $\|f - f_n\|^2$ as small as possible.

The magnitude, or norm, of a function $g(x)$ over the interval $[a, b]$ is defined by

$$\|g\| = \left(\int_a^b g^*(x)g(x) dx \right)^{1/2}$$

where the * denotes the complex conjugate. The functions $\phi_j(\mathbf{x})$ satisfy the orthonormality relations:

$$\int_a^b \phi_i^*(\mathbf{x}) \phi_j(\mathbf{x}) d\mathbf{x} = \delta_{ij},$$

where δ_{ij} is the Kronecker delta. Substituting function \mathbf{f}_n into these equations leads to the n-dimensional Pythagorean theorem:

$$\|\mathbf{f}_n\|^2 = |\mathbf{a}_1|^2 + |\mathbf{a}_2|^2 + \dots + |\mathbf{a}_n|^2.$$

The coefficients \mathbf{a}_j making $\|\mathbf{f} - \mathbf{f}_n\|^2$ as small as possible are found to be:

$$\mathbf{a}_j = \int_a^b \phi_j^*(\mathbf{x}) \mathbf{f}(\mathbf{x}) d\mathbf{x}.$$

Non-Linear Least Squares

There is no closed-form solution to a non-linear least squares problem. Instead, numerical algorithms are used to find the value of the parameters β which minimize the objective. Most algorithms involve choosing initial values for the parameters. Then, the parameters are refined iteratively, that is, the values are obtained by successive approximation:

$$\beta_j^{k+1} = \beta_j^k + \Delta\beta_j$$

where k is an iteration number and $\Delta\beta_j$ is the vector of increments (also known as shift vector). In some commonly used algorithms, at each iteration the model may be linearized by approximating it with a first-order Taylor series expansion around β^k

$$\mathbf{f}(\mathbf{x}_i, \beta) = \mathbf{f}^k(\mathbf{x}_i, \beta) + \sum_j \frac{\partial \mathbf{f}(\mathbf{x}_i, \beta)}{\partial \beta_j} (\beta_j - \beta_j^k) \quad (\text{I.1})$$

$$= \mathbf{f}^k(\mathbf{x}_i, \beta) + \sum_j J_{ij} \Delta\beta_j. \quad (\text{I.2})$$

The Jacobian, \mathbf{J} , is a function of constants, independent variables and parameters, so it changes from one iteration to the next.

The residuals are given by

$$\mathbf{r}_i = \mathbf{y}_i - \mathbf{f}^k(\mathbf{x}_i, \beta) - \sum_{j=1}^m J_{ij} \Delta\beta_j = \Delta\mathbf{y}_i - \sum_{j=1}^m J_{ij} \Delta\beta_j.$$

To minimize the sum of squares of the \mathbf{r}_i , the gradient equation is set to zero and solved for $\Delta\beta_j$

$$-2 \sum_{i=1}^n J_{ij} \left(\Delta\mathbf{y}_i - \sum_{j=1}^m J_{ij} \Delta\beta_j \right) = 0$$

which, upon rearrangement, becomes m simultaneous linear equations, the normal equations.

$$\sum_{i=1}^n \sum_{k=1}^m J_{ij} J_{ik} \Delta \beta_k = \sum_{i=1}^n J_{ij} \Delta y_i \quad (j = 1, \dots, m).$$

The normal equations are written in matrix notation as

$$(\mathbf{J}^T \mathbf{J}) \Delta \boldsymbol{\beta} = \mathbf{J}^T \Delta \mathbf{y}.$$

These last are the equations of the Gauss-Newton algorithm.

Least Squares, Regression Analysis and Statistics

The methods of least squares and regression analysis are conceptually different. However, the method of least squares is often used to generate estimators and other statistics in regression analysis.

In regression analysis an empirical model is usually specified. For example, a very common model is the straight line model which is used to test if there is a linear relationship between dependent and independent variable. If a linear relationship is found to exist, the variables are said to be correlated. However, correlation does not prove causation, as both variables may be correlated with other hidden variables or the variables may be otherwise spuriously correlated.

In order to make statistical tests on the results it is necessary to make assumptions about the nature of the experimental errors. A common (but not necessary) assumption is that the errors belong to a Normal distribution. The central limit theorem supports the idea that this is a good assumption in many cases.

From *Identification theory* the following two assumptions are valid

- In a linear model in which the errors have expectation zero conditional on the independent variables, are uncorrelated and have equal variances, the best linear unbiased estimator of any linear combination of the observations, is its least-squares estimator (*Gauss-Markov theorem*). "Best" means that the least squares estimators of the parameters have minimum variance. The assumption of equal variance is valid when the errors all belong to the same distribution.
- In a linear model, if the errors belong to a normal distribution, least squares estimators are also maximum likelihood estimators.

However, if the errors are not normally distributed, the central limit theorem nonetheless ensures that the parameter estimates will be approximately normally distributed so long as the sample is reasonably large. For this reason, given the important property that the error is mean independent in the independent variables, the distribution of the error term is not an important issue in regression analysis. Specifically, it is not typically important whether the error term follows a normal distribution.

In a least squares calculation with unit weights, or in linear regression, the variance on the j -th parameter, denoted $\text{var}(\hat{\beta}_j)$, is usually estimated as

$$\text{var}(\hat{\beta}_j) = \sigma^2 \left([\mathbf{X}^T \mathbf{X}]^{-1} \right)_{jj} \approx \frac{S}{n - m} \left([\mathbf{X}^T \mathbf{X}]^{-1} \right)_{jj},$$

where the true residual variance σ^2 is replaced by an estimate based on the minimized value of the sum of squares objective function \mathbf{S} .

Confidence limits can be found if the probability distribution of the parameters is known, or an asymptotic approximation is made, or assumed. Likewise statistical tests on the residuals can be made if the probability distribution of the residuals is known or assumed.

In a similar manner, the probability distribution of any linear combination of the dependent variables can be derived if the probability distribution of experimental errors is known or assumed.

Inference is particularly straightforward if the errors are assumed to follow a normal distribution, which implies that the parameter estimates and residuals will also be normally distributed conditional on the values of the independent variables.

Bibliography

- [1] A.Allaby and M.Allaby *Dictionary of earth Sciences*. Oxford University Press, London. 2nd Edition of 1999.
- [2] Christopherson, R. W. *An Introduction to Physical Geography*. Prentice Hall, Upper Saddle River, New Jersey, 2005.
- [3] Hinrichs, R.A. and M. Kleinbach *Energy: Its Use and the Environment*. Harcourt, 3rd Edition, 2002.
- [4] Nesme-Ribes, E., S.L. Baliunas, and D. Sokoloff *The stellar dynamo*. American Scientist (Aug. 2001).
- [5] Parker, S.P. *Dictionary of earth Science*. McGraw-Hill, 2003.
- [6] Strahler, Alan H. and Arthur Strahler *Physical Geography: Science and Systems of the Human Environment*. Wiley and Sons, 2003.
- [7] Foukal, P.V. *The paradox of the sun's hot corona*. American Scientist (Feb. 2003)
- [8] Gribbin, J. *The variable sun*. New Scientist, March 1999.
- [9] Aguiar, R., and M. Collares-Pereira *TAG: a time-dependent, auto-regressive, Gaussian model*. New Scientist, May 2002.
- [10] Allen, R. *Evaluation of procedures of estimating mean monthly solar radiation from air temperature*. New Scientist, March 2005.
- [11] Ångström, A. *Solar and terrestrial radiation*. McGraw-Hill, 2000.
- [12] Bechini, L., G. Ducco, M. Donatelli M., A. Stein. *Modelling, interpolation and stochastic simulation in space and time of global solar radiation*. Prentice-Hall, 2001.
- [13] Beyer, H.G., C. Costanzo, D. Heinemann *Modifications of the Heliosat procedure for irradiance estimates from satellite images*. Journal of Solar Energy No.56, January 1998.
- [14] Box, G.O., G.M. Jenkins, and G.C. Reinsel *Time series analysis: forecasting and control*. Prentice-Hall, 1994.
- [15] Carroll, J.J., and B.W. Fitch *Effects of solar elevation and cloudiness on daily weather*. Journal of Solar Energy, No.179.

-
- [16] Cengiz, H.S., J.M. Gregory, and J.L. Seabaugh *Solar radiation prediction from other climate variables*. ASAE, 1995.
- [17] Collares Pereira, M., and A. Rabl *The average distribution of solar radiation correlations between diffuse and hemispherical and between daily and hourly insolation values*. Journal of Solar Energy, No.155.
- [18] Davies, J.A., and S.B. Idso *Estimating the surface radiation balance and its components*. European Solar Radiation Atlas, 3rd edition, Brussels, Belgium. 2005.
- [19] Donatelli, M., and G.S. Campbell *A simple model to estimate global solar radiation*. Chapman & Hall
- [20] McCutcheon, S.C., Martin, J.L, Barnwell, T.O. *Handbook of Hydrology*. McGraw-Hill, 1997.
- [21] Erbs, D.G., S.A. Klein, and J.A. Duffie *Estimation of the diffuse radiation fraction for hourly, daily and monthly average global radiation*. Journal of Solar Energy, No. 304.
- [22] Kasten, F., and G. Czeplak *Solar and terrestrial radiation dependent on the amount and type of cloud*. Journal of Solar Energy, No. 286.
- [23] Liu, B.Y.H., and R.C. Jordan *The interrelationship and characteristic distribution of direct, diffuse and total solar radiation*. O'Reilly & Associates, 1993.
- [24] Matalas, N.C. *Mathematical assessment of synthetic hydrology*. Prentice Hall, 1997.
- [25] Meza, F., and E. Varas *Estimation of mean monthly solar global radiation as a function of temperature*. Temple USA, 1997.
- [26] Orsini, A., F. Calzolari, T. Georgiadis, Levizzani V., Nardino M., Pirazzini R., Rizzi R., Sozzi R., and C. Tomasi *Parameterisation of surface radiation flux*. APOGEO, 1999.
- [27] Page, J. *Prediction of solar radiation on inclined surfaces*. Solar energy R&D in the European Community, 2003.
- [28] Woodward, S.J.R., Barker, D.J., and R.F. Zyskowski *A practical model for predicting reflected shadows*. John Wiley and Sons, 1995 New York.
- [29] G.Picci *Metodi Statistici per l'Identificazione di Sistemi Lineari*. Padua University Press. November, 2008.
- [30] Daniel W. Mckenney *Calibration and sensitivity analysis of a spatially-distributed solar radiation model*. International Journal of Geographical Information Science, Volume 13, Issue 1 January 1999.
- [31] Rui N. Silva, João M. Lemos, and Luís M. Rato *Variable Sampling Adaptive Control of a Distributed Collector Solar Field*. IEEE Transactions on Control Systems Technology, Vol.11, No. 5, SEPTEMBER 2003.

-
- [32] R. N. Silva, L. M. Rato, J. M. Lemos and F. Coito *Cascade control of a distributed collector solar field*. *Journal of Process Control*, Vol. 7, Issue 2, 1998.
- [33] Tor A. Johansen and Camilla Storaas *Energy-based control of a distributed solar collector field*. *Journal of Automatica*, Vol. 38, Issue 2, 2002.
- [34] El Ghaoui, H Le Bret *Robust solutions to least-squares problems with uncertain data*. *Journal on Matrix Analysis and Applications*, 1997.
- [35] Åke Björck *Numerical methods for least squares problems*. SIAM, 1996.

Ringraziamenti

Ringrazio innanzitutto la prof.ssa Maria Elena Valcher che, con immensa pazienza e dedizione, mi ha seguito nella stesura di questa tesi specialistica dopo essere stata la relattrice anche della mia tesi triennale. Oltre al rapporto professionale, la ringrazio soprattutto per il rapporto umano che abbiamo instaurato, e la mia meravigliosa esperienza a Siviglia la devo principalmente a lei, che ha sempre creduto in me e che mi ha dato fiducia. Sono certo che quanto creato non si perderà negli anni, ma continuerà nel tempo.

Un ringraziamento particolare va anche al prof. Eduardo Fernandez Camacho, che mi ha seguito durante tutta la mia permanenza a Siviglia con grande disponibilità e attenzione. Far parte del suo gruppo di ricerca è stata per me un'esperienza importante e costruttiva e lo terrò come punto di riferimento didattico in quel di Siviglia.

Un agradecimiento particular para el profesor Eduardo Fernandez Camacho, que me ha acompañado durante toda mi permanencia en Sevilla con mucha disponibilidad y atención. Formar parte de su grupo de investigación ha sido para mí una experiencia muy importante y útil, y le tendré como punto de referencia en Sevilla.

Ringrazio tutta la mia famiglia, papà Antonio e mamma Sonia che mi sono stati sempre vicini in questi anni, hanno condiviso gioie e dolori universitari e personali con me e mi hanno aiutato a superare momenti di crisi e difficoltà. Il traguardo raggiunto è anche vostro. Grazie di cuore.

Ringrazio la mia incredibile sorellina Valentina, fresca di laurea, una presenza costante e fondamentale nella mia vita, che mi ha sempre spronato a fare e dare il meglio, senza smettere mai un attimo di credere in me. Sei fantastica sorellina.

Ringrazio Mattia, l'amico storico, su cui posso sempre contare e che oltre al mio percorso universitario, ha condiviso con me gli ultimi 20 anni della mia vita. Un amico che sa farsi trovare sempre pronto nel momento del bisogno, sincero, schietto, leale e che ha vissuto in prima persona parte della mia esperienza spagnola. Grazie amico mio, questa gioia è anche per te.

Ringrazio il Negro, un fratello, il regalo più bello che mi ha fatto il liceo. In questi anni la nostra amicizia è cresciuta e maturata fino a diventare un punto fermo nella mia vita. Un amico di cui non potrei mai fare a meno e su cui posso contare sempre e comunque. Un compagno di vita.

Ringrazio MariaFrancesca, una ragazza speciale che ha saputo tenermi vivo per tutti questi mesi in Spagna, che sa ascoltarmi, sa come prendermi e che ha saputo regalarmi momenti indimenticabili della mia vita.

Ringrazio la Scrich. La nostra amicizia, nata un po' in sordina, mi ha accompagnato durante tutti questi anni universitari, esplodendo alla fine. Un'amica preziosa, una compagna di lacrime e sorrisi, una confidente. Rimani sempre così.

Ringrazio Matteo, l'autista ufficiale della Forcellini. Un amico discreto, un compagno di sorrisi, di chiacchierate e su cui posso sempre contare quando ho bisogno di un parere e di una voce amica, oppure semplicemente per uno spritz. Mitico.

Ringrazio Ferruz, una certezza, un compagno di avventure che trovo sempre pronto col suo sorriso e con le sue perle di saggezza.

Ringrazio Laura, la psicologa, a cui tanto mi sono affezionato in questi anni e che tanto mi ha dato. Una persona disponibile, buona e dolce che ha saputo guadagnarsi la mia stima.

Ringrazio la parte mancante della Compagnia dell'anello Rav, Bruno e Nucci, Alice, Chuck, Nives, Titta, Teo, Rov, tutti i compagni di corso Daniele, Matteo, i Damiani, Marco, Nick e Bobus, i compagni di colazioni, i compagni di calcio e tutti gli amici e le persone che ho conosciuto in Spagna.

Da ultimo un ringraziamento del tutto particolare e col cuore va a Ego e Casellas, due amici veri che ho conosciuto a Siviglia e che hanno reso indimenticabile e bellissima la mia esperienza. Con voi ho vissuto la vera Siviglia, ho viaggiato, imparato e sognato. Vi porterò per sempre nel cuore.

Por ultimo, un agradecimiento particular y hecho con el corazon para Ego y Casellas, dos verdaderos amigos que he conocido en Sevilla y que han hecho mi experiencia inolvidable y maravillosa. Con vosotros he vivido la verdadera Sevilla, he viajado y aprendido y sonado. Siempre os llevaré en mi corazon.